Abstract Book

2024 Spring Meeting

March 22-23, 2024

I. Platform Presentations
II. Posters

Platform Presentations

Platform 1: Pediatric Malignancies (I)

1709784

Clinicopathogenetic Heterogeneity of Lineage Switch in Pediatric Acute Leukemia

X Liang [1], B Siegele [2], B Carstens [3], M Haag [3]; [1] Children's Hospital Colorado, [2] Children's Hospital Colorado, [3] Colorado cytogenetic laboratory

Background: Lineage switch of acute leukemia (AL) refers to a relapse of an AL with the lineage different from that of the diagnostic leukemia and the preservation of the original genetic clone with or without additional genetic abnormalities. It is rare. Most of reported cases are from acute lymphoblastic leukemia (ALL) to acute myeloid leukemia (AML) and are often associated with KMT2A rearrangement. Only rare cases of atypical lineage switch (AL → non-AML) with or without atypical clinical manifestation at the relapse (AL → a focal mass lesion) are documented in the literature. We performed a retrospective review of lineage switch cases in our institution to characterize their clinicopathogenetic features and provide a more comprehensive landscape of this disease.

Methods: Between 9/1999 and 9/2023, cases of lineage switch/plasticity of AL in patients less than 20-years-old were searched in the pathology data base among newly diagnosed AL (B-ALL, T-ALL, and AML) cases at our institution. The types of lineage switch/plasticity including typical type (ALL → AML) and atypical type (AL → non-AML and/or AL → a focal mass), age, gender, cytogenetic features, and outcomes are assessed.

Results: Twelve out of 1281 new AL cases demonstrated lineage switch/plasticity during their course of the diseases, including 8 cases of typical type and 4 cases of atypical type (Table 1).

Conclusion: 1. AL lineage switch/plasticity occurs predominantly in male with male exclusive in adolescent patients, suggesting male hormones may have some promoting impact on AL lineage switch especially during the period of puberty. 2. Atypical AL lineage/plasticity cases are clinically heterogeneous, including from B-ALL to a focal MS (case 9), B-ALL to CML (case 10), AML to B-ALL (case 11), and AML to a benign tumor (case 12). 3. Regardless of typical or atypical types, all cases from one type of AL relapsed to another type of AL or MS have a dismal outcome (10/10, 100%). Cases transformed from AL to a chronic leukemia or a benign tumor have a favorable outcome. 4. KMT2A gene rearrangement occurs in 50% of cases, suggesting that it is an important factor but not the only factor in driving lineage switch.

Table 1 Clinicopathogenetic Features of Lineage Switch Cases in Pediatric Acute Leukemia

Case #	**Age at 1st diagnosis/Sex**	**Type of Lineage Switch**	**Preserved genetic feature**	**Outcome**
Typical type				
1	6 y/M	B-ALL → AML	Non-specific	Died
2	3d/F	B-ALL → AML	*KMT2A*	Died
3	2y/F	T-ALL → AML	Non-specific	Died
4	10d/F	B-ALL → AML	*KMT2A*	Died
5	4m/M	B-ALL → AML	*KMT2A*	Died
6	18y/M	B-ALL → AML	Non-specific	Died
7	16y/M	B-ALL → AML	Non-specific	Died
8	15y/M	B-ALL → AML	*KMT2A*	Died
Atypical type				
9	19y/M	B-ALL → Focal myeloid sarcoma (MS) of the skin	*KMT2A*	Died
10	14y/M	B-ALL → CML	*BCR-ABL1*	Alive
11	2y/M	AML → B-ALL	*KMT2A*	Died
12	8m/M	AML → histiocytic tumor of the brain (lineage plasticity)	*Inv(16)*	Alive

Platform 1: Pediatric Malignancies (II)

1719526

Recurrent SRF Gene Fusions and Biallelic TP53 Inactivation in Two Histologically Distinct Subsets of Pediatric Leiomyosarcoma of Soft Tissue

E Alston [1], A Bakker [2], M Sabbagh [3], A Church [2], D Papke [4], C Fletcher [4], A Al-Ibraheemi [2];
[1] Boston Children's Hospital, [2] Boston Children's Hospital, [3] Mass General Brigham, [4] Brigham and Women's Hospital

Background: Pediatric leiomyosarcomas (pLMS) are rare tumors. Despite limited studies with long-term follow-up, they seem to differ from their adult counterparts, exhibiting low-grade morphology and indolent behavior. The molecular landscape of pLMS remains uncharacterized. This study presents the largest cohort of pLMS of soft tissue to date, providing insights into their clinical, morphologic, and molecular characteristics.

Methods: pLMS were retrieved from institutional and consult archives and morphologic, clinical, and molecular data was reviewed. Targeted next generation sequencing was performed on cases with available material that had not undergone clinical testing.

Results: 49 pLMS of soft tissue were identified occurring at a mean age of 9y (11m–20y) with no sex predilection (25M:24F). Tumors were 4.3 cm on average (0.8–18.2 cm) occurring on the extremities (47%), trunk (31%), head/neck (12%), pelvis (6%), and intraabdominal (4%). Tumors arose equally in subcutaneous (42%) and deep (42%) locations (16% of unknown depth). Clinical follow-up was available for 21 patients at a mean follow-up interval of 53m, with recurrence in 6 patients (29%), including 2 patients with 2 recurrences (mean time to first recurrence 24m). No metastases or deaths due to disease were reported. Tumors showed fascicles of monomorphic, predominantly ovoid to spindled cells in a nodular growth pattern. Most cases showed mild to occasional moderate atypia, with little mitotic activity (mean 5 mitoses/10 hpf). Intratumoral calcifications were common (49%), with occasional ossification (12%). A subset (10%) showed nuclear pleomorphism and higher mitotic rate (mean 15 mitoses/10 hpf). 33 cases underwent molecular testing, of which 5 showed SRF fusions and 5 demonstrated TP53 biallelic inactivation. No recurrent molecular alterations were identified in the remaining tested cases (Table 1). SRF fusion partners included NCOA2 (n=3), C3orf62 (n=1), and unknown (n=1, identified by FISH). All cases with SRF gene fusions were monomorphic, low-grade tumors with classic smooth muscle morphology. All tumors with significant pleomorphism showed biallelic TP53 inactivation.

Conclusion: We identified 2 small distinct subsets of pLMS. The first exhibits low-grade morphology and SRF gene fusion, prompting speculation about a connection to cellular myofibroma. The other displays marked nuclear atypia, pleomorphic morphology, and biallelic inactivation of TP53, suggesting a potential link to underlying Li-Fraumeni cancer predisposition syndrome. Except for the small subset with pleomorphic morphology, most pLMS are indolent with low-grade morphology; hence, conventional malignancy criteria may not be applicable to pLMS of soft tissue. Until there are longer follow-up data for these or other cases, we propose using the term “pediatric smooth muscle neoplasm” for the

Platform 1: Pediatric Malignancies (III)

1722604

Integrated Characterization of Soft Tissue and CNS CIC-Rearranged Sarcomas Reveals Shared Epigenetic Signatures Across Fusion Types and Anatomic Locations

J Van Arnam [1], F Lin [2], D Parsons [2], A Major [2], M Shafiekhani [3], H Voicu [2], M Hicks [2], K Patel [2], D Lopez-Terrada [2], K Fisher [2], C Mohila [2], M Blessing [2], A Roy [2]; [1] Texas Children's Hospital, [2] Texas Children's Hospital, [3] Baylor College of Medicine

Background: CIC-rearranged sarcoma is a high-grade undifferentiated sarcoma defined by CIC fusions with DUX4 or less common non-DUX4 partners. While the majority arise in soft tissue (ST), primary CIC-rearranged sarcomas are also reported in the central nervous system (CNS). While known to share histopathologic, genetic, and clinical features, it remains unclear if CIC-rearranged sarcomas from diverse locations and varied fusion partners are epigenetically related. We sought to characterize a set of CIC-rearranged sarcomas in an integrated fashion by examination of their histologic, immunophenotypic, and molecular findings including methylation profiling classification.

Methods: XXX pathology archival search identified CIC-rearranged sarcomas as detected by XXX Solid Tumor next-generation sequencing panel. Whole transcriptome sequencing (RNA-seq) of previously uncharacterized undifferentiated sarcomas or DNA methylation profiling identified additional cases. RNA-seq libraries were sequenced (2×100-bp reads) and analyzed by ensemble fusion callers. DNA methylation profiling was conducted with Infinium MethylationEPIC arrays (Illumina) and analyzed with the DKFZ neuropathology classifier version 12.5. Histomorphology and available immunostains were reviewed, blinded to the CIC mutation.

Results: We identified 25 cases from 13 patients (8 male, 5 female). Eleven presented with a ST primary, and 2 as CNS tumors. Of these, 19 cases from 12 patients ages 5-17 were available for review. Of the 11 ST cases, 10 had CIC::DUX4 fusions and one had a CIC::FOXO4 fusion. The 2 CNS cases harbored one each of CIC::NUTM1 and CIC::LEUTX fusion. Two histomorphologic patterns predominated: a densely cellular “Ewing-like” pattern with scant stroma and primarily round to ovoid cells with high N:C ratio, and another with myxoid stroma where tumor cells demonstrate eccentrically located nuclei with eosinophilic cytoplasm. One case, a left frontal lobe primary with CIC::LEUTX fusion, showed sheets of ganglion-like cells. When performed, at least partial CD99 staining was observed, sometimes dot-like; two cases from different patients were WT1-negative. Methylation profiling performed on 7 cases (5 soft tissue, 2 CNS) showed all cases with different CIC fusions to co-cluster as CIC-rearranged sarcomas.

Conclusion: Despite varied locations, morphologic and immunophenotypic features and fusion partners, methylation profiling demonstrates co-clustering of both ST and CNS CIC-fused sarcomas. Given CIC’s role as a transcriptional repressor, profound changes induced by its alteration may overwhelm prior methylation states present in the original cell of origin. These results further reinforce the need for molecular classification of Ewing-like neoplasms for final diagnosis in all body sites.

Platform 1: Pediatric Malignancies (IV)

1722892

Thyroid cytology in pediatric thyroid nodules; comparing our institutional risk of malignancy to the 2023 Bethesda System for Reporting Thyroid Cytopathology (BSRTC): A 15 year institutional experience

L Balikani [1], K Nicol [2], S Chekuri [2]; [1] Department of Pathology and Laboratory Medicine, Nationwide Children's Hospital, [2] Nationwide Children's Hospital

Background: The most recent Bethesda System for Reporting Thyroid Cytopathology (BSRTC) 2023 update included pediatric pathology risk of malignancy (ROM) for the first time since the first BRSTC publication in 2010. This study was conducted to compare the ROM of pediatric thyroid nodules at our institution to the BSRTC ROM.

Methods: A search of our laboratory information system was conducted to identify all pediatric (< 19 years old) thyroid nodules that underwent ultrasound-guided fine needle aspiration (FNA) between January 1999 and December 2013. All cytology was interpreted according to the 2023 BSRTC, wherever a descriptive diagnosis was used an appropriate BSRTC category was assigned. For each case, follow-up clinical management including surgery, repeat fine-needle aspiration FNA, or ≥ 6 months of clinical/imaging monitoring was collected. For cases that did not undergo surgery, nodules were considered benign if repeat FNA was benign, or if the nodule size remained stable or decreased in size after ≥ 6 months of clinical/imaging monitoring.

Results: We identified 176 thyroid FNA cases from 134 patients (120 females and 14 males, 7 weeks-18 years old), including 37 (21%) Non-diagnostic (ND), 119 (68%) Benign, 6 (3%) Atypia of Undetermined significance (AUS), 7 (4%) Follicular neoplasm (FN), no (0%) Suspicious for Malignancy (SM) and 7 (4%) Malignant. 12 ND, 55 Benign, 3 AUS, 4 FN, and 7 malignant cases underwent surgery and histologic examination revealed carcinoma in 10% of ND, 3% of Benign, 50% AUS, 17% of FN, and 100% of Malignant cases. Of the 95 cases that did not undergo surgery, 37 were considered benign based on follow-up FNA and/or clinical/imaging monitoring. Compared to the 2023 BSRTC pediatric ROM, the overall ROM in our cohort is within the range for each category except FN (17%) which is below the BSRTC average (50%) and below the lower limit of the range (28%). The ROM associated with AUS (50%) in our cohort is higher than the 2023 BSRTC average (28%). The ROM associated with ND (10%) and benign (3%) are slightly below the 2023 BSRTC averages of 14% and 6% respectively. The ROM for cases classified as malignant in our cohort (100%) is comparable to the 2023 BSRTC average (98%). See Table 1.

Conclusion: Pediatric thyroid ROM at our institution is within the BSRTC pediatric ROM range for each category. The non-diagnostic, benign and malignant category risk of malignancy are close to the average except FN. However, when the cases are stratified into pre and post - BSRTC the ROM is comparable to the average ROM for each category except for AUS. These findings could be attributed, at least in part, to the low number of AUS (6/176) and FN (7/176) cases.

Table 1: Thyroid FNA cytology cases by BSRTC, follow up, surgical resection and risk of malignancy (XXX)

Cytology category	Cases		Follow up (F/U)		Surgical resection	Malignant			ROM	2023 BSRTC ROM	
ALL CASES 1999 - 2013											
	n	%	No F/U	F/U	n	n	% of resected	% of F/U	NCH	Average	Range
ND	37	21	16	21	12	2	17	10	10	14	0–33
B9	119	68	39	80	55	2	4	3	3	6	0–27
AUS	6	3	2	4	3	2	67	50	50	28	11–54
FN	7	4	1	6	4	1	25	17	17	50	28–100
SM	0	0	0	0	0	0	0	0	0	81	40–100
M	7	4	0	7	7	7	100	100	100	98	86–100
Total	176	100	58	118	81	14					
PRE-BSRTC 1999 - 2009											
Category	#	%	No f/.u	F/U	n	n	% of resected	% of F/U	NCH	Average	Range
ND	28	29	13	15	10	2	20	13	13	14	0–33
B9	60	63	24	36	28	0	0	0	0	6	0–27
AUS	1	1	0	1	0	0	0	0	0	28	11–54
FN	3	3	0	3	1	0	0	0	0	50	28–100
SM	0	0	0	0	0	0	0	0	0	81	40–100
M	4	4	0	4	4	4	100	100	100	98	86–100
Total	96	100	37	59	43	6					
POST-BSRTC 2010-2013											
Category	n	%	No F/U	F/U	n	n	% of resected	% of F/U	NCH	Average	Range
ND	9	11	3	6	2	0	0	0	0	14	0–33
B9	59	74	15	44	27	2	7	5	5	6	0–27
AUS	5	6	2	3	3	2	67	67	67	28	11–54
FN	4	5	1	3	3	1	33	33	33	50	28–100
SM	0	0	0	0	0	0	0	0	0	81	40–100
M	3	4	0	3	3	3	100	100	100	98	86–100
Total	80	100	21	59	38	8					

Platform 2: Liver & Kidney Pathology (I)

1720032

Molecular profiling in pediatric hepatocellular adenomas: does it help with the diagnosis and subtyping?

Y Zhou [1], X Zhang [2], A Church [3], J Putra [3]; [1] Boston Children's Hospital, [2] Yale University School of Medicine, [3] Boston Children's Hospital

Background: Hepatocellular adenomas (HCAs) comprise less than 5% of hepatic tumors in children. While there are series of pediatric HCAs with an emphasis on clinicopathologic findings, the literature on molecular characterization remains limited. We aimed to study the utility of molecular testing in diagnosis and subtyping of pediatric HCAs.

Methods: Pediatric patients (≤21 years) with diagnosis of HCA and available liver biopsy/resection specimens were identified (2000-2023). Clinical information and characteristics of liver lesions were collected. Histologic evaluation (diagnostic confirmation and HCA subtyping) was performed by 2 pathologists, including re-review of reticulin and immunohistochemical (IHC) stains (β-catenin, LFABP, SAA/CRP, glutamine synthetase, CD34, glypican 3) when available. Targeted DNA NGS by a clinically validated panel was attempted on cases with available materials.

Results: 23 specimens from 22 patients (15F, 7M; 1-21y, median 17y) were analyzed. Relevant medical history included OCP use (n=9, 41%), obesity/hyperlipidemia/diabetes (n=6, 27%), glycogen storage disease (GSD) (n=4, 18%), malignancy (n=6, 27%), congenital anomalies (n=3, 14%), and primary immunodeficiency (n=2, 9%). 17 (77%) patients presented with multiple liver lesions and only 5 (23%) patients had solitary lesion. Diagnoses based on histology and IHC were unclassified HCA (U-HCA; n=13, 59%), inflammatory HCA (I-HCA; n=5, 23%), and HNF1 -inactivated HCA (H-HCA; n=4, 18%). 10 cases with available molecular data are summarized in table 1. Of the 5 U-HCAs, one occurring in GSD revealed a tier 2 variant in GNAS, supporting I-HCA; the other 4 cases harbored multiple tier 3 or 4 variants, and therefore, remained unclassified. HNF1A variants were detected in 2 of the 3 H-HCAs, confirming the phenotypic impression. One H-HCA occurred in the setting of FAP with a germline APC mutation. The 2 I-HCAs did not reveal variants involved in IL-6/JAK/STAT activation. Interestingly, one I-HCA with characteristic histology and IHC harbored a tier 3 HNF1A variant. This variant has not been reported in H-HCAs and the significance is uncertain. Genetic variants associated with malignant transformation (e.g., TERT promoter) were not identified in all cases.

Conclusion: U-HCAs make up more than half of cases in our pediatric cohort. Molecular testing improves subtyping in 1 of 5 U-HCAs (U-HCA to I-HCA in a patient with GSD). Signature molecular alterations are identified in the majority of H-HCAs, but not seen in I-HCAs. Molecular profiling in pediatric HCAs provides helpful clues for subtyping; further studies are warranted for cases with discordant phenotypic and molecular features.

Table 1. Clinicopathologic features and molecular alterations in ten HCAs with available molecular data

#	Sex	Age (y)	Procedure	Medical history	BMI	Focality	Size (cm)	Immunohistochemical profile	Histologic diagnosis	Molecular alteration
1	M	21	B	Hepatoblastoma s/p segmentectomy/ chemotherapy	26.1	S	1.0	Nuclear β-catenin: NEG LFABP: Loss SAA: Equivocal GS: weak/patchy CD34: no increase GPC3: NEG	H-HCA	*HNF1A* c.715G>C (p.A239P); *HNF1A* c.197dup (p.T67Dfs*29) (Tier 3)
2	F	18	B	OCP, endometriosis	34.2	M	14	Nuclear β-catenin: Equivocal LFABP: Retained SAA: NEG GS: weak/patchy CD34: no increase GPC3: NEG	U-HCA	Multiple Tier 4 variants (*CALR, FANCB, MET, setd2, WHSC1L1*)
3	F	11	B	Multiple congenital anomalies, immune deficiency, Evans syndrome, prior steroid use	17	M	4.0	Nuclear β-catenin: NEG LFABP: Loss CRP: NEG GS: NEG CD34: n/a GPC3: NEG	H-HCA	*HNF1A* c.544C>T (p.Q182*), exon 3 (Tier 2)
4	F	16	R	Prematurity, OCP	28.1	S	5.9	Nuclear β-catenin: NEG LFABP: Retained SAA: POS GS: patchy CD34: n/a GPC3: NEG	I-HCA	*BCORL1* c.2912C>G (p. A971G), exon 4; *HNF1A* c.1310-6C>T() (Tier 3) Multiple Tier 4 variants
5	F	11	R	Bilateral Wilm's tumor s/p chemotherapy/nephrectomies	25.9	S	1.7	Nuclear β-catenin: NEG LFABP: Retained CRP: POS GS: NEG CD34: n/a GPC3: n/a	U-HCA	*APC* c.6532A>G (p.T2178A), exon 16; (Tier 3) Multiple Tier 4 variants (*BCL2L12*, *RAD51C*)
6	F	17	B	16p11.2 microdeletion, multiple bilateral ovarian cysts, DM, hyperlipidemia, OCP	45.1	M	4.3	Nuclear β-catenin: NEG LFABP: Retained CRP: patchy GS: patchy CD34: n/a GPC3: n/a	U-HCA	Multiple Tier 4 variants: (*CALR*, *KMT2D*, *NOTCH3*, *PRKDC*, *PTPN14*, *WHSC1*)
7	M	18	R	GSD type 1A	N/A	M	4.7	Nuclear β-catenin: NEG LFABP: retained CRP: patchy GS: patchy CD34: n/a GPC3: n/a	U-HCA, background GSD	*GNAS* c.601C>T (p.R201C), exon 8 (Tier 2)
8	M	20	B	GSD (compound heterozygosity in SLC37A4)	28.7	M	13	Nuclear β-catenin: NEG LFABP: Retained SAA: POS GS: weak/patchy CD34: sinusoidal capillarization GPC3: n/a	I-HCA	*CHEK2* c.190G>A (p.E64K); *POLQ* c.6721C>T (p.R2241*); *TP53* c.847C>T (p.R283C) (Tier 3)
9	F	21	R	Global developmental delay, epilepsy, DM2, OCP	33.5	M	11.1	Nuclear β-catenin: NEG LFABP: Retained SAA: patchy GS: patchy CD34: n/a GPC3: NEG	U-HCA	*CDKN1A* c.145_148dup (p.N50Mfs*14), exon 2; *FAH* c.670C>T (p.H224Y), exon 9 (Tier 3)
10	F	1	R	FAP, colonic adenocarcinoma, Hepatoblastoma, ESRD, incidental finding on liver explant	16.7	M	2	Nuclear β-catenin: NEG LFABP: Loss CRP: patchy GS: patchy CD34: n/a GPC3: n/a	H-HCA	Germline *APC* pathogenic variant, c.531+1G>C; *POLE* VUS c.1366G>C (p.A456P)

F: female; M: male; y: year; B: biopsy; R: resection; S: single; M: multiple; GS: glutamine synthetase; GPC3: glypican 3; NEG: negative; POS: positive; n/a: not available.

Platform 2: Liver & Kidney Pathology (II)

1719990

Progressive Familial Intrahepatic Cholestasis Type 3 (PFIC3): Clinical, Molecular and Hepatic Findings in Children and Adolescents

M Mejia Bautista [1], H Wu [2], J Putra [3], A Perez-Atayde [3]; [1] Boston Children's Hospital, [2] Yale School of Medicine, [3] Boston Children's Hospital

Background: Progressive familial intrahepatic cholestasis (PFIC) is a heterogeneous group of rare disorders with variable progression to liver failure and cirrhosis. PFIC3 is an autosomal recessive disorder caused by mutations in ABC4 that encodes the ATP binding cassette protein MDR3; this protein transports phospholipids into the canalicular lumen to neutralize and solubilize bile salts to prevent precipitation and epithelial injury. Due to the rarity of the disease, pathology literature is limited. We aimed to describe the spectrum of clinical, molecular, and hepatic pathologic findings in a series of pediatric patients.

Methods: Pediatric patients (< 18 years) with PFIC3 diagnosis and available liver tissue were identified through a pathology database search (2003-2023). Demographic, clinical information and molecular features were documented. Histopathologic findings, including immunohistochemistry, of the liver in 7 patients were studied (Biopsies=7, Hepatectomies=0). Progressive disease was observed in 3 patients who had serial biopsies or biopsy followed by hepatectomy for liver transplantation.

Results: Seven patients (4F, 3M; age: 7m- 12y, Median 2y) were identified, and all had molecular diagnostic confirmation (NGS or PCR). Pruritus (N=3/7) was the most common initial manifestation, followed by epistaxis (N=2/7). Hepatosplenomegaly (at least borderline) was present in most of the patients (N=6/7). Most patients showed a stature and/or weight below the 25th percentile expected for their age (N=6/7). Elevated liver enzymes (AST and GGT) were noted in 6 patients. One clinically healthy, asymptomatic patient with a family history of cholestasis was diagnosed with PFIC3 by genetic testing at the age of 3.5 months. The majority of patients (6/7) showed marked fibrosis/cirrhosis (METAVIR F3-F4), including 3 patients with micronodular cirrhosis. Cholangiolar damage with sparse neutrophilic infiltrate and bile duct proliferation was present in all livers. Immunohistochemical staining for MDR3 in the livers was performed in all patients; 5 showed an absence of canalicular expression. Four patients showed previously described variants (Homozygous=3, Heterozygous =1). Three patients had novel variants: ABCB4: c.1714C>T (heterozygous), ABCB4 Allele 1: 1783 C>T (R595X) and Allele 2: 2479 G>C (A827P), and ABCB4 Allele 1: 3368 C>A (S1123Y) and Allele 2: 3416 A>G (Y1139C). Two of these patients had preserved canalicular expression of MDR3. The clinical and histological data of the 7 patients are summarized in Table 1.

Conclusion: • Children with PFIC3 are usually diagnosed at an early age; in rare cases, the diagnosis is performed later in life, likely due to mild clinical manifestations. • Advanced fibrosis and cholangiolar damage with neutrophilic infiltrate and bile duct proliferation are frequently observed; children with the diagnosis of “cryptogenic cirrhosis” should have molecular genetic studies and immunohistochemical staining for MDR3 on their livers. •

Children with PFIC3 mutation may have preserved MDR3 expression, particularly in patients with heterozygous non bona fide deleterious mutations.

Table 1. Clinical features, liver pathology, and molecular findings of patients with progressive familial intrahepatic cholestasis type 3 (PFIC3).

Category		Patient 1		Patient 2	Patient 3		Patient 4	Patient 5	Patient 6	Patient 7
Sex		F		M	F		F	M	F	M
Age at liver biopsy		2y		4 y	13y		7m	7 y	8 m	2y
Initial presentation		Epistaxis		Epistaxis and pruritus	Incidental (elevated liver enzymes)		Incidental (hepato-splenomegaly at routine clinic visit)	Pruritus	Scleral icterus and pruritus	Healthy (family history)
Hepatomegaly		Present		Present	Borderline splenomegaly		Present	Present	Present	Absent
Stools		Normal		Pale/ yellow	Normal		Normal	Normal	Acholic	Normal
Stature/Length (%ile)		25		16	47		9	12	<1	23
Weight (%ile)		37		28	75		10	3	<1	28
Lab values	**AST**	155		87	147		238	160	137	91
	GGT	266		108	311		85	150	516	368
Portal inflammation		Mild, mixed		Moderate chronic	Mild, mixed		Moderate, mixed	Minimal, lymphocytic	Mild, mixed	Mild, chronic
Cholestasis		Absent		Absent	Absent		Absent	Absent	Present	Absent
Additional findings		Cholangiolar hypertrophy and ductal metaplasia		Reactive chorangioles	Marked cholangiolar damage		Bile duct proliferation and reactive changes	Reactive ductules	Bile duct proliferation, neutrophilic cholangiolitis	Bile duct proliferation, acute pericholangitis
METAVIR		F4 (micronodular)		F3	F1-F2		F3	F4 (micronodular)	F3	F4 (micronodular)
MDR3 IHC		Retained		Absent	Retained		Absent	Absent	Absent	Absent
	ABCB4 Variants	Hetero-zygous 1783 C>T (R595X)	Hetero-zygous 2479 G>C (A827P)	Hetero-zygous c.1714C>T	Hetero-zygous 3368 C>A (S1123Y)	Hetero-zygous 3416 A>G (Y1139C)	Homozygous c.1326_1327 delinsGT	Heterozygous c.1006-1G>T	Homozygous c.1378 A>T (p.I460F)	Homozygous c.1326_1327
	Mutation	Nonsense	Missense	Nonsense	Missense	Missense	Del/Ins	Splice-site	Unknown	Del/Ins
	Reported	No	No	No	No	No	Yes	Yes	Yes	Yes
	Clinical significance	Predicted likely pathogenic	VUS (predicted likely pathogenic)	Predicted pathogenic	VUS (predicted likely pathogenic)	VUS (predicted likely pathogenic)	Pathogenic	Pathogenic	VUS	Likely pathogenic

Abbreviations: F: female, M: male, y: years, m: months, %ile: percentile, AST: aspartate aminotransferase, GGT: gamma-glutamyl transpeptidase, VUS: variant of uncertain significance, Del/Ins: deletion/insertion.

Platform 2: Liver & Kidney Pathology (III)

1722621

Histologic Porto-sinusoidal Vascular Disease is Frequent in Native Liver Biopsies of Children with Cystic Fibrosis

E Taylor [1], N Cortes Santiago [2], K Patel [2]; [1] Baylor College of Medicine, [2] Texas Children's Hospital

Background: Cystic fibrosis liver disease (CFLD) has long been postulated to be secondary to dysfunctional cystic fibrosis transmembrane conductance regulator in the apical biliary epithelium, leading to bile stasis and eventually cirrhosis with portal hypertension (PHTN). Recent studies in young adults have described obliterative portal venopathy (OPV) and noncirrhotic portal hypertension (NCPH) as the predominant pathophysiology. It is unknown if OPV develops early in childhood. We aim to systematically study native liver biopsies in children with CF with a focus to identify porto-sinusoidal vascular disease (PSVD), the new proposed terminology for a wide array of disorders manifesting as NCPH.

Methods: The pathology database at our institution was queried to identify all patients with CF who underwent liver biopsy, between 2000 and 2020. All available pathology material was studied. Electronic medical records were reviewed for clinicopathologic correlation.

Results: We identified 20 liver biopsies corresponding to 18 CF patients (15 molecularly confirmed). Age at biopsy ranged from 1 month to 16 years (median, 6.5 years) with male predominance (M:F 13:5). Significant lung disease was present in 13/18 (72%) patients, none having undergone lung transplant at the time of liver biopsy. The most frequent histologic finding was that of a cholangiopathy with cholangiolar proliferation in 14/18 (78%) of patients, usually accompanied by pericholangitis (13/18, 72%), and less frequently bile plugs (11/18, 61%). Hepatocellular/canalicular cholestasis was infrequent (35%) as was biochemical jaundice (17%). PSVD was equally common and present in 14/18 (78%) patients, including 3 of the 4 patients with clinical PHTN. Of the 10 patients with PSVD without PHTN, follow up data was available for 7, of whom 3 developed PHTN within 3 months to 9 years. Macrovesicular steatosis without lobular inflammation or ballooning was also frequently seen (10/18, 56%). Fibrosis was characteristically variable within a single biopsy with advanced fibrosis (F3-F4) seen focally in 8 (40%) biopsies, including from 2 patients with PHTN. At the conclusion of the study, 1 patient had undergone isolated lung transplant, 2 had isolated liver transplants, 1 had dual lung-liver transplant, and 6 had died at last follow up (including 2 with isolated lung and liver transplant each).

Conclusion: Male predominance in our cohort is in keeping with recent literature showing male sex as a risk factor for CFLD. PSVD changes are equally as common as cholangiopathy in native liver biopsies from pediatric CF patients. Importantly, histologic PSVD can accompany, and may precede clinical PHTN. As such, PSVD changes should be actively sought in these patients.

Platform 2: Liver & Kidney Pathology (IV)

1722637

A Retrospective Review of Borderline T-Cell-Mediated Acute Rejection Cases in Pediatric Transplanted Kidneys Using the 2019 Banff Classification

R Ryan [1], L Biederman [2], A Dasgupta [1], A Shenoy [2]; [1] Ohio State Wexner Medical Center, [2] Nationwide Children's Hospital

Background: The diagnosis of borderline acute cellular rejection (bACR) based on the criteria in the Banff Classification of Allograft Pathology is a consistently heterogenous diagnosis among pathologists. Although changes have been made to the criteria in recent iterations of the Banff classification, it remains a challenging and controversial diagnosis both pathologically and clinically. The current Banff classification requires both tubulitis and interstitial inflammation for a diagnosis of bACR.

Methods: Institutional pathology records were queried for kidney transplant biopsies with a diagnosis of borderline acute cellular rejection between 1/2005 to 08/2023. Archived slides were re-classified based on current Banff (2019) criteria by two renal pathologists. Clinical records were reviewed for demographic and follow up data.

Results: Forty-six cases were included in the study. Twenty-six (56.5%) cases continued to meet the diagnostic criteria for bACR. Of the cases that remained classified as borderline ACR, 65% (n=17) showed microvascular inflammation on biopsy consistent with antibody mediated rejection (ABMR). Twenty cases (43.5%) no longer met criteria for bACR on re-review because they did not have both components necessary for a diagnosis of bACR under the current classification. Of these patients, 55% (n=11) also exhibited microvascular inflammation consistent with a component of ABMR. Sixty-five percent of patients with ABMR and bACR had a worse serum creatinine at 1 year out (if 1 year out was not available most current serum creatinine was used). This number increased to 82.4% if the time frame were increased to the most recent available creatinine, excluding re-transplanted patients. This is compared to only 44% of patients at 1 year and 55% at most recent follow-up with a worse serum creatinine in the subgroup with only bACR without ABMR.

Conclusion: The presence of ABMR was one of the confounding variables which made classification using the Banff system more difficult to render a diagnosis of bACR. Both cases that remained bACR and no longer met bACR criteria had high rates of concurrent ABMR. Therefore, when entertaining a diagnosis of bACR, a possible concurrent ABMR should be carefully considered. Unsurprisingly, concurrent bACR and AMBR portends a worse renal prognosis. However, in keeping with the pathophysiology of ABMR, it is borne out over a longer time course.

Platform 3: Lung & Perinatal Pathology (I)

1722761

Histologic Correlates of Failed Lung Allografts in the Pediatric Population

S Gulino [1], S Vargas [2]; [1] Children's National Medical Center, [2] Boston Children's Hospital

Background: Second-time lung transplantation provides a unique opportunity to identify histologic correlates of allograft failure. Histologic phenotypes in this condition are not well-characterized in the pediatric population. We aimed to characterize the spectrum of histologic changes in pediatric patients with chronic lung allograft failure.

Methods: Patients undergoing lung resection (2005-2023) for re-transplantation in the setting of chronic graft failure were identified. Clinical data and histologic features were examined and correlated.

Results: We identified 12 patients (10 female, 4 male), initially transplanted at age 1-18 years (median, 13 years) for cystic fibrosis (n=4) and other genetic/developmental lung disease (n=8). Interval from transplant to re-transplant ranged from 7 months to 10 years (median, 30 months). Previous biopsy showed acute rejection in 7 (58%) and airway fibrosis in 7. Eleven had previous infection. Clinically suspected reason for failure included chronic rejection/bronchiolitis obliterans/chronic lung allograft dysfunction/restrictive allograft syndrome (n=11) and Pseudomonas abscess (n=1). Common histologic patterns identified in failed allografts included airway fibrosis (n= 12; Fig. 1A), acute airway inflammation (n=8; most prominent in large airways), chronic airway inflammation (n=8), parenchymal fibrosis (n=7), and pulmonary arterial intimal thickening (n=7). Parenchymal fibrosis included fibrous thickening of alveolar septa (n=7); it also manifested as confluent alveolar fibroelastosis-like effacement (n=7), often (n=3) with fibrin at its periphery (Fig 1B). Other notable findings included vascular cuffing by lymphocytes (n=3), extensive lymphoplasmacytic infiltrate consistent with nondestructive post-transplant lymphoproliferative disorder (n=1), venous fibrosis (n=1), and prominent usual-interstitial-pneumonia-like fibroblastic foci (n=1).

Conclusion: Histologic features of chronic lung allograft failure in the pediatric population consist of a spectrum of changes including the “alveolar fibroelastosis” that characterizes restrictive allograft syndrome in adults; fibrin at the periphery suggests a “leading edge” phenomenon. Airway fibrosis is a consistent feature, and acute large airway inflammation is unexpectedly prevalent. The vascular lymphocytic cuffing traditionally used to gauge cellular rejection in transbronchial biopsies is infrequent. These findings provide insights into the pathobiology of lung allograft dysfunction in children.

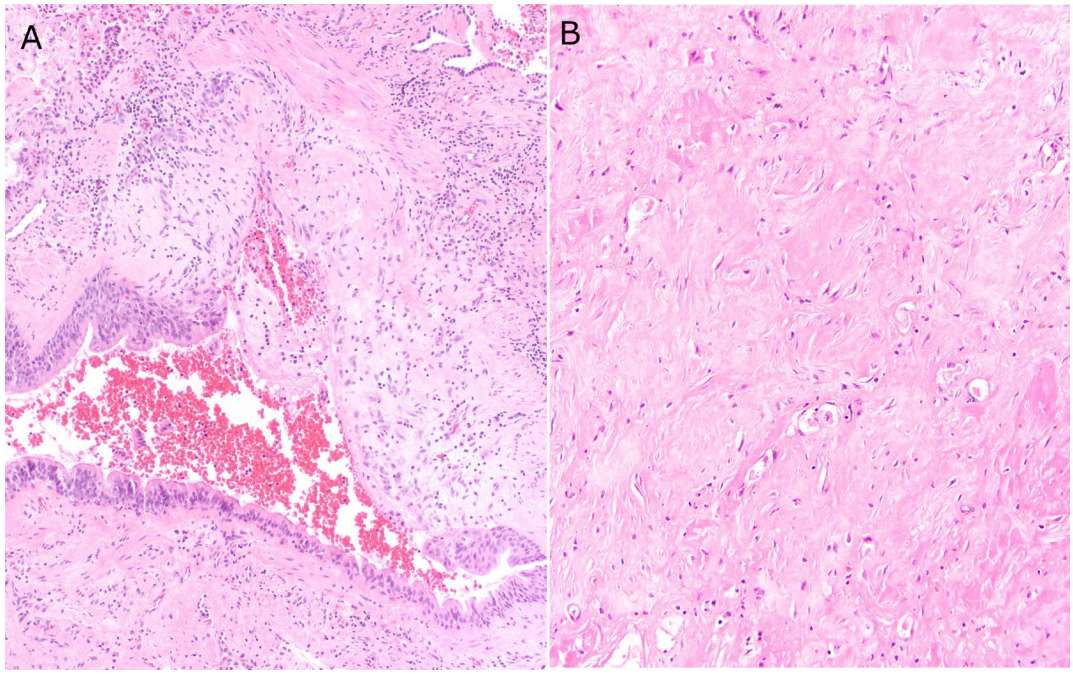
A
B

Platform 3: Lung & Perinatal Pathology (II)

1722079

Antibody-mediated Rejection in Pediatric Lung Transplantation: Unraveling Histopathological Insights

M Abdelhammed [1], D Leza-Rincon [2], D Moreno-McNeill [3], D Schady [3], S Nicholas [3], N Cortes-Santiago [3]; [1] Baylor College of Medicine, Department of Pathology & Immunology, [2] The University of Texas Health Science Center at McGovern Medical School, [3] Texas Children's Hospital, Baylor College of Medicine

Background: Diagnosing antibody-mediated rejection (AMR) post-lung transplantation remains an intricate and complex task. We aim to delineate the histopathological findings within a group of pediatric lung transplant recipients who were deemed to have at least possible AMR per ISHLT criteria at a large pediatric institution.

Methods: Institutional database was searched to identify pediatric lung transplant patients who underwent treatment for AMR between 2017-2022. Relevant demographic, clinical, and laboratory data were obtained from the electronic medical records. Diagnostic and follow up biopsy slides, including C4d immunohistochemistry were reviewed. Acute cellular rejection (ACR) and lymphocytic bronchiolitis (LB) were graded according to ISHLT criteria. The presence of eosinophils was categorized as absent (0), rare (1), or greater than rare (2). A score higher than rare was assigned if there was at least 1 eosinophil in three or more high-power fields (hpf) or if eosinophil microabscess-like clusters were observed, even if only focally. Neutrophils were graded as absent (0), less than 10/hpf (1), 10-20/hpf (2), and more than 20/hpf (3). Distribution and strength of C4d was graded as focal/diffuse and weak/strong, respectively with diffuse staining (>50%) considered positive.

Results: Nine patients met inclusion criteria. The indications for transplantation were varied and included cystic fibrosis (n=2), pulmonary veno-occlusive disease (n=2) and surfactant deficiency (n=2), among others. The median age at transplantation was 34 months (3-191 months), and median post-transplant interval at AMR was 1 month (0.2-53 months). Five patients developed AMR within 3 months of transplant. DSA were seen in all patients, 4 patients had allograft dysfunction at the time of biopsy and 2 had concomitant infection. Diagnostic biopsy findings included tissue eosinophils (any) in 5 cases, acute lung injury in 4, and septal neutrophilia (2+) in 3. Diffuse capillary C4d staining was seen in 5 patients. Two biopsies showed significant concomitant ACR (>A1) and 4 had LB. Overall, 3 patients each met ISHLT criteria for definite, probable and possible clinical (n=4) or sublinical (n=5) AMR (see Table 1). Four patients had died at the conclusion of this study, at a median post-AMR diagnosis of 1.5 months (range: 1-20 months). Three deceased patients had evidence of persistent acute lung injury with death occurring less than 3 months after AMR diagnosis.

Conclusion: Tissue eosinophils were the most common finding in pediatric patients with at least possible AMR and may be an important histologic feature. Acute lung injury is an important injury pattern in these patients and portends an unfavorable prognosis. High mortality rate in this cohort highlights the importance of accurate and timely diagnosis.

Table 1. AMR diagnosis according to ISHLT criteria

Patient	Allograft Dysfunction	DSA	Histology	C4d	Other causes excluded	Diagnostic certainty
1	+	+	+	-	-	Possible clinical AMR
2	+	+	+	+	+	Definite clinical AMR
3	+	+	+	+	-	Probable clinical AMR
4	+	+	+	-	+	Probable clinical AMR
5	-	+	+	+	+	Definite subclinical AMR
6	-	+	-	-	+	Possible subclinical AMR
7	-	+	-	-	+	Possible subclinical AMR
8	-	+	-	+	+	Probable subclinical AMR
9	-	+	+	+	+	Definite subclinical AMR

Platform 3: Lung & Perinatal Pathology (III)

1719886

Placental pathology and umbilical cord blood gene expression

L Ernst [1], A Freedman [1], A Franklin [1], L Keenan-Devlin [1], A Borders [1], A Crockett [2], G Miller [3]; [1] Endeavor Health, [2] Prisma Health, [3] Northwestern University

Background: Placental pathology is categorized into four key types: acute inflammation (AI), chronic inflammation (CI), maternal vascular malperfusion (MVM), and fetal vascular malperfusion (FVM), with each having different implications for adverse pregnancy and neonatal outcomes. Prior work has demonstrated that gene expression of placental villous tissue differs based on the type of placental pathology present. The purpose of this analysis is to build on these findings by investigating whether types of placental pathology are also associated with alterations in gene expression of umbilical cord blood.

Methods: Placental tissue and umbilical cord blood were obtained at delivery from participants in a randomized controlled trial of group prenatal care (n=1,256) and a subset were selected for analysis of umbilical cord blood gene expression (n=248). Hematoxylin and eosin-stained placental histology slides were reviewed by a single perinatal pathologist and findings were classified as AI, CI, FVM, and MVM based on Amsterdam consensus criteria. Umbilical cord blood was stored in PAXgene tubes prior to RNA extraction and mRNA profiling. Regression models were used to test associations between umbilical cord blood gene expression and types of placental pathology. Models included all four types of placental pathology, thus comparisons reflect placentas with a given type of pathology as compared to placentas without that pathology (e.g., AI vs. no AI), controlling for the other types of pathology. Models were additionally adjusted for maternal age, body mass index at the first prenatal visit, education, and smoking status. Differential expression was determined based on an adjusted p-value < 0.1 and a fold change threshold of > 1.5 or < 0.67.

Results: 235 participants had both placental pathology and umbilical cord blood gene expression. 40% of placentas had AI, 46% had CI, 29% had MVM, and 24% had FVM. 59 transcripts were differentially expressed in at least one type of pathology (Figure 1). 41 transcripts were identified as differentially expressed in AI, characterized predominantly by upregulation (40/41), including transcripts related to neutrophil activation (CD177) and cytokine signaling (SOCS3, IL18R1, OSM, IL1R2). 17 transcripts were differentially expressed in MVM, with upregulation of 7 transcripts, including those related to hypoxia (HIF3A) and cell proliferation and differentiation (FOSB, EGR1). Only one transcript was differentially expressed in FVM (upregulation of IFI27), and no transcripts were differentially expressed in CI.

Conclusion: A majority (41/59) of differentially expressed transcripts in umbilical cord blood were identified in placentas with AI as compared to those without AI. There was no overlap in the identified transcripts across types of placental pathology, indicating that pathology types may have different impacts on umbilical cord blood gene expression.

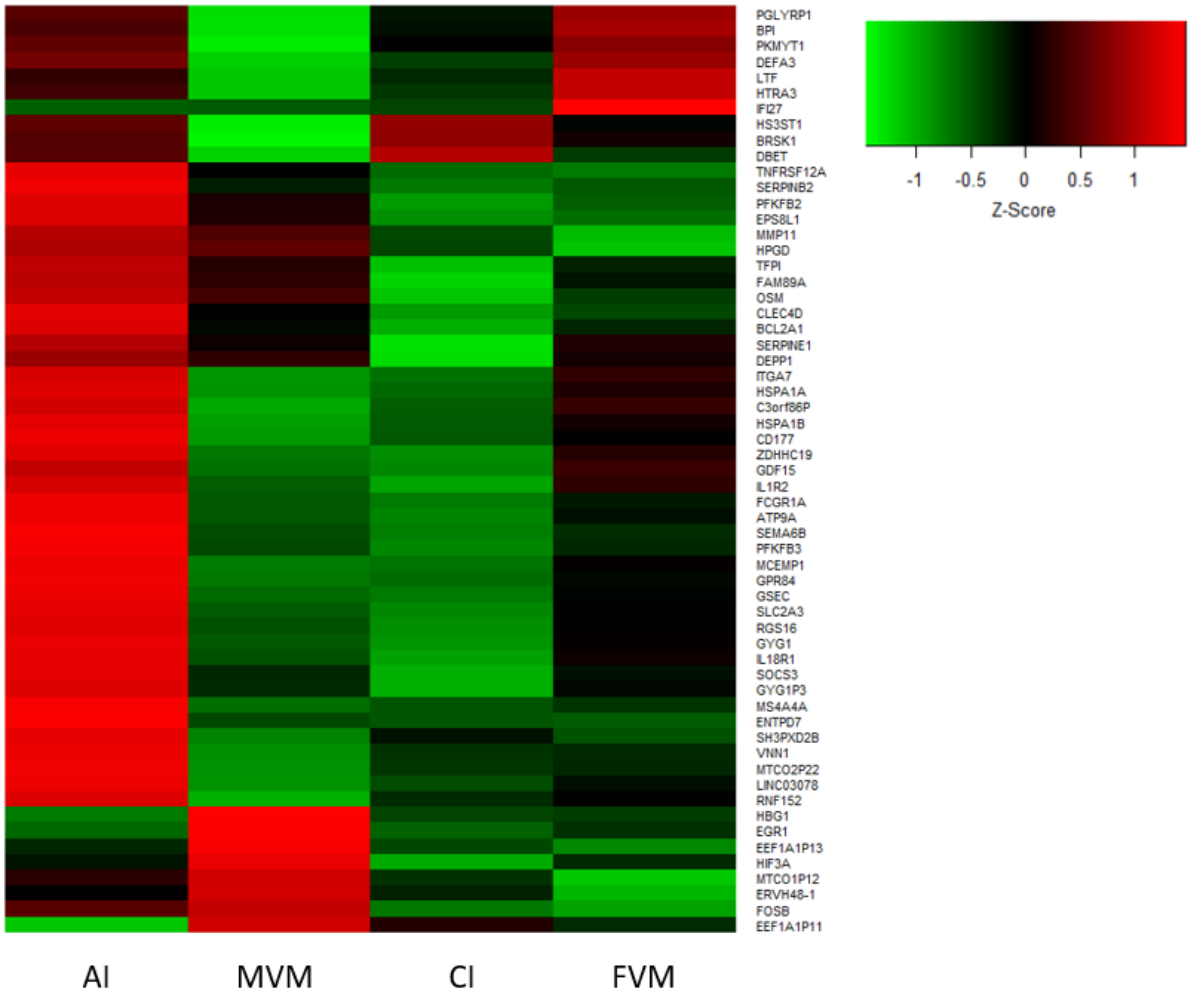
PGLYRP1
BPI
PKMYT1
DEFA3
LTF
HTRA3
IFI27
HS3ST1
BRSK1
DBET
TNFRSF12A
SERPINB2
PFKFB2
EPS8L1
MMP11
HPGD
TFPI
FAM89A
OSM
CLEC4D
BCL2A1
SERPINE1
DEPP1
ITGA7
HSPA1A
C3orf86P
HSPA1B
CD177
ZDHHC19
GDF15
IL1R2
FCGR1A
ATP9A
SEMA6B
PFKFB3
MCEMP1
GPR84
GSEC
SLC2A3
RGS16
GYG1
IL18R1
SOCS3
GYG1P3
MS4A4A
ENTPD7
SH3PXD2B
VNN1
MTCO2P22
LINC03078
RNF152
HBG1
EGR1
EEF1A1P13
HIF3A
MTCO1P12
ERVH48-1
FOSB
EEF1A1P11
-1
-0.5
0
0.5
1
Z-Score
AI
MVM
CI
FVM

Platform 3: Lung & Perinatal Pathology (IV)

1720010

Pregnancy Loss Associated with COVID-19 infection: Correlations with viral RNA in placental and fetal tissue

L Ernst A Mehreen, E Price, V Wang, S Suresh, K Mangold, L Sabatini; Endeavor Health

Background: SARS-CoV-2 infection is known to be associated with adverse perinatal outcomes including pregnancy loss. Pathologic studies have shown a SARS-CoV-2 placentitis characterized by chronic histiocytic intervillositis (CHI) with massive perivillous fibrin deposition (MPVFD) with trophoblastic necrosis in cases of fetal demise and in liveborns with vertical transmission. The purpose of this study was to compare the placental pathology and cause of death in stillbirths associated with SARS-COV-2 infection and to determine if the pathology correlates with differences in detectable presence of virus in the placental tissue and fetal organs.

Methods: Methods: We searched for fetal autopsy cases between 3/1/2020 and 12/31/2022 where the history indicated the mother tested positive for SARS-CoV-2 during her pregnancy or SARS-CoV-2 infection was suspected after autopsy. We selected representative FFPE tissue blocks from the placenta, fetal liver and fetal lung and extracted total nucleic acid from 10 micron FFPE sections using the Pin-Point Slide RNA Isolation System. We then performed a real-time RT-PCR assay for SARS-CoV-2 based on the CDC designed protocol.

Results: Results: We identified 14 autopsies representing 5.6% of 248 perinatal autopsies performed in the study period. Maternal and fetal demographic characteristics did not differ between the 5 cases with SARS-CoV-2 positive placental tissue and the 9 cases with negative placenta. The SARS-CoV-2 positive placentas exclusively demonstrated both CHI and MPVFD (100% vs 0%, $p< 0.001$) and cause of fetal death was exclusively determined to be placental insufficiency in the SARS-CoV-2 positive placentas. The cause of death in the cases with SARS-CoV-2 negative placentas included umbilical cord blood flow obstruction, hydrops fetalis, thrombosis of the umbilical vein, and termination of pregnancy for lethal anomalies or obstetric complications incompatible with life. Fetal liver was positive for SARS-CoV-2 by PCR in only 2 cases, both in the group with negative PCR for SARS-CoV-2 in the placenta and cause of death related to obstruction of fetal blood flow. The lung tissue was negative in all cases.

Conclusion: Conclusion: In this series of 14 autopsies of pregnancy loss associated with prenatal SARS-CoV-2 infection, we found a correlation between detectable virus in the placenta at the time of death and the presence of CHI and MPVFD. When virus was not detected in the placenta, this classic placental pathology was not present; however, surprisingly in two cases without detectable virus in the placenta, SARS-CoV-2 was detected in the fetal liver. These findings may be important for understanding the impact of COVID infection on neonates and children born to COVID positive mothers.


2024 SPP
SPRING MEETING
March 22 & 23, 2024
Hyatt Regency Baltimore Inner Harbor
Baltimore, Maryland

Posters

1718563

Fusion-negative Rhabdomyosarcoma: Clinical application of targeted RNA sequencing
A Glembocki G Somers; SickKids Hospital, Toronto

Background: Rhabdomyosarcoma (RMS) is the most common soft tissue sarcoma of childhood and is divided into fusion-positive RMS (alveolar rhabdomyosarcoma, ARMS) and fusion-negative RMS (often embryonal, FN-RMS) subtypes. In our center, ARMS-defining fusions were identified by performing either FISH or NanoString assays. This study aims to highlight the pathologic and molecular characteristics of a cohort of FN-RMS using a targeted NGS RNAseq assay.

Methods: Archival material from pediatric patients (n=32) diagnosed with FN-RMS from 2018 to June 2023 was retrieved. A subset of cases (12) had undergone targeted RNAseq as part of the clinical workup. The RNAseq results were reviewed for significant genetic changes and were correlated with the clinicopathological features. The study was approved by the Hospital's Research Ethics Board.

Results: Among the 32 FN RMS cohort, 20 cases underwent FISH or NanoString. Twelve cases underwent RNAseq, yielding clinically significant results, as follows: - oncogenic DICER1 mutations in two endocervical lesions (both 15-year-old girls); one presenting with heterologous cartilage formation, - pathogenic TP53 and NF1 mutations in a buttock tumour with features of anaplasia in a 10-year-old boy, - TEAD1::NCOA2 rearrangement in an arm spindle cell lesion in a 2-week-old girl, - FUS::TFCP2 rearrangement in a skull base spindle cell lesion in a 12-year-old boy, - hotspot mutations in HRASp.G13R and PIK3CAp.C420R in a thigh lesion with solid and alveolar histology in a 2-year-old boy, enabling the potential use of a MEK inhibitor, - oncogenic mutation FGFR4p.V550L in a pelvic lesion of a 6-year-old boy, - no reportable SNVs in one case (6-day-old boy, bladder), and - four cases with hotspot mutations: HRASp.G13R in an abdominal lesion in a 6-month-old boy, NRASp.Q61K with PTENp.F341V in an orbital lesion in a 12-year-old boy, NRASp.Q61K in a cheek lesion in a 10-year-old girl and KRASp.G12V in a neck lesion in a 9-year-old boy; all of them enabling the potential use of a MEK inhibitor. The last six tumors exhibited typical embryonal RMS morphology and immunophenotype.

Conclusion: In 11 of 12 patients, targeted NGS RNAseq discovered significant genetic findings that helped guide diagnosis, predict prognosis, and provide specific alterations for targetable therapy. In this small series, the utility of RNAseq has been clearly demonstrated. Future work will further characterize the genomic and epigenomic landscape of FN-RMS using total RNAseq and EPIC methylation arrays in larger numbers of tumours.

1720998

MYOD1 mutation in Pediatric Rhabdomyosarcoma

A Glembocki G Somers; SickKids Hospital, Toronto

Background: Rhabdomyosarcoma (RMS) is a soft tissue malignancy exhibiting skeletal muscle differentiation. Four histologic subtypes have been defined: alveolar, embryonal (ERMS), pleomorphic and spindle cell/sclerosing (SSRMS). The SSRMS subtype is infrequent and is histologically and biologically a heterogenous disease. Four subsets are further distinguished by recurrent molecular alterations: (1) A 'congenital/infantile' group, harboring gene fusions and showing very good prognosis, (2) An 'intraosseous spindle cell RMS' with TFCP2/NCOA2 rearrangements only described in adults, (3) A MYOD1-mutant SSRMS, and (4) A 'genetically negative group'. MYOD1-mutant SSRMS has an aggressive nature and limited responses to current therapeutic regimens, which highlights the need to identify these cases. This study aims to (1) characterize a large cohort of pediatric fusion-negative RMS (FN-RMS) to identify MYOD1 mutations; (2) to compare diagnostic test(s) for MYOD1 mutation, and (3) have a better understanding of the morphology of MYOD1-mutant RMS.

Methods: A retrospective analysis of archived paraffin-embedded tissue materials was approved by the Hospital's Research Ethics Board. All tests performed were done according to the Hospital Research Ethics Board Protocol. Archival material from pediatric patients (n=24) diagnosed with FN-RMS from 2018 to June 2021 and paratesticular FN RMS diagnosed since 1985 (n=15) was retrieved. All 39 tumors underwent MYOD1 immunostaining (clone EP212, monoclonal rabbit), followed by targeted polymerase chain reaction (PCR) amplification of the MYOD1 hot spot region (pLeu122Arg) and Sanger sequencing of the amplicon.

Results: In the series of 39 tumors, diffuse expression of MYOD1 was present in 12 tumors (defined as staining in greater than 80% of tumor cell nuclei). Two tumors harbored MYOD1 mutations by PCR. Both mutation-positive tumors also showed strong MYOD1 immunostaining. One tumor was a para-pharyngeal lesion showing sclerosing/spindle-shaped RMS histology, while the second tumor was an abdominal RMS with classical embryonal morphology.

Conclusion: This study found high immunohistochemical expression of MYOD1 protein in 12 of 39 cases of FN-RMS (31%), and two of 39 tumors harbored the MYOD1 hotspot mutation (5%). Both MYOD1 mutant-positive tumors also showed strong immunohistochemical staining, and only one showed the classical SSRMS morphology. Although the study numbers are small, this suggests that the presence of MYOD1 mutation cannot reliably be predicted on morphological or immunohistochemical grounds, and highlights the need for molecular studies to confirm the presence of the mutation.

1719661

Focused placental gross examination in the detection of decidual arteriopathy: A quality improvement project in an Academic Pediatric Hospital

A Glembocki I Gu, A Lafreniere; SickKids Hospital, Toronto

Background: Diseases of maternal vascular malperfusion (MVM) are among the most common placental conditions leading to uteroplacental insufficiency. MVM is associated with maternal conditions with a component of vascular disease, including hypertensive disorders, diabetes mellitus, and autoimmune diseases, and may have an increased risk of recurrence in future pregnancies. One study of greater than 16,000 placentas demonstrated increased frequencies of MVM in patients with pre-eclampsia (10.2%) and fetal demise (9%). Furthermore, fetal vascular malperfusion may be seen in association with or caused by MVM. Decidual arteriopathy (DA) reflects incomplete adaptation of maternal vessels for pregnancy, resulting in placental insufficiency, and is an important histologic correlate of MVM. Detection of DA requires sampling of maternal vessels from the decidua. We hypothesize that focused gross sampling of maternal vessels in the maternal disc will improve the detection of DA.

Methods: We developed a new grossing protocol (see Figure 1) incorporating focused sampling of the maternal vessels for surgical and autopsy placentas. To evaluate the impact of the protocol, we compared a prospective cohort of singleton placentas grossed using the new protocol (July 1, 2022, to June 30, 2023) to a matching cohort from the previous year. We developed a case report form (CRF) and collected appropriate, limited patient demographic information (i.e. maternal age and gravidity, gestational age). We reviewed finalized pathology reports for the presence or absence of DA. In turn, we documented the presence of other features of MVM (i.e. low placental weight, accelerated villous maturation). To evaluate the new protocol's impact, we elaborated a survey on ease of gross sampling, successful sampling of maternal vessels, perceived utility in rendering a clinical diagnosis, perceived impact on turn-around-time, and overall interest in adopting the new protocol in the future.

Results: By reviewing 47 finalized pathology reports, we found that DA was identified in 66.6% of cases where we performed wedge-sampling of the maternal surface (14/21), while only 50% of cases with no wedge-sampling showed DA (13/26).

Conclusion: Our findings support our hypothesis that, with systematic wedge sampling, we will identify DA in a significantly higher proportion of MVM cases. Future work will compare double-blinded histologic evaluation of the placenta in the detection of MVM with and without maternal wedge samples.

Received ***, labeled with patient identifiers, maternal name (***) and "***", is a singleton placenta with attached umbilical cord and membranes. The specimen is placed in formalin and photographed prior to examination. The umbilical cord measures *** cm length x *** cm diameter. The trimmed placenta weighs *** g and measures *** cm.

The membranes are [colour/semitranslucent] with a [normal, circummarginate, circumvallate] insertion; [point of rupture is *** cm from the nearest margin][cannot be determined]. The umbilical cord is [colour] and inserts [centrally, eccentrically, marginally], *** cm from the placental edge; it contains *** vessels and approximately *** coils per 10 cm.

The fetal surface is [colour/fibrin/vascularization]. The maternal surface is [colour/completeness/blood clots]. Multiple maternal vessels are identified on the maternal surface. The parenchyma is [colour/consistency/lesions].

Section code (representative)**:**

*** - umbilical cord, placental end, with fetal membranes
*** - umbilical cord, fetal end, with fetal and maternal surfaces
*** to *** - full thickness placenta; ***.
*** - maternal vessel wedge sections

1722914

Congenital Disseminated Extrarenal Rhabdoid Tumor with Placental Metastases

B AlTarawneh M Pinar, N Tatevain; Women and Infant hospital and Brown University

Background: Malignant congenital tumors of fetal origin with placental metastases are exceedingly rare, with only seven cases in the literature describing the pathologic characteristics of placental metastases in a congenital extrarenal rhabdoid tumor. We report the rare case of the disseminated congenital extrarenal rhabdoid tumor in the stillborn at 33 weeks discovered at autopsy, with pulmonary hypoplasia due to the large mediastinal nodule, together with the detailed examination of the placental metastasis.

Methods: CASE REPORT: 1635 gram male stillborn at 33 weeks of gestation by clinical estimate and 9-week ultrasound, with mild dysmorphic features, corresponding with 29-30 weeks by postmortem toe-heel measurements. Autopsy showed a right superior-posterior mediastinal mass and multiple nodules on the right visceral pleura, diaphragm, and parenchyma of the liver and kidney. Microscopic examination of the fetal necrotic and autolyzed masses revealed tumor cells with prominent nucleoli and abundant eosinophilic cytoplasm. alnog with placental examination and a panal of immunohistochemical stains.

Results: Placental examination revealed tumor cells within the villous parenchyma and stem villous vasculature, which seemed to be more viable than the tumor cells in the mediastinum. The cells show atypical round cells, anisonucleosis with eccentric nuclei, hyperchromasia, fine to coarse chromatin, prominent nucleoli and abundant eosinophilic cytoplasm with inclusions. The panel of immunohistochemical stains performed on the fetal tumor tissue and placenta favored a rhabdoid tumor. Microarray was unsuccessful due to the poor preservation of the tissue; genetic testing was declined.

Conclusion: Conclusion. Very rare published cases reported placental metastases, including description of as few as two villi placental involvement; in contrast, our case demonstrated conspicuous tumor cells within the vessels of the stem villi, as well as in the stroma/vessels of the chorionic villi.

1722204

Placental Mesenchymal Dysplasia with Unique Chromosomal Abnormality and Unusual Morphology - Case Report and Literature Review

B AlTarawneh [1], N Tatevain [1], C Carabano [2], C Claus [2], S Kostadinov [1]; [1] Women and Infant hospital and Brown University, [2] Rhode Island Hospital

Background: Placental mesenchymal dysplasia (PMD), a rare placental lesion characterized by placentomegaly, can be associated with fetal intrauterine growth restriction (IUGR), stillbirth, Beckwith-Wiedemann syndrome (BWS), some chromosomal abnormalities, or phenotypically normal fetuses. The most common karyotype associated with PMD is 46,XX. Other instances were associated with androgenic/biparental mosaicism, and aneuploidy. BWS has been related to imprinting alterations on 11p15.5, which may affect the expression of IGF-2, thus influencing growth of the fetus and placenta. Partial trisomy of 11p15.5 (two paternal copies and one maternal copy) has been found in an enlarged placenta with edematous villi. Another gene implied in the pathogenesis of this condition is Xp22.31, which is expressed as VEGF-D, related to angiogenesis and thus potentially to the mesenchymal abnormalities found in PMD and eventually in the fetus. Uniparental disomy 6, trisomy 13, aneuploidy, and Klinefelter syndrome were additionally mentioned to be associated with PMD.

Methods: We reviewed PMD case from our institution and performed a systematic review of the existing literature. Inclsion Criteria for the reveiw were diagnosis of PMD as Defined by placental pathology grossly and microscopically, description of placental morphology, immunohistochemical stain, ultrasound, findings and genetic/chromosomal alteration

Results: (Case report). 31-year-old woman (gravida 2) was referred to the clinic at 18 weeks of gestation for a placenta with vesicular lesions discovered on prenatal routine examination. An ultrasound exam at 19 weeks of gestation showed numerous vesicular lesions, which gradually augmented as the pregnancy advanced. The maternal serum β-human chorionic gonadotropin level remained in normal ranges, and she had low risk cell free fetal DNA. A live fetus was noted to have IUGR and multiple anomalies, including small thoracic circumference and enlarged heart (likely because of the small chest size), omphalocele with protruding bowel and large cystic structure (possible omphalomesenteric duct cyst), hyperechoic kidneys, and large adrenal gland. The ultrasound differential diagnosis was broad and included aneuploidy, triploidy, BWS, congenital adrenal hyperplasia, and skeletal dysplasia. Multidisciplinary medical consensus considered the termination of the pregnancy. PMD was retrospectively diagnosed after reviewing the data from ultrasound, pathological examination, and immunohistochemical stain. Chromosomal microarray analysis revealed unique chromosomal abnormality - duplication at 1p31.1

Conclusion: In this case, PMD was associated with duplication at 1p31.1, previously undescribed genetic abnormality, which adds to the existing pool of knowledge. In addition, placental slides show villous pseudoincluions, previously unreported in this entity placental histological feature.

1720009

Abnormal Paneth cell histomorphology as a distinct feature in gastrointestinal biopsies of XLAG patients

C Thoeni [1], J Bush [2]; [1] BC Children's Pathology, [2] BC Children's Pathology

Background: Patients with Bruton's (X-linked) agammaglobulinemia (XLAG), a rare disorder characterized by loss of B cells and lack of antibody production due to loss of a functioning tyrosine kinase, which regulates B-cell signaling and function, show a morphological spectrum of gastrointestinal (GI) diseases with patterns mimicking graft-versus-host disease (GVHD), or inflammatory bowel disease (IBD), but often lacking some of the diagnostic features of those disease entities within the GI tract. We aimed in this study to investigate GI biopsy samples of XLAG patients to further analyze histological patterns specifically seen in XLAG guts and not in others such as patients with GVHD or IBD.

Methods: Three patients were identified who underwent endoscopic evaluation and had a confirmed diagnosis of XLAG by genetic sequencing that harbored a loss of function mutation within the Bruton's tyrosine kinase. Hematoxylin and Eosin stained sections of GI biopsies of XLAG patients were compared to biopsies of five patients with GVHD, five patients with Crohn's disease, and five patients with ulcerative colitis. Ethics approval was obtained from the XXX Research Ethics Board.

Results: Table 1 summarizes the comparison of histomorphological features of XLAG patients with either GVHD or IBD patients. In our XLAG patients, there were abnormal patterns within Paneth cells of the duodenum, ileum, cecum and ascending colon, which was not evident in GVHD or IBD patients. These abnormalities included Paneth cells which were either decreased in number or showed an abnormal distribution or secretion pattern in XLAG when compared to non-XLAG patients.

Conclusion: XLAG patients can present with a spectrum of histomorphological features within the gastrointestinal tract, which may make it difficult to differentiate from other more common mimickers such as IBD and GVHD. Our preliminary investigation found that in addition to some relative lack of features, such as the absence of chronic architectural changes, eosinophilia, and plasma cells, that assessment of Paneth cells may be advantageous. XLAG may be higher on the differential when Paneth cells are reduced in number or found higher in the crypt epithelium. Future plans include evaluating a larger cohort to confirm these findings in a multi-institutional study.

Histopathology feature	XLAG	GVHD	IBD
Lack of plasma cells	yes	no	no
Eosinophilia	no	no	yes
Architectural distortion	no	yes	yes
Paneth cell abnormalities (abnormal distribution/decrease in number)	yes	no	no

1706614

Type 3 CPAM or Hyperplasia of an Immature Lobe? A Mechanistic Approach to the Controversial Solid Fetal Lung Lesion

E Nelson [1], M Takeda [2], F Xu [3], M Li [2], R Linn [2], J Pogoriler [2]; [1] The Children's Hospital of Philadelphia, [2] Children's Hospital of Philadelphia and University of Pennsylvania, [3] Children's Hospital of Philadelphia

Background: The diagnosis of solid (Stocker type 3) congenital pulmonary airway malformation (CPAM) is contentious, with some authors believing that they represent hyperplasia of an immature lobe related to obstruction during development. Given recent publications suggesting a mechanistic approach to classification independent of cyst size, we hypothesized that a solid fetal morphology could arise from either obstruction or KRAS mosaic mutation. We further sought to determine whether previously described post-natal histologic features were also applicable to this age group. To address this challenge, we evaluated 2nd trimester autopsies with solid lung lesions and compared them to post-natal resections.

Methods: Clinical histories and gross descriptions were obtained via review of records. Gelatin-dye perfusion via the trachea was used in one case to evaluate airway patency. In two cases, regions of interest were enriched via macrodissection of FFPE, DNA was isolated, and exon 2 of KRAS was amplified. PCR products were Sanger sequenced and analyzed using Mutation Surveyor. Histologic features of each case were evaluated by two pathologists.

Results: One case was received partially fragmented but with a largely intact lung lesion that showed irregularly branching airways with papillary projections, multiple foci of mucinous cell clusters, and intervening small glandular spaces lined by epithelium with prominent subnuclear vacuoles (Figure 1). This case was positive for KRAS p.G12V. A second intact 2nd trimester fetus had bronchial obstruction confirmed by exclusion of tracheal dye. This case was negative for KRAS codon 12 mutation and showed evenly sized minute “cysts” without mucinous cells (Figure 1). Two additional 2nd trimester fetal autopsy cases (20 and 24 weeks gestation) with bronchial atresia affecting mainstem bronchi were identified in the archives. Both cases were primarily composed of lung parenchyma with enlarged and simplified alveolar structures, with one showing very focal type 2 CPAM changes with minute cysts. A third surgical pneumonectomy at 26 weeks gestation had similar histologic features, although operative reports were not available to confirm atresia. None of the 5 cases showed mucostasis or significant foamy macrophages.

Conclusion: 2nd trimester lung lesions with a grossly solid morphology may arise either due

to obstruction or to KRAS mutation. In intact autopsies, bronchial obstruction can be easily confirmed at autopsy by instillation of a gelatin/dye mixture via the trachea. 2nd trimester cases of obstruction have morphology similar to previously published post-natal cases; however, in contrast to term infants, mucostasis and foamy macrophages are not reliably present to assist in the recognition of an obstructive etiology. Solid fetal lung lesions due to KRAS mosaic mutation are histologically similar to cases of KRAS -related type 1 and/or 3 surgical resections and may contain markedly immature types of epithelium. Mucinous cell clusters were only seen with KRAS mutation.

1706701

Current Utilization of Molecular Testing in the Pediatric Pathology Setting: A Survey by the SPP Practice Committee

C Gestrich [1], S Besmer [2], P Kreiger [3], D Lopez-Terrada [4], L Surrey [3], A Church [5]; [1] UPMC Children's Hospital of Pittsburgh, [2] Saint Louis University, [3] Children's Hospital of Philadelphia, [4] Texas Children's Hospital, [5] Boston Children's Hospital

Background: The increased accessibility and utilization of molecular testing including next-generation sequencing (NGS) has impacted the practice of pediatric pathology, with diagnostic, prognostic, and therapeutic implications for our patients. This survey is the first to describe the utilization of molecular testing in the routine practice of pediatric pathology for the care of children with known or suspected neoplasms.

Methods: The Society of Pediatric Pathology Practice Committee distributed a survey to our membership asking 25 questions about training, practice setting, molecular ordering practices and barriers to testing.

Results: Seventy-five pathologists responded to the survey. Seventy-three respondents (97%) are currently ordering molecular tests, including FISH (99%), NGS DNA panels (80%), and NGS RNA fusion panels (69%). 83% reported that they are ordering molecular testing more than they were five years ago. 42% reported that their institution has restrictions on ordering molecular testing; 51% have test utilization guidelines. Respondents report that NGS has been helpful for diagnosis (91%), prognosis (69%) and treatment selection (90%) for their patients. Most pathologists feel comfortable with the ordering process (82%) and understanding the results (74-77%). 42% would order tests more often if they were confident that the costs would be covered by insurance or their government health program.

Conclusion: The survey provides valuable insight into the current use of molecular testing in the care of children with known or suspected solid tumors. The majority of pathologists reported that they are increasingly using a variety of molecular techniques, with increased use over time, and that NGS is useful. These results highlight a variety of barriers to molecular testing, including cost, insurance coverage, turn-around time, limitations of available assays (including limited coverage of pediatric-specific alterations), and difficultly in determining the most appropriate test to order. This data may be useful in supporting pediatric pathologists in their practice.

1707061

Pulmonary pathologic manifestations of DOCK8 deficiency

M Zhao [1], J Gaffin [2], E Lee [2], J Chou [2], S Vargas [2]; [1] Brigham and Women's Hospital, [2] Boston Children's Hospital

Background: DOCK8 immunodeficiency is an autosomal recessive hyperimmunoglobulin E syndrome characterized by DOCK8 mutations; clinical manifestations include frequent/recurrent respiratory tract infections. Pathologic findings in DOCK8 deficiency have not been systematically studied. Herein, we characterize features of this syndrome in pulmonary samples.

Methods: We searched clinical and pathology databases to identify patients with genetically confirmed DOCK8 deficiency treated at our institution from 2010-2023. All pulmonary pathology samples except those acquired post bone marrow transplant were included. Archival material was examined. In 6 BAL samples for which cytopathology slides were not available for review, cytopathology reports were relied upon.

Results: BAL material included 22 specimens (sampled at ages 2-17) from 11 patients (9 female, 2 male). In 3 patients, BAL showed innumerable prominent granular cytoplasmic inclusions, bright red on H&E stain, within airway epithelial cells; despite absent correlative microbiologic findings, electron microscopic examination (available in 1 of these 3) showed extensive intra-epithelial viral particles. Other BAL findings included ciliocytophthoria (3/22 specimens), degenerative (5/22) or reactive (3/22) respiratory epithelial cells, phagocytized bacteria (2/22), and abundant multinucleate giant cells (1/22). In differential counts, predominating cells were most often macrophages (11/20 evaluable samples) or neutrophils (6/20). Eosinophilia (≥10%) and lymphocytosis (>5%) were seen in 6/20 and 1/20 evaluable samples. Surgical pathology material included 6 lung specimens (sampled at ages 6-13) from 4 patients. One core biopsy showed EBV-associated lymphoproliferative disease, 1 transbronchial biopsy showed lymphocytic bronchitis, 1 wedge biopsy showed CMV pneumonitis and lymphocytic bronchitis, another showed increased intra-alveolar macrophages and interspersed eosinophils, and 2 resections (1 lobectomy, 1 lingulectomy) showed chronic airway disease with severe bronchiectasis.

Conclusion: Our study characterizes detailed pulmonary pathology features in patients affected by DOCK8 deficiency, many attributable to viral infection. The findings provide insight into pathologic susceptibilities in DOCK8 deficiency and furthermore demonstrate that pathologic examination, including BAL, contributes pertinent diagnostic information in this disorder.

1709283

Novel SMC1A Variant Mutation in Cornelia de Lange Syndrome: Gastrointestinal/Pulmonary Sequelae Repair Complications

D Dirnberger D Dirnberger BS, Y Zhang MD PhD, T Chen MD. PhD., R Olson, E Cochran MD., J Fanburg-Smith, MD.; Penn State Health, Penn State Children Hospital

Background: Cornelia de Lange Syndrome (CdLS) is a rare, multisystem genetic disorder characterized by midline craniofacial dysmorphism and upper axial developmental delay. CdLS complications are complex that can be repaired and compatible with young adult survival. This study observes repair sequela for a unique molecular subtype of CdLS, resulting in unfortunate early demise. SMC1A (structural maintenance of chromosomes 1A) encodes cohesion complex regulatory proteins, is often c.586C>T (p.Arg196Cys) and one of the genes associated with CdLS.

Methods: A nine-month-old female with CdLS presents for post-mortem examination with unknown final etiology of demise.

Results: During a restricted internal chest and abdominal post-mortem examination, full spectrum of classic external features of CdLS were observed, including midface hypoplasia, short stature, hypertrichosis, synophrys, micrognathia, long eyelashes, upturned nose, down turned mouth, long philtrum, and thin upper lip. Upon internal examination, congenital diaphragmatic hernia repair caused multiple adhesions above and below the diaphragm, with a fixed diaphragm, resulting in observed gastrointestinal obstruction/volvulus as well as restricted cardiopulmonary movement, pulmonary hypoplasia, aspiration pneumonia, and evidence for sepsis. Features of disseminated intravascular coagulation including clots and hemorrhages were observed, resulting in final demise. Phenotypic and mutational analysis revealed a unique subtype of CdLS: X-linked pathogenic 100% gene coverage heterozygous de novo SMC1A (NM_006306.4, chr X:53432776) c.1658G>T, pGly533Val in exon 10 mutation associated with a full spectrum of phenotypic features.

Conclusion: This study reports a de novo p.Gly533Val exon 10 SMC1A variant that has not previously reported in CdLS and is associated with a full spectrum of phenotypic syndromic sequela. Adhesion complications after repair of gastrointestinal/pulmonary syndromic features led to early demise. Understanding the specific features, mutation, and possible complications associated with this unique SMC1A variant of CdLS may improve outcome and lifespan in patients with CdLS.

1709458

An Early Presentation of Pediatric Desmoplastic Small Round Cell Tumor with Heterologous Features and Systematic Review of the Literature

R Azimi [1], C Brathwaite [2], L dehner [3], M fader [4], F Pedroso [4], E Nayman [5]; [1] Mount Sinai Medical Center, [2] Nicklaus Children's Hospital, Miami, FL, [3] V. Ackerman Laboratory of Surgical Pathology, Washington University Medical Center, St. Louis, MO, [4] Nicklaus Children's Hospital, [5] Florida International University

Background: Background: Desmoplastic small round cell tumor (DSRCT) has an incidence of 0.3 cases/million with 76% occurring in those 10 to 39 years-old. They typically present late with widespread peritoneal seeding. Overall survival (OS) rates are dismal. We present an incidentally found DSRCT with heterologous elements and provide a systematic review of the literature.

Methods: Design: Our patient was a 13-year-old female who presented with acute abdominal pain. Imaging and laparoscopy revealed an 11.0 x 9.2 x 13.4 cm torsed fallopian cyst and an incidental 2 cm multicystic tumor attached to the pelvic floor, which were excised. Histologically, the tumor had a variably myxoid stroma with nests and cords of small cells accompanied by glands lined by a ciliated epithelium (Figure 1). Some of the glands had papillary projections that mimicked a sex-cord stromal, teratomatous, or mixed Müllerian tumor. Desmoplasia was not observed. On IHC (Table 1), the nests co-expressed desmin and keratin (Figure 2). WT1-C was not available. The ciliated epithelial cysts were ER+/PR+. The tumor was positive for EWSR1 rearrangement and EWSR1-WT1 fusion. The sample matched for DSRCT by the Sarcoma DNA Methylation Classifier. Repeat exploratory laparotomy was performed 2 months later, which revealed numerous DSRCT nodules < 1 cm throughout the pelvis. There was pronounced desmoplasia in these nodules. Vincristine was started and will be followed by total resection of any residual disease and hyperthermic intraperitoneal chemotherapy. All DSRCTs indexed in PubMed from 2018 – July 2023 (n = 66) were reviewed, along with 40 cases from 1999 – 2018.

Results: Results: 106 cases of DSRCT were systematically reviewed. The mean age of presentation was 24 years-old with a 3:2 male predominance. Patients mostly presented with widespread intra-abdominal seeding, but several extra-abdominal sites were also reported. Calculated OS curves were 90.5%, 83.1%, 41.7%, and 9.7% at 6 months, 1, 3, and 5 years, respectively. In contrast to the usual DSRCT, our case was found incidentally, and had a nested pattern with ER+/PR+ ciliated cysts, mimicking a sex-cord stromal, teratomatous, or mixed Müllerian tumor. This made the diagnosis more challenging.

Conclusion: Conclusion: To our knowledge, this is the first report of a DSRCT with heterologous, ciliated glands. Co-expression of desmin and keratin should prompt consideration of DSRCT. Although OS rates are low, diagnosis at an early stage followed by aggressive, multimodal therapy provides the best chance of cure.

Figure 1.

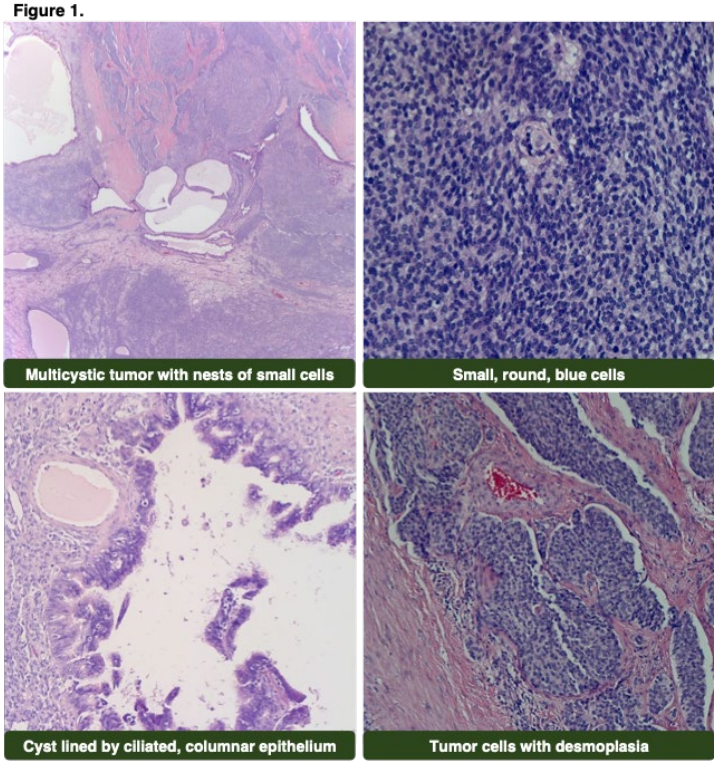

Figure 2.

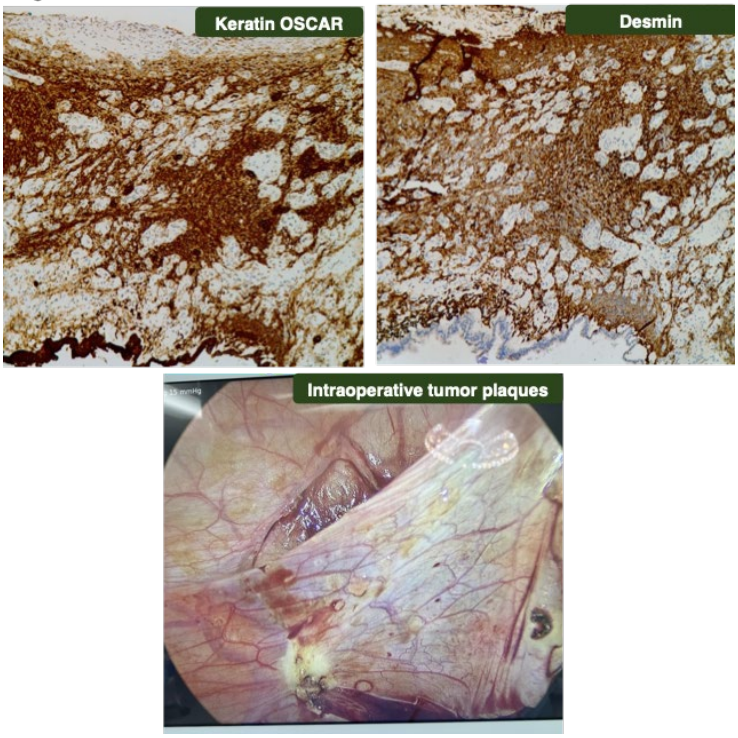

Table 1. Immunohistochemical Stains		
Positive	**Focally Positive**	**Negative**
EMA, Desmin, OSCAR Keratin, AR, ER, PR (cyst lining)**, INI1 retained**	**CD56** (tumor cell nests cords)**, Vimentin** (tumor cell nests, stroma, cyst lining)	**AFP, hCG, OCT3/4, Glypican, HPL, D-240, LH, FSH, GATA3, SALL4, CEA, Myoglobin, MyoD1, GLUT1, SOX10, TLE1, BCL2, CD99, SS18-SSX, CDX2, Chromogranin, Synaptophysin, TTF1, Napsin A, INSM1, Inhibin, Calretinin, SF1, Beta-Catenin**

Platform 1: Pediatric Malignancies
I

1709565

E Cadherin/CD34 Double Immunostaining in Placental Diagnosis
J Stanek; Cincinnati Children's Hospital

Background: Fetal vascular malperfusion (FVM) is one of the four major patterns of placental injury that may be responsible for complicated fetal or neonatal conditions. By highlighting endothelial fragmentation, the double E cadherin/CD34 immunostain (34ECI) highlights distal villous endothelial fragmentation of recent FVM that is not seen either grossly or on hematoxylin-eosin (H&E) stained sections.

Methods: We routinely perform the stain on a grossly unremarkable placental section in our population of placentas predominantly from pregnancies with mass-forming fetal anomalies and umbilical cord complications at high risk for FVM.

Results: 34ECI can upgrade the FVM, and/or reveal the temporal heterogeneity of FVM lesions (Figure), both useful in establishing the cause of fetal death or poor neonatal condition. It also highlights the basement membranes of trophoblastic cells and helpful in diagnosis of distal villous hypomaturity. It can distinguish mineralized stem occluding thrombi from mineralized trophoblastic pseudo inclusions, the first outlined by CD34, the second by E-cadherin, thus helping to differentiate FVM from placental aneuploidies. The CD34 component helps in timing placental infarctions, allows for more precise diagnosis of chorangiosis and diagnosis of the combined hypoxic/FVM lesions. The E cadherin component helps in the diagnosis of trophoblastic lesions of shallow placental implantation featuring the increased number of extravillous trophoblasts in placental membranes and chorionic disc.

Conclusion: 34ECI is very useful for placental diagnosis. However, the significance of focal villous endothelial fragmentation associated with chronic villitis of unknown etiology, chorangioma/chorangiomatosis, intervillous thrombi, Kline hematomas, massive perivillous fibrinoid deposition, and isolated focal perivillous fibrinoid deposition still needs clarification.

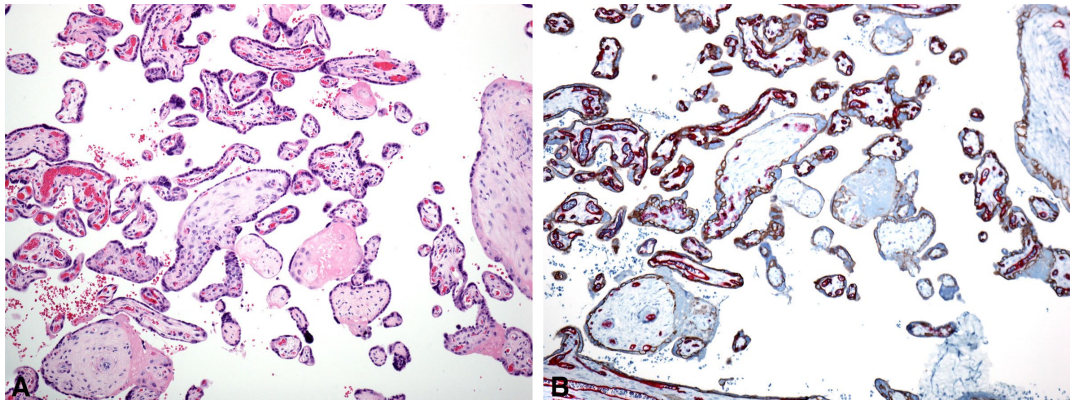

1709791

Pathologist review of pediatric peripheral blood smears is an overutilized order: the XXX) experience

N Roy [1], A Herrera [2], L Xue [2], M Jimeno [2], C Lee [2], J Medina [2], T Desiree [2], S McCarthy [2], M Deardorff [2], E Leung [2], S Chamala [2], M O'Gorman [2], A Kovach [2]; [1] Department of Pathology and Laboratory Medicine, Children's Hospital Los Angeles, [2] Children's Hospital Los Angeles

Background: Pathologist review of peripheral blood smears can be a valuable adjunct to automated and manual review of complete blood counts (CBC). In the modern era of robust laboratory automation systems, clinician requested peripheral blood smear review (PBSR) has low clinical yield (Beckman et al, Diagnostic Pathology 2020: 23% with potentially added clinical value) and may be curtailed without clinical consequence (Lollie et al, J Clin Pathol 2021: reduction in orders by 42.5% through policy change and education). The value of a PBSR given today's detailed parameter reporting by CBC analyzers and manual review has not been addressed in a primarily pediatric setting, and at our Children's Hospital, criteria for PBSR are currently undefined.

Methods: The XXX Laboratory Stewardship Program retrospectively reviewed consecutive PBSRs over a 7-month period in an effort to ascertain its clinical value. Patient demographics, ordering providers' department, clinical question, and CBC values were gathered.

Results: The study included 299 PBSR orders (average 9 orders/week) from patients (0 - 35.0 years of age, median 6.2 years) in intensive care (25.5%), other inpatient units (41.1%), and outpatient (33.4%) settings. Submitted indications for PBSR included evaluation for hemolysis (19.4%), "malignancy" (11.7%), bi-lineage / pancytopenia (10.4%) or isolated quantitative and/or qualitative abnormality of red blood cells (15.1%), leukocytes (12.2%), or platelets (5.4%). In 25.8% of cases, no specific clinical indication was included with order, among which 52.8% had CBC values within normal limits. No morphologic findings not already reported on the CBC were identified in any case (0 out of 299). Among patients with a reported concern for hemolysis, 44.8% were not concurrently anemic. Among orders requesting evaluation for "malignancy," no smear reviews identified abnormal cell types.

Conclusion: These data support the conclusion that PBSR in our primarily pediatric practice setting is overutilized, similar to that reported in primarily adult practice settings. Education of ordering providers about the capabilities of modern CBC analyzers and technologist expertise at manual review may help appropriately curtail inappropriate orders. Future directions of this study include correlation with documented clinical acknowledgement and/or action based on the PBSR pathology report, and educational and informatics initiatives to direct clinician effort towards effective interpretation of existing detailed CBC data.

1714259

A Rare and Challenging Case of Poorly Differentiated Pulmonary Adenocarcinoma with an EML4::ALK Fusion in a Pediatric Patient

Background: ALK-positive non-small cell lung cancers (NSCLC) represent a minority of malignant pediatric neoplasms. Identification of ALK alterations are critically important for determining additional therapeutic options for patients with this diagnosis. We report a rare, challenging case of poorly differentiated pulmonary adenocarcinoma with EML4::ALK fusion in a 14-year-old patient.

Methods: We reviewed available clinical, radiologic, pathologic, immunohistochemical (IHC) and molecular data related to this case.

Results: A 14-year-old male presented to the emergency department with persistent back pain following a sports related injury, recent fevers, and night sweats. MRI demonstrated two 3-4 cm masses in the left hilum and subcarinal region, as well as abnormal marrow signal in the T1 vertebral body. A CT chest confirmed multiple enlarged mediastinal lymph nodes. Lymph node biopsy showed small cohesive clusters of eosinophilic cells with hyperchromatic and enlarged nuclei and prominent nucleoli. Extensive IHC workup of the tumor cells revealed CAM 5.2 positive staining. ALK (D5F3) stain was diffusely positive. The tumor cells were negative for germ cell tumor markers (SALL-4 and OCT3/4), hematologic markers (MUM-1, PAX-5, CD30 and CD45), and skeletal muscle markers (Desmin, Myogenin, and MyoD1). Additional stains, including p63, ERG, calretinin, WT1, SMA, S100, and NUT were all negative. INI-1, BRG-1, and BAP-1 were retained. Subsequent CT of the abdomen and pelvis showed numerous hypoattenuating subpleural and hepatic nodules. A PET CT demonstrated hypermetabolic activity within the identified nodules and enlarged lymph nodes. A hepatic nodule was then biopsied, showing the same morphology as the original lymph node biopsy. A TTF-1 stain was performed which was diffusely positive within the tumor cells, suggestive of pulmonary origin. Again, ALK overexpression was noted. FISH subsequently identified an ALK rearrangement. Molecular studies revealed an EML4::ALK fusion. Additional studies revealed a TP53 mutation, low tumor mutation burden, and microsatellite stability. The patient initially had an excellent response to the ALK inhibitor alectinib, but unfortunately had disease progression a few months after therapy initiation.

Conclusion: Primary lung cancers are exceptionally rare in the pediatric population, representing 0.2% of all pediatric malignancies. ALK-driven tumors make up approximately 3-7% of overall NSCLC cases, with a tendency to be found in younger patients. While rare, it should be considered on the differential diagnosis in adolescents presenting with unknown primaries with widespread metastases and malignant epithelioid morphology. With the advent of newer precision drug therapies, ALK rearrangements are now successfully targetable with ALK inhibitors. Given the rarity of these tumors, there is limited data for ALK inhibitor use in pediatric patients; however, successful disease response has been reported in this

population. Identification of a targetable ALK rearrangement in pulmonary adenocarcinoma in a pediatric patient is critical for offering additional therapeutic options.

1714297

Sclerosing Angiomatoid Nodular Transformation (SANT) of the Spleen in the Pediatric Population: Report of a Case, Feasibility of Diagnosis on Core Needle Biopsy, with Comprehensive Review of Literature (2004-2024)

J Salise D Grier, C Talbott, O Lopez-Nunez, J Stanek, S Szabo; Cincinnati Children's Hospital Medical Center

Background: Sclerosing angiomatoid nodular transformation (SANT) is a non-neoplastic, mass-forming vascular lesion of the spleen, first reported in 2004. While a benign condition of uncertain pathogenesis, it mimics a variety of neoplasms, often necessitating splenectomy. Only rare cases are diagnosed less-invasively, by biopsy, which is more challenging given the broad differentials. Most are reported in adults, with few anecdotal pediatric cases. We aim to (1) expand the literature with a case of pediatric SANT, (2) widen the differential pitfalls to granulomatous disorders of the spleen and (3) demonstrate feasibility of diagnosis on a core needle biopsy (CNB).

Methods: Clinical and pathologic data were obtained retrospectively from medical records, with IRB approval. Tabulated data from our literature review is provided, focusing on the 14 pediatric cases identified (among the 426 cases reported in PubMed.)

Results: Our 10-year-old female patient presented with splenomegaly, failure to thrive, vomiting, anemia, elevated ESR (107) and CRP (2.3). US, CT and MRI revealed a 6.8 cm solid splenic mass, with perisplenic lymphadenopathy. Differentials included lymphoma, sarcoma and inflammatory myofibroblastic tumor (IMT). An initial CNB of the spleen favored a granulomatous disease, with negative stains for fungi and AFB. SANT was diagnosed on repeat CNB, with micronodular pattern of concentric sclerosing fibrosis, formed around remnant foci of vascularized ("angiomatoid') splenic parenchyma – a mimicker of granulomatous disease on H&E. The central "angiomatoid" component can be highlighted on CD34 and CD31, with remnant CD8+ Littoral cells. The background (SMA-positive) myofibroblastic/fibroblastic proliferation may ultimately be obliterative and a mimicker of IMT on a small CNB. With progressive sclerosis, an associated (lympho)plasmacytic infiltrate may evoke the differential of an inflammatory or an immune dysregulatory process, notably IgG4-Related Disease. Given chronic fatigue and anemia, eventually splenectomy was pursued for our patient. Morcellated fragments amounted to 158.5 grams, with histology as previously. The patient remains recurrence free 5 months later. A comprehensive review of the literature of SANT (2004-2024, PubMed) yielded a total of 14 pediatric cases (8 female and 6 male) between ages of 9 weeks - 17 years (median of 8.5 years). Presenting symptoms were abdominal pain, splenomegaly and incidental splenic mass (in 8, 3 and 3 patients, respectively,) with diagnoses on partial or total splenectomy (in 4 and 10 patients, respectively) and without recurrence on follow-up.

Conclusion: SANT of the spleen is a benign entity, non-infectious and with low risk of bleeding. With review of presentations in children and of differentials, we demonstrate that a reliable pathologic diagnosis is feasible on core needle biopsies. This in turn affords non-

invasive management or less-invasive surgery (morcellation), for better outcome.

1715970

Gastrointestinal Histology in Early-onset IBD and Behcet's-like disease due to RELA haploinsufficiency

S Chen [1], R Abraham [2], S Akoghlanian [2], B Boyle [2], K Lecerf [2], R Maltz [2], V Prasad [3], V Sivaraman [2]; [1] Nationwide Children's Hospital/The Ohio State Universty, [2] Nationwide Children's Hospital, [3] Nationwide Children's Hospital/ The Ohio State University

Background: RELA haploinsufficiency is caused by pathogenic heterozygous variants in RELA, encoding the p65 subunit of the canonical pathway of NFkB. Key clinical manifestations include an autoinflammatory phenotype with mucocutaneous ulcers and variable degrees of combined immunodeficiency including Behcet's-like disease and early-onset inflammatory bowel disease. Up to one third of patients present with gastrointestinal symptoms but the histopathology has not been well described. We identified and describe a cohort of patients diagnosed and treated at a tertiary care children's hospital.

Methods: Gastrointestinal biopsies and reports from patients with known RELA pathogenic variants were reviewed along with the demographic and clinical information.

Results: Six adult and pediatric patients were identified (4 males, 2 females including one parent; age at diagnosis: 11 months - 20 years). Two-thirds of patients presented with diarrhea. All patients had colonoscopy with a subset having upper endoscopy. Each patient had at least one set of biopsies with half having more than one biopsy time point. At colonoscopy, all but one patient had colonic inflammation (edema, erythema, friability). Histologic review showed esophageal eosinophilia (range: 13-22 intraepithelial eosinophils/hpf) in 50%, focal active ileitis in 50% and chronic, mild to moderately active colitis in 33% of patients. Microgranulomas were identified in at least one set of biopsies in patients with active colitis. Figure 1 highlights endoscopic and histologic images. Treatment included colchicine, TNF inhibitors, and IL-1 inhibitors.

Conclusion: RELA haploinsufficiency is a new immune dysregulation disorder that can manifest as early-onset IBD and Behcet's-like disease. The phenotype is variable and includes recurrent oral and genital ulcers, uveitis, episcleritis, and GI manifestations including diarrhea and failure to thrive. Histopathologic features overlap with chronic, active ileocolonic inflammation as well as microgranulomas seen in classic inflammatory bowel disease, causing potential diagnostic pitfalls. Correlation with clinical and immunological phenotype and laboratory findings is vital for targeted therapy and genetic counseling.

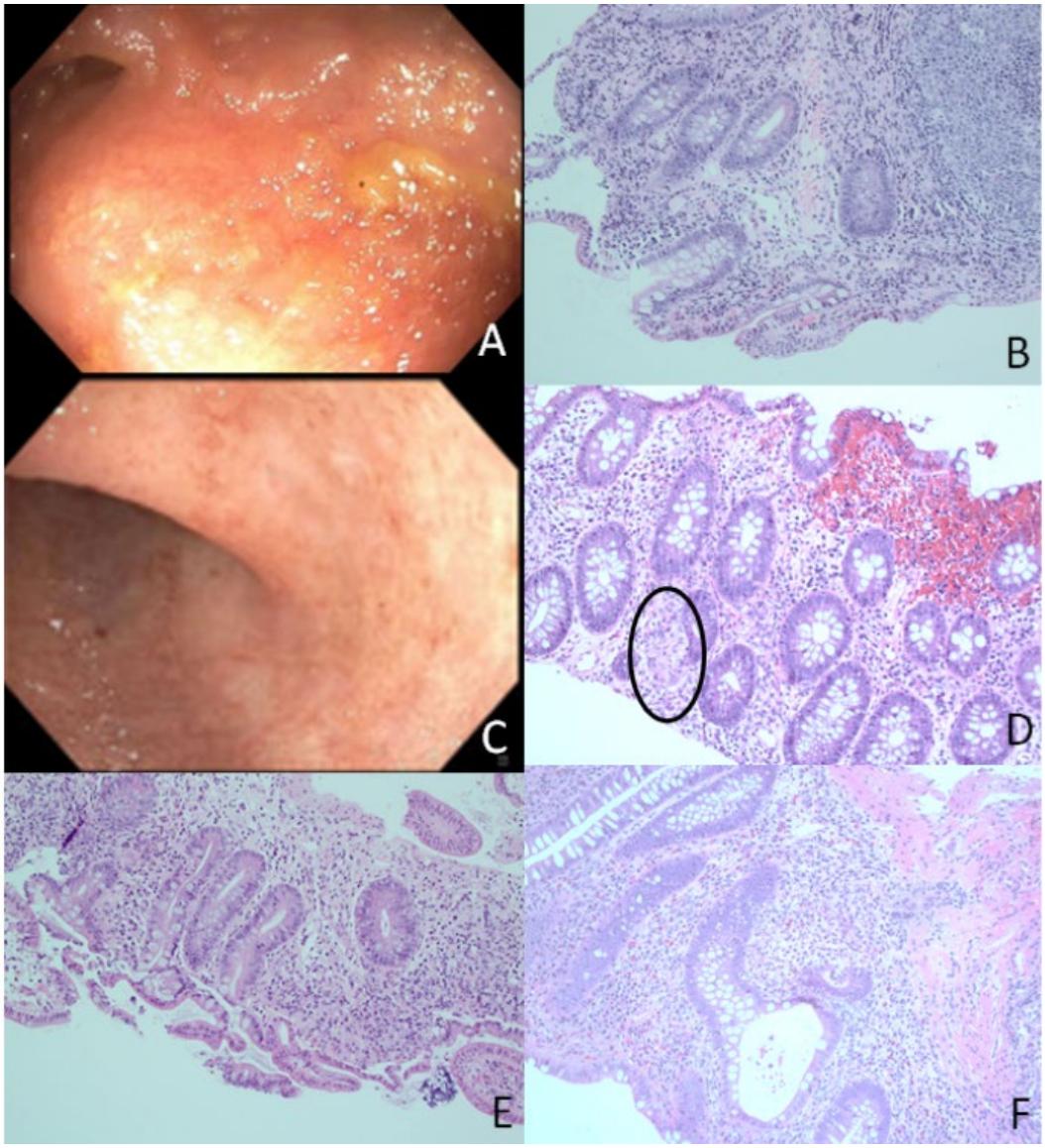
A
B
C
D
E
F

1718881

ROR gamma T-positive lymphocytes in colon of children with inflammatory bowel disease

F Mohammadi [1], P Kapur [2], V Singh [2]; [1] Childrens Medical Center, Dallas, [2] UT Southwestern Medical Center

Background: Ulcerative colitis (UC) and Crohn's disease (CD) are major subtypes of inflammatory bowel disease (IBD). TH1 cells play a prominent role in the gut inflammation of CD. In contrast, TH2 cells are more prominent in UC. TH17 cells, another class of T helper cells, were identified as significant players in the pathogenesis of CD. Most studies of TH17 have utilized flow cytometry techniques to assess TH17 cells in the human intestine. Histological studies of TH17 cells in children affected with IBD are rare. Retinoic acid-related orphan receptor Gamma T(ROR-γt) is expressed by the nuclei of TH17 helper T cells and has been used to identify TH17 cells. In this study we present the use of ROR-γt immunohistochemistry as a tool to evaluate TH17 cells in colonic mucosa.

Methods: A retrospective search of our hospital's pathology records was conducted for cases of inflammatory bowel disease that had surgical resection of colon and diagnosed with either UC or CD. We identified 15 consecutive cases from each of the two diagnostic categories and selected one representative formalin-fixed paraffin embedded tissue block for obtaining unstained slides. The 30 cases comprised the study group. We selected 10 cases of colonic resection done for non-IBD diagnoses, which comprised the control group. One representative formalin-fixed paraffin embedded tissue block was identified for cutting unstained slides from the ten control cases. Immunohistochemical staining for ROR-□t was performed following the automated immunostainer protocol on the unstained slides of all 40 samples. Positively staining cells were counted in 3 high power fields (40x objective) of the mucosal lamina propria in area of maximal density.

Results: The age of the subjects in the study group ranged from 3 to 17 years with a mean of 13.3. In colons affected with CD the ROR-γt immunohistochemistry showed a range of 5 to 28 cells per high power field (hpf) with a mean of 13.2 +/- 2.8 per hpf. The colons affected with UC had a range of 5 to 23 cells hpf with a mean of 14.5 +/- 3.3 hpf. Colons from controls had a range of 3 to 20 cells per hpf with a mean of 8.2 +/- 4.2 per hpf. When UC and CD cases were combined, the colons from all IBD cases had a range of 5 to 28 hpf with a mean of 13.8 +/- 2.1 per hpf. A t-test showed a statistically significant difference ($P=0.004$; significance threshold $P< 0.05$) between IBD cases versus the controls, but there was no statistically significant difference between the UC and CD colons.

Conclusion: TH17 cells, as identified by nuclear staining for ROR-γt, are increased in the colonic mucosa of children with IBD. Interestingly, we found that the TH17 cells are increased not only in CD but also UC. Since the number of infiltrating TH17 cells are not different between CD and UC, the ROR-γt immunohistochemistry may not be helpful as a diagnostic aid to discriminate between the 2 entities.

1719374

Injury or Lividity: A Case of Fetal Demise with Maceration Mimicking Traumatic Subgaleal Hemorrhage

A Cardenas O Aisagbonhi, M Parast, J Hu; UC San Diego Health

Background: Subgaleal bleeding in neonates is typically associated with injury secondary to assisted vaginal delivery, particularly when vacuum or forceps assistance is employed. While subgaleal hemorrhage (SGH) is often considered life-threatening in newborns, the implications in the context of intrauterine fetal demise and especially in the absence of significant trauma remain unclear. There is currently no literature that links SGH with external cephalic version, and there is just one case report published that suggests the leakage of autolytic fluid may present as blood in the subgaleal space.

Methods: This case study investigates the autopsy findings of an intrauterine fetal demise at 38 weeks, to a secundigravida in her mid-thirties, hours after a successful, uncomplicated, external cephalic version. Fetal monitoring one hour after the procedure was reassuring. The following morning, there were no heart tones appreciated on ultrasound and reduced fetal movement overnight. The fetus was delivered via unassisted vaginal delivery less than 24 hours after demise.

Results: Autopsy revealed a grossly normal infant, with small (15-25 mL) apparent subgaleal hematoma. Despite initial concerns of the possibility of head trauma secondary to external cephalic version completed the day prior, placental pathology was more revealing. Examination demonstrated a small placenta with decidual vasculopathy and infarcts consistent with features of maternal vascular malperfusion. Additionally, the placenta was found to have a marginal cord insertion, dilated chorionic plate vessels, early vascular mural thrombus and multifocal avascular villi (fetal thrombotic vasculopathy) supporting a diagnosis of fetal vascular malperfusion. These findings suggest a combination of uteroplacental insufficiency and partial intermittent cord blood flow obstruction as the most likely cause of demise. We opine that the cranial hematoma most likely represents post-mortem leakage of autolytic fluid into the subgaleal space given the small fluid volume, cephalic position of the fetus, cephalic lividity, and the absence of evident trauma to the calvarium or surrounding soft tissue. Further, if the hematoma were sustained in antemortem period, the small volume of hemorrhage would be insufficient to cause demise on its own.

Conclusion: This case highlights the uncertainty surrounding the significance of fetal cranial bleeding at autopsy. While it is important to recognize signs of trauma at autopsy, it is equally important to consider the possibility of maceration related changes. Our case demonstrates the uncommon and seldom published phenomenon of postmortem autolytic fluid leakage that may mimic traumatic SGH and ultimately underlines the importance of cautious interpretation, particularly in the context of relatively minor findings.

		No molecular driver identified	*SRF* fusion	*TP53* biallelic inactivation
N		23/33 (70%)	5/33 (15%)	5/33 (15%)
Molecular Findings	Recurrent alterations	None	*SRF* fusion partners: -*NCOA2* (3/5) -*C3orf62* (1/5) -Unknown (1/5)	-Rearrangement with TP53 intron 1 breakpoint (n=3) -Two copy deletion of TP53 (n=2)
	Other molecular findings	-Flat copy number profile -*SDHA* nonsense mutation (n=1) -*FOX::PLAG1* fusion (n=1)	-Flat copy number profile	-Genomic instability with recurrent copy number alterations -2 copy deletion of *RB1* (n=1) -2 copy deletion of *CDKN2A/B* (n=1)
Clinical Features	Mean age years (range)	9 (11 m-18)	8 (2-14)	11 (6-17)
	Sex (M:F)	10:13 (0.8)	4:1 (4.0)	3:2 (1.5)
	Site	Extremities (9/23) Trunk (7/23) Head/neck (4/23) Pelvis (2/23) Intraabdominal (1/23)	Extremities (4/5) Head/neck (1/5)	Extremities (3/5) Trunk (2/5)
	Depth	Subcutaneous (10/23) Deep (12/23) Unknown (1/23)	Subcutaneous (3/5) Deep (1/5) Unknown (1/5)	Subcutaneous (4/5) Unknown (1/5)
	Mean size in cm (range)	4.1 (0.8-18.2)	5.6 (1.0-10)	5.0 (3-10)
	Local recurrence (mean follow-up interval)	4/11 (63 months) No follow-up data: 12/23	0/2 (38 months) No follow-up data: 3/5	0/1 (6 months) No follow-up data: 4/5
Histologic Features	Cyto-morphology	Ovoid to spindled Epithelioid features (6/23) Rhabdoid features (1/23)	Spindled	Spindled and pleomorphic Epithelioid features (1/5)
	Pleomorphism	Mild (16/23) Moderate (7/23)	Mild (3/5) Moderate (2/5)	Severe (5/5)
	Necrosis	3/23	0/5	0/5
	Calcifications	9/23	4/5	0/5
	Mitotic count per 10 HPF (SD)	5 (4.6)	2.6 (2.6)	15 (7.7)

1719879

Prevention of Neonatal Death Secondary to Disseminated Herpes Simplex Virus: Can Molecular Analysis of Placenta Aid in Early Detection?

L Ernst [1], E Price [2], L Sabatini [1], S Suresh [1], A Franklin [1]; [1] Endeavor Health, [2] Endeavor Heath

Background: Perinatal herpes simplex virus (HSV) infections can have deadly consequences for the newborn and early detection can be key to live-saving treatment. Placental histologic findings may be mild and/or non-specific; therefore, using placental pathology to decrease time to treatment has proven challenging. We hypothesize it may be possible to detect placental HSV DNA which ascended into the uterine cavity prior to delivery in perinatally-acquired infections and sought to determine retrospectively if molecular evidence of HSV was present in the placenta.

Methods: Autopsy and placental pathology reports for cases of neonatal demise associated with disseminated HSV infection were reviewed. We extracted genomic DNA from 10 micron FFPE sections of the umbilical cord and extraplacental membranes using the Pin-Point Slide Isolation System. PCR was performed using the Simplexa HSV1 & 2 Direct assay validated in-house for use with FFPE tissue.

Results: We identified the autopsies of two neonates with disseminated HSV infection who died within 2 weeks of birth. The first was a female born vaginally at 33 weeks gestation to a 30 year old female who developed acute chorioamnionitis and fetal tachycardia. Examination of the placenta was completed on day of life 4 and confirmed acute chorioamnionitis, acute umbilical phlebitis, acute umbilical arteritis, and funisitis, as well as low grade maternal and fetal vascular changes. Special stains were negative for bacterial and fungal organisms. For the first few days of life, the infant had respiratory distress and feeding problems thought to be related to aspiration, but she ultimately developed apnea and acidosis, concerning for sepsis. Lumbar puncture was positive for HSV-2 on day 9 of life, and she died the next day. Molecular studies were negative for HSV-1&2 in the membranes and umbilical cord. The second was a male born vaginally at 34 weeks gestation to a 19-year-old female who presented with preterm labor. Pathology examination was completed on day of life 2 demonstrating a small for gestational age placenta with sparse acute subchorionitis, chronic deciduitis with plasma cells, and changes consistent with maternal vascular malperfusion. The infant was initially stable; however, 2 days after delivery he was noted to be grunting with nasal flaring and tachypnea. The infant continued to have worsening respiratory distress and developed hyperbilirubinemia, thrombocytopenia and metabolic acidosis. Despite maximal efforts, he died on day 6 of life. Molecular studies of the membranes and umbilical cord were both positive for HSV-2.

Conclusion: It is possible to identify HSV by molecular analysis of FFPE umbilical cord tissue and/or extraplacental membranes even in placentas with no specific histologic evidence of HSV. While this is unlikely to be cost effective screening method, use of molecular methods to diagnosis perinatal HSV infection in the placenta requires more investigation, as

earlier diagnosis of HSV infection may be life saving.

1720014

Challenges and Limitations in the Histopathologic Evaluation of Pediatric Acute Liver Failure: An Illustrative Case

P Jafari A Hutchison, L Osnis, R Hunter, A Husain, V Tesic, C Lehmann, J Hart; University of Chicago Medicine

Background: Pediatric acute liver failure (PALF) carries significant morbidity and mortality and raises a vexingly broad differential that includes infection, toxin/drug-mediated injury, and autoimmune processes. Liver biopsy is central to work-up, but diagnostic value may be limited by morphologic overlap between entities, underscoring the importance of close clinical correlation. Etiology remains unclear in at least 30% of cases. Here, we present a case of PALF that highlights these unique challenges and diagnostic considerations. A previously healthy 7-year-old presented with ~3 days of jaundice, nausea, and vomiting. History was notable for recent travel to Belize and negative for medication use or known toxin ingestions. Immunizations were complete for age except for hepatitis A (1 of 2 doses). Total bilirubin was 12.8 mg/dL (conjugated, 9.2 mg/dL), alkaline phosphatase 668 U/L, AST 1526 U/L, ALT 1142 U/L, GGT 60 U/L, and INR 2.4. Despite supportive care, liver chemistries remained elevated; the patient was ultimately listed for liver transplant. Before transplant could be performed, the patient developed profound coagulopathy complicated by subarachnoid hemorrhage and died (admission day 9).

Methods: Liver biopsy (admission day 3) and complete autopsy were performed. Histologic findings were reviewed.

Results: Biopsy (Fig 1A-H) revealed striking lobular disarray, centrilobular dropout, patchy hepatocyte swelling, brisk mixed sinusoidal inflammation, and scattered acidophil bodies. No viral inclusions were identified. There was no cholestasis or steatosis. Portal tracts contained a CD8-rich lymphocytic infiltrate but plasma cells were not conspicuous and interface activity was not appreciated. EBER RNA ISH showed nonspecific reactivity. Overall, an infectious or toxin-mediated process was favored. The findings were not compatible with Wilson disease or autoimmune hepatitis. Autopsy revealed massive panacinar necrosis of the liver (Fig 1I) without identifiable viral inclusions. Clinical work-up included anti-liver/kidney microsomal, mitochondrial, and smooth-muscle antibodies; serum copper and ceruloplasmin; alpha-1-antitrypsin phenotype (MM); serum acetaminophen; stool/respiratory pathogen multiplex PCR panels (e.g., adenovirus); and serology for hepatitis A-E, Leptospira, Strongyloides, HIV, syphilis, and non-hepatotropic viruses (HSV-1/2, VZV, EBV, West Nile virus, measles, dengue, chikungunya, Zika). Stool panel was positive for C. difficile toxin and STEC. All other results were negative or normal/noncontributory. The case was discussed in consultation with the CDC Infectious Diseases Pathology Branch, which performed PCR testing for yellow fever, dengue, and adenovirus and IHC for adenovirus and HSV-1/2 on autopsy liver tissue (all results negative).

Conclusion: Liver biopsy may yield important insights in PALF by determining the pattern of liver injury and narrowing the differential. An etiology may nonetheless remain elusive. A

CD8-rich T-cell infiltrate, as seen here, has been previously described in cases of indeterminate PALF, suggestive of immune dysregulation in this population; further investigation is necessary. Close clinicopathologic correlation is essential in these potentially devastating cases.

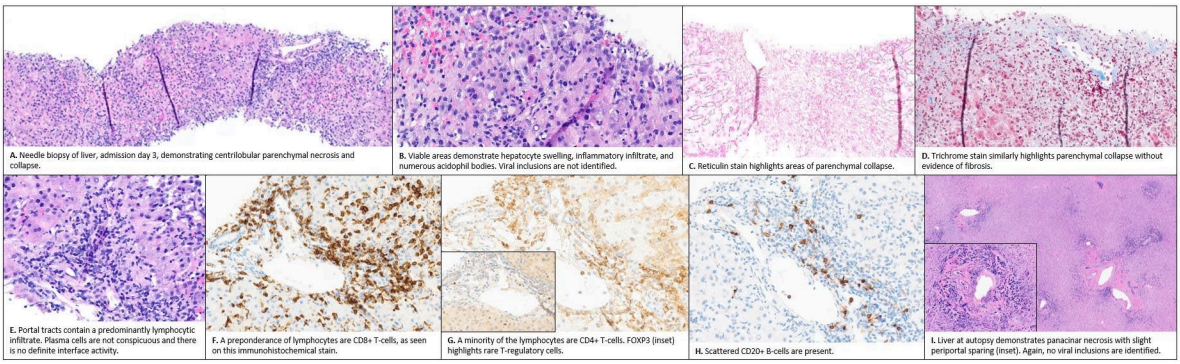

1720346

Morphological and clinical findings in placentas and newborns with a history of tobacco, alcohol and other substance abuse during pregnancy

M Franco O Canon, M Delgado, M Olaya-C, J Uribe, M Velasquez, H Mendez; Pontificia Universidad Javeriana

Background: During pregnancy, exposure to substances in the environment affects both the placenta and the fetus. Abundant documentation confirms the effects that alcohol, opioid, cannabis and other substance consumption has on pregnancy. Smoking produces risk factors for small for gestational age newborns (SGA), intrauterine growth restriction (IUGR), preterm- labor, hypertensive disorders of pregnancy, stillbirth, miscarriage, placental abruption and adult morbidities. In this paper, we examine gross and microscopic placental features in women who reported exposure to tobacco, alcohol, or other psychoactive substances, and, subsequently, seek to establish their link to maternal and neonatal outcomes.

Methods: We examined 706 placentas, from a high complexity hospital. Placental processing and analysis had complied with international standards. All procedures were approved by the Ethics Committee of our institutions. Clinical variables of interest included general information on the mother, and on pregestational diseases and pregnancy complications; additionally, we included descriptions of newborn clinical conditions and complications. We collected gross and microscopic findings on the placentas such abnormal placental weight, umbilical cord abnormalities and histological alterations. We collected data on mothers who had admitted tobacco, alcohol or other psychoactive substance exposure. The hypothesis test to determine P-value was null hypothesis (H0), OR=1 and the two-tailed alternative hypothesis (Ha), different from OR=1. Variables with $P< 0.05$ were highlighted in the final statistical results. We carried out statistical analysis with Stata 14.2.

Results: Out of the 706 placentas received, 4.8% of mothers(34) admitted to having consumed some type of toxic substance during pregnancy; of these, 37.5% used tobacco, 16.6% psychoactive substances and 12.5% alcohol. The most commonly pre-existing maternal conditions were obesity (20.3%) and hypothyroidism (2.9%). During pregnancy, prevalent complications included amniotic infection(32.3%), urinary tract infection (14.5%) and hypertensive disorders of pregnancy(14.5%). In newborns, respiratory distress syndrome: p0; OR 8.53(CI 3.82-19.04), congenital heart defects: p0; OR 14.56(CI 5.31-40) and as expected, IUGR: p0.006; OR 5.4(CI 1.9-15.3). Among exposed women, placentas exhibited weight above percentile 90: p0.00; OR 26.81(CI 12.5-57.6), true knots (p0.04; OR 8.07(CI 1.47-42.1)) and SUA (p0.02; OR 5.81(CI 1.54-22)). In our histological analysis, a statistically significant association was presented by vascular ectasia (p0.05; OR 2.13 (CI 1.03-4.41)) and thrombosis (p0.00; OR 5.33(CI 2.3-12.4).

Conclusion: It is a long-established fact that exposure to toxins during pregnancy affects the placenta, and consequently the fetus. We have described precise lesions that occur in the histological interaction in the placenta. These descriptions concur not only with the etiology and what we know about modifications in the microenvironment but help explain the poor

fetal and neonatal outcomes affected by FVM. Tobacco, alcohol and other psychoactive substance abuse persists as the main modifiable behavioral pattern that can lead to fetal and neonatal risks, and the placenta as a witness.

1720397

Pediatric high-grade sarcoma with nuclear anaplasia leading to a diagnosis of Malignant peripheral nerve sheath tumor, Neurofibromatosis Type 1, and somatic TP53 mutation.

P Rungsiprakarn [1], L Surrey [2], S MacFarland [2], L Schwartz [3], M Santi [2], P Kreiger [2]; [1] Children's Hospital of Philadelphia, [2] Children's Hospital of Philadelphia and Perelman School of Medicine, University of Pennsylvania, Philadelphia, Pennsylvania, [3] St. Joseph's Children's Hospital, Paterson, New Jersey

Background: Malignant peripheral nerve sheath tumor (MPNST) is a rare soft tissue sarcoma arising sporadically, post-radiation, or in the setting of Neurofibromatosis type 1 (NF1). MPNST is rare in the pediatric population but most commonly occurs in older children with known NF1. Both NF1-associated and sporadic MPNSTs can show multiple somatic genomic alterations, such as mutations/deletions in NF1, CDKN2A/B, PRC2, TP53. We report a 3-year-old child with a high-grade sarcoma with nuclear anaplasia leading to a diagnosis of MPNST in the setting of previously undiagnosed NF1 and somatic TP53 mutation.

Methods: Clinical information was obtained from chart review and the clinical team. Pathology reports, genomic reports, and histologic sections were reviewed.

Results: A 3-year-old male presented with intermittent right leg pain, limping, and palpable abdominal mass, found to have a 13 cm right intra-abdominal mass. Additional clinical examination revealed multiple café au lait spots and axillary freckling. He underwent surgical biopsy and histological examination revealed a proliferation of spindled to round tumor cells with a sheet-like to fascicular growth pattern and areas of background myxoid change. Tumor cells showed hyperchromatic nuclei with occasional macronucleoli and scant eosinophilic to vesicular cytoplasm. Scattered nuclear anaplasia was apparent along with frequent mitotic figures and focal necrosis (< 5%). An extensive immunohistochemistry panel was inconclusive. Tumor cells were negative for ALK, bcl2, CD163, CD31, CD34, chromogranin, CK7, desmin, erg, inhibin, MSA, myoD1, myogenin, MUC4, Nkx2.2, NTRK, S100, SATB2, SMA, SOX10, synaptophysin, and TLE1, with retained nuclear staining for INI1 and ATRX. Positive immunostaining was seen for CD56, FLI1, O13 (patchy perinuclear dot-like), p16 (patchy), p53 (diffuse strong nuclear), and WT-1 (cytoplasmic). H3K27me3 showed partial loss. Molecular testing of the tumor showed NF1 (NM_001042492.3) c.1185+2T>A(p.?) with evidence of copy neutral loss of heterozygosity, a TP53 variant (NM_000546.6) c.843C>A (p.Asp281Glu), and MYC amplification. Paired germline testing revealed the same pathogenic (heterozygous) variant in NF1, consistent with a diagnosis of NF1; no TP53 variant was identified in the blood. Given NF1 diagnosis and histologic and molecular features, he was started on chemotherapy and radiation per MPNST treatment protocol.

Conclusion: This case highlights the importance of including MPNST in the differential diagnosis of a high-grade sarcoma, even in a young patient without a pre-existing diagnosis of NF1. In addition, the nuclear anaplasia seen in this tumor correlated with somatic TP53

mutation.

1720691

Supratentorial brain tumor harboring EWSR1::PLAGL1 fusion with heterogeneous morphology – a diagnostic pitfall

V Singh N Uddin, V Rajaram; UT Southwestern Medical Center

Background: Tumors of the central nervous system harboring fusion of EWSR1 gene with different gene partners have been frequently described. Furthermore, PLAGL1 gene fusion with different gene partners has been observed in rare supratentorial brain tumors. However, EWSR1::PLAGL1 fusion has only been rarely observed in brain tumors, which are remarkably disparate such as atypical teratoid rhabdoid tumor, ependymoma and a glioneuronal tumor. The protein product of the PLAGL1 gene encodes a zinc finger protein, which acts as a transcription factor and in glioblastomas, may facilitate tumor progression. We report a brain tumor with EWSR1::PLAGL1 fusion that on the intraoperative consultation presented with a papillary appearance and on permanent sections revealed heterogeneous morphology.

Methods: A 2-year-old girl presented to our hospital with acute onset of limping and difficulty walking. Diagnostic imaging revealed a large right frontal mass with involvement of the central gray structures as well as protrusion into lateral ventricle. Microscopic examination of the resected tumor with H&E and immunohistochemical stains was performed. Ancillary techniques included Next-Generation Sequencing (NGS)with fusion analysis for a panel of genes and karyotyping of tumor tissue.

Results: During intraoperative examination of the tumor, a portion of this specimen was received that presented a predominantly papillary pattern resembling a papillary ependymoma or a choroid plexus tumor. The permanent sections of the resected tumor comprised a focally infiltrative cellular neoplasm with a heterogeneous appearance. A significant portion of the tumor consisted of primitive appearing cells that were small to medium sized with scant to moderate cytoplasm and nuclei that varied from round to ovoid appearance. There was a basophilic staining mucoid, extracellular, matrix in these areas. There were frequent apoptotic cells, and 12 mitoses per 10 high-power fields. In another area, the tumor had a papillary appearance with cells featuring low nuclear to cytoplasmic ratio, and abundant eosinophilic cytoplasm. The tumor cells in these areas had a perivascular distribution with stout processes that tapered to rest on blood vessels. Mitotic figures are rare in these papillary areas. In a third pattern of morphology, the tumor cells had a neuroblastoma-like appearance with cells resembling immature ganglion cells, and areas of necrosis with scattered calcifications. Finally, in rare foci, the tumor cells had a rhabdoid appearance. Immunohistochemical staining revealed retention of INI 1, patchy positive staining with GFAP, synaptophysin, occasional cells with positive cytokeratin AE1/AE3 and dot like staining with EMA in a few tumor cells. P53 immunostain was positive in 50% of tumor cells. The karyotype of the tumor was 46,XX,t(6;22)(q25;q13). The NGS based fusion panel revealed EWSR1::PLAGL1 fusion.

Conclusion: The histologic, immunohistochemical, and molecular findings were consistent

with a high-grade neuroepithelial/embryonal tumor of the supratentorial region of brain. Based on the rare reported brain tumors with EWSR1::PLAGL1 fusion, and the case presented here, we bring to attention the varied morphology of brain tumors with EWSR1::PLAGL1 fusion.

1720714

Histopathologic Spectrum of Native Liver in Methylmalonic and Propionic Acidemias

Y Zhou [1], T Al Doheyan [2], X Zhang [3], I Gonzalez [4], A Perez-Atayde [5], L Teot [5], S Vargas [5], K Patel [6], J Putra [5]; [1] Boston Children's Hospital, [2] Baylor Collage of Medicine, [3] Yale University School of Medicine, [4] Indiana University, [5] Boston Children's Hospital, [6] Texas Children's Hospital

Background: Methylmalonic acidemia (MMA) and propionic acidemia (PA) are 2 major inherited inborn errors of organic acid metabolism affecting multiple organ systems with variable clinical course. Patients usually develop long-term multisystem complications requiring liver transplantation (LT). Despite the significant role of liver in organic acid metabolism, literature on liver pathology in MMA/PA is limited. We aimed to characterize the histologic and ultrastructural findings in the native liver of patients with MMA/PA.

Methods: Pathology databases of 4 institutions were queried to identify native liver tissue on patients with MMA/PA. Available pathology materials including electron microscopy (EM) images were studied. Electronic medical records were reviewed for clinicopathologic correlation.

Results: We identified 25 liver explants (12 MMA, 13 PA) and 1 autopsy (PA) specimen from 26 patients (M:F = 1:1) over a period of 23 years. The age at LT/autopsy ranged from 5m-24y (median 8y). Genetics were available in 16 patients, revealing MUT or MMAB mutation in MMA (n=10) and PCCA or PCCB mutation in PA (n=6). Clinicopathologic features of MMA and PA are summarized in Table 1. The majority of patients (18/25, 72%) showed elevated liver enzymes at the time of LT/autopsy, and half (12/24, 50%) had abnormal liver ultrasound findings (heterogeneous echogenicity (n=7), hepatomegaly (n=6), hypoechoic lesion (n=1)). Overall, the most frequent liver pathology was megamitochondria (n=19, 73%), followed by mild portal inflammation (n=10, 38%), glycogenated hepatocyte nuclei (n=9, 35%), mild lobular inflammation (n=5, 19%), macrovesicular steatosis (n=5, 19%), and hepatocyte cytoplasmic clearing (n=4, 15%). Rare histologic findings included canalicular/hepatocellular cholestasis (1 PA), mild ductular proliferation (1 PA), extramedullary hematopoiesis (1 PA), Ito cell hyperplasia (1 PA), and mild anisonucleosis (1 MMA). Mild portal/periportal fibrosis was identified in only 2 patients with MMA (17%) and 2 patients with PA (15%). Histologic parameters between the 2 groups showed no significant differences, except glycogenated hepatocyte nuclei (p=0.0145). EM (1 MMA, 1 PA) revealed enlarged mitochondria with abnormal shapes and matrical osmiophilic or paracrystalline inclusions. There was no significant difference in ages between cases with and without megamitochondria, or with and without fibrosis.

Conclusion: This is the largest series of pathologic evaluation of native liver in patients with MMA and PA. Both groups show similar histologic and ultrastructural spectrum of findings. The most common finding of megamitochondria is in keeping with the theory of mitochondrial dysfunction as a contributing factor to multisystem complications. Despite the

chronic nature of the disease, advanced fibrosis is absent.

Table 1. Clinical features and liver pathology of patients with MMA and PA

Category		MMA (n=12)	PA (n=14)
Sex	F:M	5:7	8:6
Age	Range (median)	2-20 y (14 y)	5 m-24 y (2.5 y)
Initial manifestation	Range	Neonatal-1.5 y	Neonatal-2 m
	Neonatal (%)	83%	83%
Gene mutation^		MUT (90%), MMAB (10%) (n=10)	PCCA (67%), PCCB (33%) (n=6)
Liver enzyme elevation, n (%) ^		8 (67%)	10 (77%)
Abnormal liver imaging, n (%) ^		6 (54%)	6 (46%)
Follow up interval (months)		4-144	45-216
Survival after LT*	Alive	11	12
	Deceased	1 (cause unknown)	1 (DOD)
Portal inflammation, n (%)		6 (50%), mild	4 (29%), mild
Lobular inflammation, n (%)		3 (25%), mild	2 (14%), mild
Macrovesicular steatosis, n (%)		2 (17%), minimal-mild	3 (21%), mild-moderate
Fibrosis	n (%)	2 (17%; portal/periportal)	2 (15%; portal/periportal)
	METAVIR	1 F1 (17 y), 1 F2 (2 y)	1 F1 (6 y), 1 F2 (3 y)
Megamitochondria, n (%)		11 (92%)	8 (57%)
Cytoplasmic clearing, n (%)		3 (25%), focal to diffuse	1 (7%), diffuse
Glycogenated nuclei, n (%)		1 (8%)	8 (57%)
Iron deposition (PPB stain^) (%)		67% (mild-moderate) h+k (n=2), h (n=1), k (n=1)	50% (mild) h+k (n=1), k (n=1)
Ceroid-laden macrophages (PAS/D stain^) (%)		57% (n=4/7)	50% (n=2/4)
Electron microscopy		Mitochondrial abnormalities; increased cytoplasmic free glycogen; microvesicular steatosis; pericanalicular lipofuscin (n=1)	Mitochondrial abnormalities; prominent peroxisomes; Ito cell enlarged with cytoplasmic lipid droplets (n=1)

F: female; M: male; y: year; m: month; LT: liver transplantation; DOD: died of disease; n, number. PPB: Perl's Prussian blue; h, hepatocellular; k, Kupffer cell.

^: Percentages were calculated based on the cases with known information or available materials.

*: when applicable; one autopsy patient without LT was excluded.

Gene names: MUT=Methylmalonyl-CoA mutase; MMAB=Methylmalonic aciduria cblB type; PCCA=Propionyl-CoA carboxylase subunit alpha; PCCB= Propionyl-CoA carboxylase subunit beta.

1721273

Congenital Neurofibromatosis Type l with Massive Involvement of Autonomic Ganglia

J Young [1], J Steele [2], K Carreon [3], A Li [3], H Lidov [3], E Yang [3], A Al-Ibraheemi [3], H Kozakewich [3]; [1] Boston Children's Hospital, [2] Children's Hospital of Philadelphia, [3] Boston Children's Hospital

Background: Congenital neurofibromatosis type l (NF1) with significant disease in autonomic ganglia is infrequently described. Herein, we present the autopsy findings in a three-year-old girl whose disease was detected at prenatal imaging, who had rapid and progressive disease despite operative intervention and MEK inhibitor therapy, and who died with an extraordinary burden of disease in autonomic ganglia.

Methods: Prenatal imaging detected bilateral large thoracic and smaller abdominal paraspinal masses, pyelectasis, and clitoromegaly/ambiguous genitalia. At birth, café-au-lait spots, macroglossia and clitoromegaly were present. Postnatal imaging revealed bilateral cervical, thoracic, and abdominopelvic paraspinal masses. At one week, biopsies of the left thoracoabdominal mass were interpreted as a benign peripheral nerve sheath tumor. Partial loss of nuclear INI-1 immunoreactivity was observed in tumoral and non-tumoral cells. Next Generation Sequencing (XXX) revealed an NF1 c.3888T>G (p.Y1296*), exon 29 nonsense mutation at 44% allele frequency. Germline testing on blood revealed an identical mutation. MEK inhibitor therapy was begun with little effect prompting debulking of the left paraspinal thoracoabdominal mass. Progressive disease, hydroureteronephrosis, hypertension, laryngeal obstruction, and left diaphragmatic paralysis led to eventual transition to comfort care.

Results: At autopsy, external examination was notable for café-au-lait spots, macroglossia, and cliteromegaly. Internal examination revealed that the cervical, thoracic, and abdominal masses were markedly enlarged, discrete or fused sympathetic ganglia or were in the vicinity thereof. The histomorphology was neurofibromatous with a minor component of mature and immature ganglion cells. Parasympathetic ganglionic involvement manifested as hyperganglionosis in the bladder, vagina, distal colon and rectum, and focally in the upper gastrointestinal tract. The bowel was dilated proximal to the sigmoid colon. Three large atrial and ventricular masses were present. Autonomic nerves including vagal, recurrent laryngeal, cardiac, and perivisceral were visibly enlarged and microscopic neurofibromatous involvement was widespread in somatic nerves in skin and soft tissue. There was megalencephaly, frontal gyral atrophy, atypical cerebral cortical astrocytosis, and slight neurofibromatous expansion of spinal nerve roots.

Conclusion: This instance of NF1 is unusual from several aspects: 1) significant disease present at birth, 2) disease dominated by massive involvement of autonomic ganglia, 3) minor component of ganglion cells accompanying the neurofibromatous element in affected autonomic ganglia and adrenal medulla mimicking ganglioneuroma, and 4) enormous and rapidly progressive disease at a very young age. One plausible explanation might be the effects of the rare NF1 mutation: it has been reported only twice in clinical genomic variant databases, although patient characteristics are not available. It is unknown if the partial loss of

nuclear INI-1 immunoreactivity in tumoral and non-tumoral cells was a factor given the role of SMARC genes in schwannomatosis and possibly in NF2.

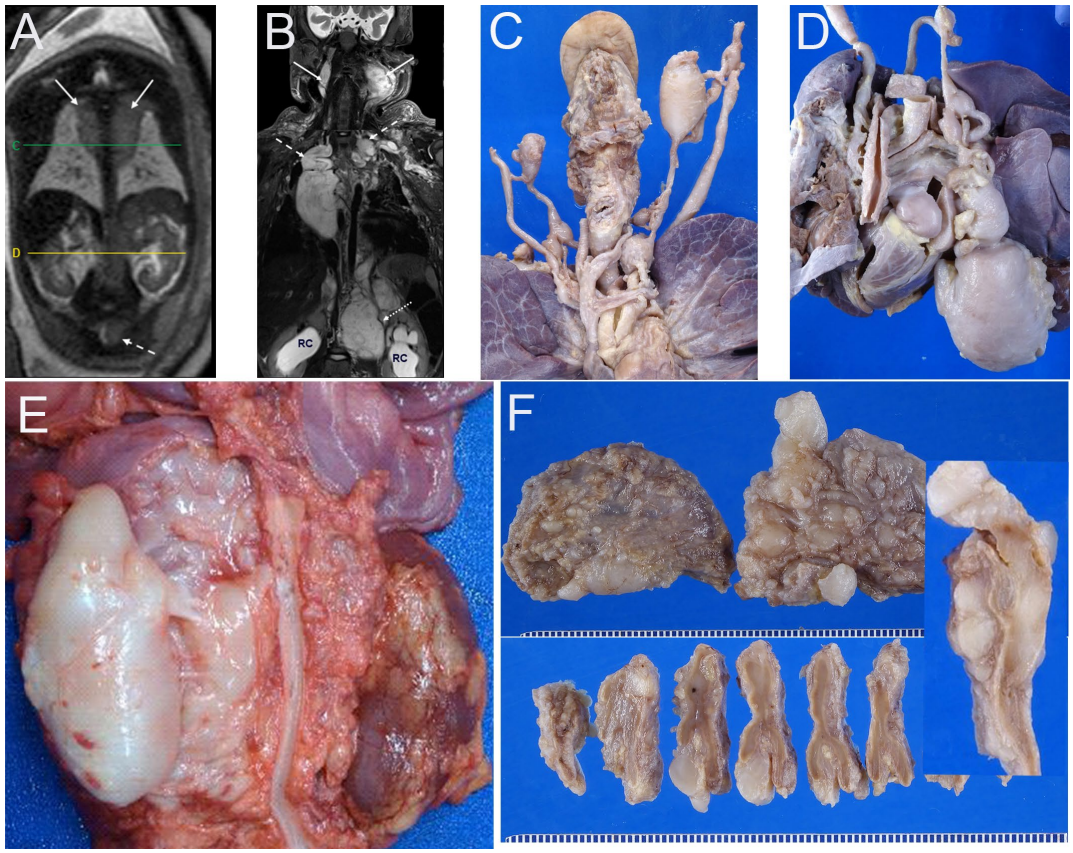

1721326

The clinicopathologic features and genetic alterations in three cases of pediatric colon adenocarcinoma.

M Bitar [1], M Harrell [2], G Raca [2], R Schmidt [2], N Shillingford [2], L Wang [2], M Warren [2], B Yang [2], P Zamiara [2], S Zhou [2]; [1] Children's Hospital Los Angeles, [2] Children's Hospital Los Angeles

Background: Pediatric colorectal cancer is primarily sporadic, yet certain risk factors, including inflammatory bowel disease (IBD) and cancer predisposition syndromes like familial adenomatous polyposis (FAP) and mismatch repair deficiency syndrome, contribute to its occurrence. To investigate this tumor, we describe the clinicopathologic findings and genetic alterations in three cases of pediatric colon adenocarcinoma.

Methods: Gross examination and histologic evaluations were performed on all cases. Molecular profiling of tumors included targeted pan-cancer next-generation sequencing (NGS), and chromosomal microarray analysis (CMA).

Results: Case 1: A 14-year-old girl with refractory ulcerative colitis underwent total colectomy, revealing a moderately-differentiated adenocarcinoma in the ascending colon. The tumor exhibited ERBB2 (HER2) amplification, a TP53 p.Arg248Gln mutation, and loss of heterozygosity of 17p that included the TP53 locus. Germline testing was recommended to evaluate for Li-Fraumeni syndrome but Sanger sequencing on peripheral blood was negative for the TP53 p.Arg248Gln variant. Case 2: An 18-year-old girl with familial adenomatous polyposis and a heterozygous germline pathogenic variant in APC p.Glu1309Aspfs*4 in 5q22.2 underwent total colectomy and was found to have a well-differentiated adenocarcinoma. The malignancy arose in two of the patient's innumerable adenomatous polyps. The adenocarcinoma harbored the same APC germline variant and a somatic ARID1A p.Glu1802* variant. CMA demonstrated multiple chromosomal gains and losses and was most notable for copy-neutral loss of heterozygosity involving the entire chromosome 5, resulting in loss of the remaining wild-type APC allele in the tumor cells. Case 3: A 16-year-old boy presented with frequent bloody stools and was found to have a moderately-differentiated adenocarcinoma in the sigmoid colon. The tumor cells were positive for MSH2 and MSH6 but negative for MLH1 and PMS2 immunostains. The tumor harbored many apparent somatic mutations suggesting a hypermutated tumor. Our standard pediatric NGS panel does not examine mismatch repair genes. Cancer predisposition panel was performed on a tumor sample and revealed MSH3 p.Pro67Alafs*18 and MSH3 p.Lys383Argfs*32 variants. CMA was non informative. Germline testing to evaluate for constitutional mismatch repair deficiency syndrome was recommended.

Conclusion: Pediatric colon adenocarcinoma can arise in various disease contexts, as illustrated by these cases. The presented cases highlight the importance of tumor genetic testing to detect targetable mutations, guide germline testing to rule out cancer predisposition syndromes, and uncover the molecular basis of tumorigenesis.

1721883

Evaluation of an immunohistochemical panel in pediatric Hepatocellular carcinoma (pHCC)

L Berklite [1], S Ranganathan [2], R Verma [2]; [1] Cincinnati Children's Hospital Medical Center, [2] Cincinnati Children's Hospital Medical Center

Background: HCC is the second most common primary malignant liver tumor in children, but remains relatively understudied in comparison to adult HCC and hepatoblastoma (HB). Recent studies have suggested pediatric HCC (pHCC) have overlapping but non-identical biology with adult HCC. In this study we evaluated a panel of immunohistochemical (IHC) markers in a cohort of pHCC to better define these tumors in comparison to adult HCC and HB.

Methods: 126 HCC cases were identified from the files of a single institution diagnosed between 1983-2023. Relevant clinical data was collected from the electronic medical record. 44 cases had available material for IHC and special stains including PROX-1, MOC31, glypican-3, beta catenin, reticulin, CK7, and glutamine synthetase (GS). Extent and intensity of stains were semi-quantitatively scored and a composite IHC score (ICS) was generated (range 0-9).

Results: Patients were aged 6 months to 43 years with a male to female ratio of 1.52. Underlying conditions included Fanconi anemia (n =2), Fontan hepatopathy, ERCC1 deficiency, Zellweger syndrome, Alagille syndrome (n = 5), alpha-1 antitrypsin deficiency (n = 3), diabetes, hepatitis C and B, PFIC2, 5-beta reductase deficiency, Turner syndrome (n=2), Abernethy syndrome, Prune belly syndrome, and Moya moya. 30/126 cases were diagnosed as fibrolamellar HCC (FLHCC). 9/126 cases HCC arose in an adenoma. IHC findings are summarized in Table 1 (insert image). Glypican-3 negative cases included 3 cases of early HCC arising in an adenoma and 2 FLHCC. Both MOC31 negative cases were from a patient with Zellweger syndrome. 3/13 cases with nuclear beta catenin arose in an adenoma. 87.5% (7/8) of cases with nuclear beta catenin showed strong diffuse GS positivity and 54.5% (6/11) showed expression of SALL4. Cases with preserved reticulin included 5 cases arising in an adenoma and 2 FLHCC. All FLHCC had diffuse CK7 expression. The only GS negative case was an early HCC arising in an adenoma. 21.4% (6/28) of cases with GS positivity showed diffuse, strong (3+) staining with the remaining cases showing heterogenous or only focal positivity.

Conclusion: We defined the immunoprofile of pHCC across a spectrum of clinical contexts. pHCC showed consistent expression of glypican-3, GS, PROX-1 and MOC31 with frequent loss of reticulin meshwork. In contrast to HB, nuclear beta catenin was rare in pHCC but seen in the context of beta catenin mutated adenomas and was frequently associated with SALL4 positivity

Table 1. Immunohistochemical features of pHCC					
	PROX-1		**MOC-31**		**GS**
+	82.6% (19/23)	**+**	90.9% (20/22)	**+**	96.6% (28/29)
-	17.4% (4/23)	**-**	9.1% (2/22)	**-**	3.4% (1/29)
Mean ICS	5.74	**Mean ICS**	4.95	**Mean ICS**	5.65
	SALL4		**CK19**		**CK7**
+	59.3% (16/27)	**+**	55% (11/20)	**+**	53.6% (15/28)
-	40.7% (11/27)	**-**	45% (9/20)	**-**	46.4% (13/28)
Mean ICS	3.1	**Mean ICS**	3	**Mean ICS**	3.5
	Glypican 3		**Beta catenin**		**Reticulin**
+	84.6% (33/39)	**M**	64.1% (25/39)	**Loss**	80.6% (25/31)
-	15.4% (6/39)	**M, C, N**	35.9% (13/39)	**Preserved**	19.4% (6/31)
Mean ICS	5.29	**M, C**	2.6% (1/39)		
ICS- Immunohistochemical composite score, M-membranous, C-cytoplasmic, N-nuclear					
Immunohistochemical distribution patterns					
PROX-1 (n = 19)		**MOC-31 (n = 21)**		**GS (n =27)**	
0	2	**0**	5	**0**	2
1+	2	**1+**	3	**1+**	3
2+	2	**2+**	1	**2+**	4
3+	13	**3+**	12	**3+**	18
SALL4 (n = 23)		**CK19 (n = 14)**		**CK7 (n =25)**	
0	9	**0**	6	**0**	13
1+	3	**1+**	3	**1+**	3
2+	3	**2+**	0	**2+**	1
3+	8	**3+**	5	**3+**	8
Glypican 3 (n = 35)					
		0	7		
		1+	1		
		2+	1		
		3+	26		
Score: 0: 0-5%, 1+: 5-30%, 2+: 30-50%, 3+: >50%					

1721906

Use of Respiratory Viral Testing in Autopsy

S Chen [1], H Wang [2], M Conces [2], A Rubrecht [2], N Ramirez [2], P Baker [2], L Balikani [2], A Shenoy [2], A Hughes [2], L Biederman [2]; [1] Nationwide Children's Hospital/The Ohio State Universty, [2] Nationwide Children's Hospital

Background: During the pandemic, respiratory viral panel (RVP) testing, particularly testing for severe acute respiratory syndrome coronavirus 2 (SARS-CoV-2), became an important pre-autopsy screening tool for infectious risk and appropriate precautions. In our institution, we offer COVID-specific testing (CST) for SARS-CoV-2 by polymerase chain reaction or nucleic acid amplification as well as respiratory viral panel (RVP) testing which includes SARS-CoV-2 and 26 other respiratory pathogens. Pre-pandemic, RVP testing was utilized in patients with a high pre-test probability of positivity. However, with the SARS-CoV-2 pandemic, utilization of RVP and CST shifted to postmortem screening tests in many patients at the discretion of the pathologist after clinical history review.

Methods: We reviewed fetopsy and autopsy case requests with RVP or CST post-mortem testing between January 2018 to December 2023. RVP testing was offered pre-pandemic though stand-alone SARS-CoV-2 testing and the inclusion of SARS-CoV-2 on the RVP was offered from 2020 onward. Autopsy reports and charts were reviewed for clinical data and symptomatology.

Results: A total of 644 autopsies/fetopsies were requested between 2018 and 2023. Five patients did not receive a full autopsy due to a postmortem positive SARS-CoV-2 test. Viral pathogens detected are summarized in Table 1. Pre-pandemic (2018-2019), 6.5% (n=15) of all autopsy/fetopsy cases had RVP testing with a positive result in two patients (13%). Utilization in 2020 increased to 18% (n=17) of cases with a positivity rate of 18%. In 2021, the utilization stayed stable at 17% (n=19) with a positivity rate of 26%. In 2022, 48% of cases were tested postmortem with a positivity rate of 16%. Between 2020-2022, testing comprised 97% RVP and 3% CST. In 2023, 59% (n=55) of cases were tested, of which 71% were CST. The positivity rate however decreased slightly to 16%. In cases with positive viral testing that also received an autopsy, 58% (11/19) had findings supporting a contributory component of the viral pathogen.

Conclusion: Viral testing in the post-mortem setting has increased institutionally and its usage has changed to a screening tool to determine infectious risk and set up appropriate precautions, reflective of the increasing prevalence of respiratory pathogens including SARS–CoV-2. The sharp increase in testing in the last year is likely attributable to less empiric testing done by outside sites. The positivity rate, including unexpected positivity, has fluctuated throughout the pandemic. The utilization of CST in a more cost effective method of screening than RVP panel, which should be employed for patients with a high clinical suspicion for a respiratory illness.

PERIOD	SINGLE VIRAL PATHOGEN	TWO VIRAL PATHOGENS
2018-2019	rhino/enterovirus (1)	adenovirus and rhino/enterovirus (1)
2020-2022	rhino/enterovirus (5) adenovirus (2) Coronavirus NL63 (1) SARS CoV2 (1) parainfluenza virus 2 (1) Influenza A H1 2009 (1)	adenovirus and parainfluenza virus 3 (1) adenovirus and rhino/enterovirus (1) parainfluenza virus 1 and rhino/enterovirus (1)
2023	SARS CoV2 (4) adenovirus (2) rhino/enterovirus (2) respiratory syncytial virus (2)	SARS CoV2 and Coronavirus NL63 (1)

1721940

A case of unique demographic and uncommon anatomical Müllerian remnant cyst favors its embryological heterotopia theory

S Wang P Repollet Otero, F Balarezo, K Haghayeghi; Hartford Hospital

Background: Müllerian remnant cysts, also known as cutaneous ciliated cysts, represent a rare and benign skin lesion initially reported in 1978. Though typically observed in the lower extremities of post-pubertal young females, these cysts have been reported in other anatomical locations and also in males. Due to their rarity, the precise pathogenesis remains elusive. Herein, we present a case of Müllerian remnant cyst persisting since birth, providing supportive evidence for the embryological heterotopia theory.

Methods: Patient clinical information was extracted from the electronic medical record, and histologic staining was conducted following standard protocols.

Results: Patient is a 2 month-old female who presented with a 2 cm skin lesion projecting 1 cm off the skin on the right shoulder. The lesion was white at birth but later adopted the color of the surrounding skin. Ultrasound revealed a fluid-filled structure which had an exophytic component and tapered to a small tract within the subcutaneous tissues. There was no internal Doppler flow. Clinical and radiologic impressions included epidermal inclusion cyst, lymphatic malformation or pedunculated skin tag. It had grown significantly in size with tenderness and redness, which led to seeking clinical care. Subsequently, incision and drainage was performed and culture revealed MRSA infection. After a course of clindamycin, the infection was resolved and the lesion was stable. Two months later, a follow-up MRI disclosed a thin linear extension into subcutaneous adipose tissue up to the trapezius muscle, favoring an epidermal inclusion cyst. Given the stable clinical state, excision was deferred. Patient returned at 14-month-old with intermittent spontaneous drainage from the lesion. Physical exam revealed similar skin lesion without significant size change, redness or concern for infection. Due to the drainage, excision was performed. Grossly, a 1.5 cm subcutaneous cyst connected to the blister-like area on the skin was appreciated. Microscopically, a ciliated columnar epithelium cyst lining with focal pseudostratification was identified. There was no evidence of cellular atypia or malignancy. Based on the distinct histologic features, a diagnosis of Müllerian remnant cyst was confirmed.

Conclusion: Based on the morphologic and immunohistochemical features of Müllerian remnant cyst, multiple hypothesis including embryological heterotopia and metaplasia of tissue or lymphatic dissemination have been proposed. However, no definitive conclusion has been reached. Our case, involving an infant with a lesion persisting since birth, may be supportive of the embryological heterotopia hypothesis. Despite its benign nature, the potential for infection underscores the importance of vigilant management.

1721961

Choroid Plexus Carcinoma and its Association with Li-Fraumeni Syndrome

K Moss [1], M Blessing [2], J Van Arnam [3]; [1] Baylor College of Medicine/Texas Children's Hospital, [2] Baylor College of Medicine/Texas Children's Hospital, [3] Texas Children's Hospital

Background: Choroid plexus carcinoma (CPC) is a rare neoplasm of the specialized epithelium that produces cerebrospinal fluid (CSF). The majority of cases occur in infants and young children and present with variable symptoms, sometimes acutely, associated with hydrocephalus. Genetic susceptibility for this neoplasm is associated with Li-Fraumeni syndrome.

Methods: We present a case of a 2 year old male, previously well, who presented with a one month history of progressive nausea, vomiting, and lethargy. His symptoms were nonresponsive to famotidine and lansoprazole. Ultimately, he presented comatose to the emergency department, where a head CT noted a 7.2 x 6.0 x 4.5 cm right posterior temporal mass with cystic/necrotic changes and herniation. During transfer for a higher level of care he developed pulseless arrest and died. A limited brain and spinal cord only autopsy was performed.

Results: At autopsy, the brain showed a 6.7 x 6.5 x 4.2 cm tan-grey papillary mass circumferentially coating and markedly expanding the temporal and occipital aspects of the right lateral ventricle with associated severe cerebral edema and mass effect resulting in midline shift and herniation. Microscopic examination demonstrated a papillary to solid neoplasm invading brain parenchyma with broadly pushing borders, variably hyperchromatic nuclei, irregular nuclear contours, brisk mitotic activity and corresponding high Ki67 labeling, and necrosis. Immunostains confirmed the choroid plexus origin of the tumor and p53 showed a wild-type pattern.

Conclusion: In this case, the family’s main question was about the genetic associations with this tumor and whether their future children were at risk of similar tumors. Pediatric autopsy is an important and valuable tool for pathologists to aid families in understanding genetic implications of a child’s death as well as future family planning. Li-Fraumeni syndrome is an autosomal dominantly inherited germline mutation in the TP53 gene which results in increased risk of developing various cancers. Most patients with this syndrome inherit an altered copy of the gene from an affected parent, but 7-20% of cases are the result of a de novo mutation. A limited genetic study of the patient and parents in this case yielded important information about their own risk as well as their future offspring’s risk of having this genetic syndrome and developing cancer.

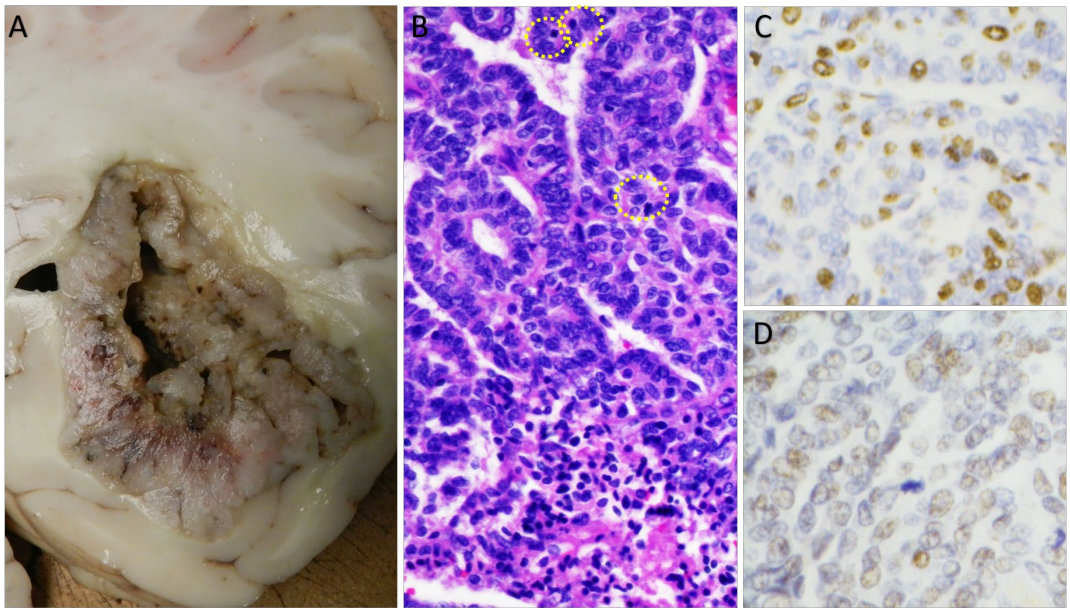
A
B
C
D

1721986

A Rare Autopsy Case of Eagle-Barrett Syndrome with Congenital Heart Anomalies

Q Zhang [1], C Castaneda [1], M Oliver [1], S Cook [2], C Bockoven [1], J Gulliver [2]; [1] University of Wisconsin-Madison, [2] University of Wisconsin Clinics and Hospitals

Background: Eagle-Barrett syndrome, also known as Prune belly syndrome (PBS), is a rare congenital disorder with male predominance and while incidence varies, there are estimates of about 4 per 100,000 live male births1. The isolated PBS cases manifest three cardinal pathological features: abdominal wall musculature deficiencies, cryptorchidism, and urinary tract abnormalities. Approximately 75% of patients with PBS have anomalies involving another organ system, including respiratory (58%), cardiovascular (25%), gastrointestinal (24%) and musculoskeletal (23%) defects2-4. The cause of PBS is unknown, but chromosomal abnormalities have been identified in some cases. Herein, we report an autopsy case of a 3-month-old male diagnosed with PBS with associated congenital heart anomaly.

Methods: Review of the clinical history, autopsy material, and histologic sections were performed.

Results: The major gross findings included gross appearance of paucity of midline abdominal muscles, cardiomegaly for age, dilated right atrium with anterior atrial septal defect, secundum type, small left ventricle, bilateral hydronephrosis, bilateral intra-abdominal gonads, and massively dilated penile urethra. The patient had a history of excision of bilateral distal narrow ureteral segments. Bilateral pleural effusions and abdominal ascites were also identified. Histologically, within the myocardium, there was mild myocyte hypertrophy with negative C4d staining. The bilateral lungs showed acute bronchopneumonia. The bilateral kidneys showed areas of disorganized immature renal parenchyma with islands of immature cartilage. Immature tubules were surrounded by collarettes of condensed mesenchyme. Dilated tubules were scattered throughout the parenchyma. The findings were consistent with segmental areas of dysplastic renal parenchyma.

Conclusion: In this case, features consistent with PBS included the gross appearance of paucity of midline abdominal muscles, urinary tract abnormalities including bilateral hydronephrosis with segmental dysplastic renal parenchyma, and bilateral cryptorchidism. The associated comorbid congenital heart anomalies were also identified. Based on the Woodard classification of PBS, the patient would fit best within Category 2 and would be considered at risk for complications of the prior urinary tract obstruction or frequent urinary tract infections. The pathogenesis is incompletely understood. Mechanical factors, genetic or chromosomal alterations, teratogens, and infectious agents have all been proposed, but there is not definitive evidence to support a clear cause. In this case, FISH and chromosomal microarray, per the provided history, were normal, underlining the unclear etiology of the described constellation of findings. The cause of death was likely multifactorial in the setting of congenital heart anomalies, features consistent with Prune Belly Syndrome, and subsequent development of acute bronchopneumonia resulting in acute hypercarbic and hypoxic respiratory failure. The associated congenital heart anomalies were unique in this

case and contributed to the poor outcome. In the future, gathering data from a multitude of cases as well as more extensive genetic testing could reveal a more definitive pathogenesis.

1721989

A Case of Fumarate Hydratase-Deficient Renal Cell Carcinoma with TFE3 Immunoreactivity in a Sickle Cell Trait Patient

C Ilagan M Zhang; The University of Texas MD Anderson Cancer Center

Background: Fumarate hydratase-deficient renal cell carcinoma (FH-deficient RCC) is a rare and aggressive subtype of RCC that occurs in patients aged 21 to 65 years old, with male predilection. This is thought to be caused by inactivating mutation of the FH gene. It can either occur sporadically or arise in the setting of hereditary leiomyomatosis and renal cell carcinoma (HLRCC) syndrome. We present a case of FH-deficient RCC with TFE3 immunoreactivity in a pediatric patient with sickle cell trait.

Methods: A 12-year-old male with family history of sickle cell trait presented with hematuria and abdominal pain. Imaging showed a 14 cm solid, cystic, and hemorrhagic left renal mass. A radical nephrectomy was performed. Concurrently, the patient was confirmed to have sickle cell trait on hemoglobin electrophoresis.

Results: Gross examination revealed a yellow-tan, hemorrhagic, multinodular and cystic mass located in the upper to mid pole of the kidney. Microscopically, the renal mass exhibited multiple growth patterns including papillary pattern with hyalinized fibrovascular cores (Figure 1A) and tubulocystic pattern. The tumor cells had prominent eosinophilic nucleoli. On immunohistochemical analysis, the tumor cells were positive for PAX8, EMA, vimentin, pancytokeratin, AMACR, while negative for CK7, CK20, WT1 and CAIX. INI-1 showed retained nuclear expression. There was diffuse nuclear and cytoplasmic staining of 2-succinocysteine (2SC) (Figure 1B), while there was loss of FH stain (Figure 1C). TFE3 immunostain was positive (Figure 1D). Fluorescence in situ hybridization (FISH) was negative for TFE3 gene arrangement.

Conclusion: The case highlights multiple diagnostic pitfalls. In a patient with sickle cell trait, diagnostic consideration usually includes renal medullary carcinoma (RMC). In this case, INI-1 showed retained expression which, along with morphology, made it unlikely to be RMC. Another pitfall was the TFE3 immunoreactivity. Caution must be taken in the interpretation of the stain since TFE3 immunoreactivity lacks specificity; therefore, confirmatory FISH studies must be performed. This case illustrates the importance of incorporating morphology, immunohistochemical and molecular findings in making a diagnosis. Furthermore, FH-deficient RCC is important to include in the differential diagnosis when encountered with a case of high grade renal tumor with papillary or tubulocystic pattern and prominent nucleoli.

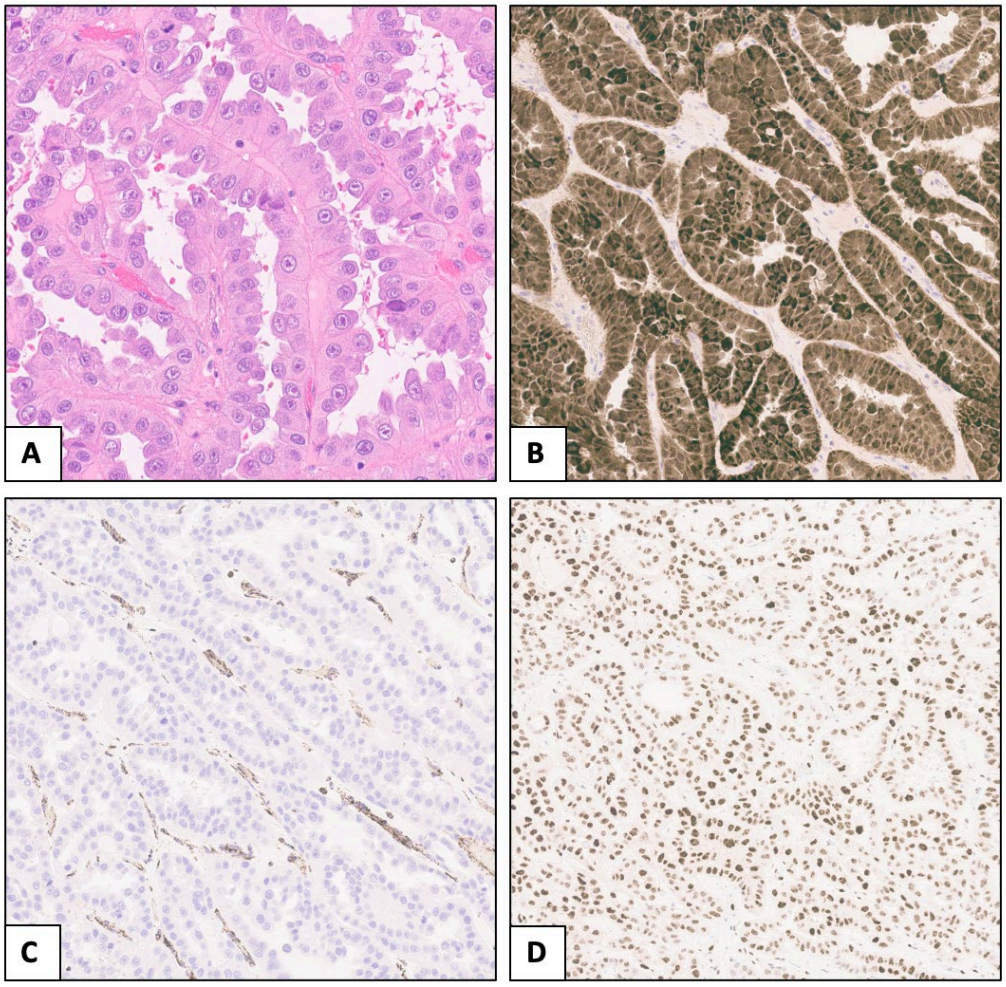
A
B
C
D

1722003

Neonatal Hemochromatosis in a Fetus with De Novo PTEN Mutation: An Autopsy Case Report and Literature Review

F Bian [1], Y Feng [1], J Angel [1], R Linn [2]; [1] Department of Pathology and Laboratory Medicine, Pennsylvania Hospital of the University of Pennsylvania Health System, Philadelphia, PA, USA., [2] Division of Anatomic Pathology, Perelman School of Medicine, Children's Hospital of Philadelphia, Philadelphia, PA.

Background: Neonatal hemochromatosis (NH) is a rare disorder that typically presents at fetal or perinatal onset, characterized by fatal liver injury associated with the iron accumulation in hepatic and extrahepatic tissues. Gestational alloimmune liver disease (GALD) is currently considered the main cause. Immunotherapy with high-dose intravenous immunoglobulin (IVIG) in subsequent pregnancy has been associated with successful pregnancy outcomes. We report a case in which autopsy revealed neonatal hemochromatosis as the cause of intrauterine fetal demise (IUFD) in a male fetus at 27 weeks of gestation. The mother, a 37-year-old female, gravida 4, had experienced 2 early spontaneous miscarriages in the interim.

Methods: A consented, unlimited autopsy was performed at our hospital. Cytogenetic testing and whole exome sequencing (WES) was performed on fetal tissue.

Results: The autopsy revealed mild dysmorphic facial features, including low-set ears and flat nasal bridge. Grossly, the liver was small for gestational age and variably nodular on cut surface. Although variable loss of nuclear basophilia was present due to maceration, extensive histologic abnormalities were identified throughout the liver, including significantly distorted liver architecture, as evidenced by reticulin stain demonstrating near diffuse abnormal reticulin framework with collapse, compatible with hepatocyte loss, highlighted by HepPar1 staining, and ductular reaction highlighted by CK7 staining (Fig 1A-D). Iron stain showed marked intracellular deposition, primarily within hepatocytes and biliary epithelium, as well as extracellular hemosiderin deposition (Fig 1E). Early periportal fibrosis was evident upon Trichrome staining (Fig 1F). Immunostaining for HSV1/2 and CMV on the liver, kidney, and placenta was negative. Other findings included a reduced number of proximal tubules, as highlighted by CD10 staining. In addition, placental examination revealed a large for gestational age placenta, likely secondary to extensive villous edema. This combined with numerous fetal erythroid precursors in the villous capillaries is compatible with fetal anemia. Cytogenetic and WES testing of fetal tissue yielded a de novo PTEN mutation. Based on the autopsy results, the mother is preparing for a subsequent pregnancy and plans to initiate IVIG therapy starting at 14 weeks of gestation.

Conclusion: This is the first reported case of NH in the presence of a PTEN mutation. While this finding is novel, no current publications demonstrate a direct relationship between PTEN and NH, suggesting that PTEN mutation may be incidental rather than etiologic. This case underscores the importance of the fetal autopsy in not only investigating the etiology of

IUFD, but also its potential to directly impact care and outcomes in future pregnancies.

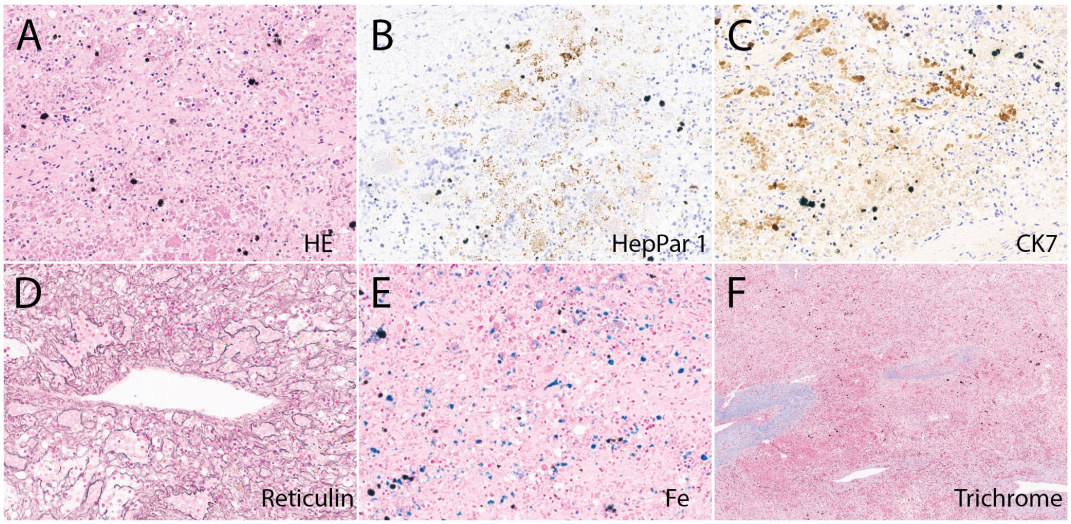

1722014

Eosinophilic Renal Neoplasm with Biallelic TSC2 Mutations in the Post-Neuroblastoma Setting

C Bodnar S Cook, C Bockoven, M Hoover-Regan, J Gulliver; University of Wisconsin Hospital and Clinics

Background: Renal neoplasms with oncocytic/eosinophilic morphology and sporadic TSC2 mutations represent a diverse group of mostly indolent tumors with some aggressive entities. Proper classification is critical in clinical decision-making, treatment, and follow-up care, as biological behavior may vary significantly among the neoplasms. We report a case of low-grade renal oncocytic neoplasm with biallelic TSC2 mutations in a pediatric patient with a history of neuroblastoma.

Methods: We reviewed all available clinical history, radiologic findings, and pathologic, immunohistochemical, and molecular data, in addition to cases described in current literature.

Results: A 14-year-old male with a history of poorly differentiated neuroblastoma presented for a renal ultrasound. He was found to have a left renal interpolar rounded abnormality with circumferential hyperemia. Subsequent MRI redemonstrated a rounded 3.2 cm mass within the mid-pole of the left kidney without calcific or adipocytic foci. No lymphadenopathy, osseous lesions, or renal vasculature extension were identified. A biopsy of the mass showed an oncocytic neoplasm with large cells containing granular pink cytoplasm and prominent nucleoli with some cytologic atypia. Occasional large, bizarre cells and scattered large atypical mitotic figures were also identified. The patient went on to have a resection. The neoplasm was encapsulated and composed of large cells with abundant eosinophilic granular to occasionally vacuolated cytoplasm with again occasional bizarre appearing cells with increased mitoses. All margins were negative for tumor. The neoplastic cells were positive for PAX-8, p504s, CD117, with patchy positivity for CD10, while negative for CK7, CK20, CAIX, S100, TFE-3, and Hales Colloidal iron. There was retained staining with SDH-B and fumarate hydratase. Molecular testing was performed and showed biallelic TSC2 mutations. However, the patient had a three-month follow-up with imaging that did not demonstrate recurrence.

Conclusion: There is a wide spectrum of tumors with TSC mutations which includes entities such as eosinophilic vacuolated tumor, post-neuroblastoma oncocytoid renal cell carcinoma, oncocytic renal neoplasm of low malignant potential NOS, and eosinophilic solid and cystic renal cell carcinoma, among others. To our knowledge, this is the first case of an eosinophilic renal neoplasm with morphology closely resembling eosinophilic vacuolated tumor to be described in the post-neuroblastoma setting. Eosinophilic renal neoplasms are increasingly able to be characterized molecularly, often those associated with TSC mutations can behave in an indolent fashion with rare reports of metastases. Early identification of these mutations could lead to appropriate genetic counseling. The ability to identify specific mutations also provides potential therapeutic options. Response to mTOR pathway inhibitors has been described.

1722174

Multi-organ Von Hippel-Lindau Disease in a 21 y/o male: development of first CCRCC while on treatment with novel drug Belzutifan

P Repollet Otero S Wang, X Song, S Ligato, F Balarezo; Hartford Hospital

Background: Von Hippel-Lindau Disease (VHL) is an autosomal dominant disease characterized by hemangioblastoma (HB) development in the central nervous system (CNS) and retina, clear cell renal cell carcinoma (CCRCC), pheochromocytoma, pancreatic neuroendocrine tumors, cystadenomas of the epididymis, and endolymphatic sac tumors (EST). Management typically involves multiple surgical resections for local control. The novel drug, belzutifan, offers a promisingly systemic alternative to reduce the surgical burden. We report a 21-year-old male with VHL, initially diagnosed at age 15 with multiple HB and subsequently developing EST, CCRCC and pheochromocytoma during follow-up. Remarkably, the CCRCC, his first reported renal manifestation of VHL, was discovered intraoperatively almost a year into belzutifan therapy.

Methods: The patient's clinical information was retrospectively reviewed using our institution's electronic medical record from presentation in 2017 to present. The histopathological features of tumors were obtained from our pathology database. Tumor processing, histological analysis and immunohistochemical tests were performed following standardized protocol.

Results: The patient, with a family history of VHL, sought medical attention at age 15 due to dysphagia, respiratory difficulty, dizziness and abnormal gait. Imaging revealed numerous CNS lesions distributed intracranially and along the spine. A cystic mass in the fourth ventricle was causing severe mass effect on the brainstem and was thought to be the source of the patient's symptoms. After resection, histologic analysis confirmed HB, and patient was diagnosed with VHL. Despite treatment with propranolol, Avastin and sorafenib, the HB increased in both number and size over the years, requiring multiple resections. In 2021, an EST developed of the right retromastoid, causing conductive hearing loss. In 2023, due to disease progression, belzutifan therapy was initiated. Six months into therapy, surveillance imaging showed stable HB with growth of the EST and a new left adrenal mass. During adrenalectomy almost a year into belzutifan therapy, an incidental left renal mass was identified and also excised. Pathology was consistent with a pheochromocytoma and CCRCC.

Conclusion: Belzutifan, a novel HIF-2α inhibitor, has variable effects on VHL-related RCC and non-RCC tumor progression, as documented in existing literature. Herein we presented a case of a young male with VHL that developed his first reported CCRCC and pheochromocytoma after switching to belzutifan therapy. During this period, overall stabilization of the HB compared to prior therapies was observed, while the EST had clear progression in size. This case report sheds more light into the effects of belzutifan therapy on VHL-related RCC and non-RCC neoplasms.

1722460

The Variable Histologic Patterns of Chronic Granulomatous Disease: Report of Two Cases and Literature Review

K Cote K Tejada, G Somers, Y Avitzur, I Siddiqui; The Hospital for Sick Children

Background: Chronic granulomatous disease (CGD) is a rare, inherited immunodeficiency that affects the phagocytes, leading to recurrent infections with catalase-positive organisms. There is phenotypic and genotypic heterogeneity with variable manifestations. As the name implies, the most common tissue reaction is granuloma formation. However, pigmented and non-pigmented histiocytes within the GI tract have been found to be more common.

Methods: This report presents two pediatric patients with diagnosis of CGD, listing their clinical presentations and histomorphology.

Results: Patient #1, a 15-month-old male, who developed intestinal failure as a neonate secondary to midgut volvulus. Following resection he had several necrotizing enterocolitis like episodes. Genetic testing confirmed CGD. The intestinal biopsies taken pre-bone marrow transplant (BMT), showed occasional pigmented histiocytes in the lamina propria with gastritis and mild ileitis. He later underwent a BMT. 1.5 years post-BMT, he needed a liver transplant for intestinal failure associated liver disease. Both the pre- and post-BMT small intestinal biopsies as well as the liver biopsy and explant specimen showed presence of pigmented histiocytes. Additionally, the explanted liver showed variable hepatoportal sclerosis and portal venopathy in the absence of cirrhosis. Patient #2, a 5-year-old previously well female, presented with worsening lower lobe pneumonia despite broad spectrum antimicrobials. Further work up and genetic testing confirmed CGD. She exhibited mild gastrointestinal symptoms and stunted growth. Upper endoscopy was unremarkable. Colonoscopy showed circular hyperpigmented lesions throughout the colon with no ulcers. Prominent foamy and pigmented histiocytes were noted throughout the lamina propria in all the colonic biopsies and fewer in the gastric biopsy. She eventually underwent successful BMT.

Conclusion: These findings in the two patients underscore the diverse histopathological manifestations of CGD. The identification of pigmented histiocytes within the lamina propria of the GI tract and within the hepatic sinusoids provide insight into their importance in diagnostically challenging or near normal GI biopsies. Hepatic involvement in CGD is described, including vascular abnormalities such as portal and central venopathy with or without nodular regenerative hyperplasia, in the absence of cirrhosis. CGD may lead to end stage liver disease. Our patient, with presence of tissue histiocytes post-BMT, had normal neutrophil oxidative burst tests, excluding the possibility of active CGD, suggesting that residual affected histocytes may remain in the GI tract for long periods post BMT. Understanding the histopathological spectrum of CGD is crucial for accurate diagnosis and management.

1722626

Very Early Onset Inflammatory Bowel Disease (VEOIBD)-Like Histopathologic Changes in Trichohepatoenteric Syndrome (THES). A Report of Two Cases

L Balikani [1], E Mezoff [2], B Chaudhari [2], R Abraham [2], C Chung [2], C Flahive [2], R Maltz [2], D Koboldt [2], A Shenoy [2], S Chen [2], M Conces [2], L Biederman [2], V Prasad [2], S Mangray [2], A Rubrecht [2]; [1] Department of Pathology and Laboratory Medicine, Nationwide Children's Hospital, [2] Nationwide Children's Hospital

Background: Trichohepatoenteric syndrome (THES) is an autosomal recessive syndrome caused by pathogenic variants in either the TTC37 or SKIV2L genes. Although hair, liver and intestines are primarily affected, there are other systemic manifestations. Immunodeficiency in these patients is highly variable, though there are reports of hypogammaglobulinemia and impaired humoral responses to vaccines. Switched memory B cells have been reported to be reduced in some patients and vaccine antibody responses are highly variable, as well as T cell proliferation and NK cell degranulation is decreased in approximately 50% of patients. Intractable diarrhea during infancy is a common manifestation hence the designation of THES/syndromic diarrhea. The gastrointestinal (GI) findings in THES patients overlap significantly with other GI conditions including VEOIBD, autoimmune enteropathy, and food-protein-induced enterocolitis. Herein, we present 2 patients with THES and VEOIBD-like findings.

Methods: Patients 1 and 2 (P1 and P2) were evaluated in our center on presentation and follow-up. The clinicopathologic, immunologic, genomic and transcriptomic findings are reviewed (Table 1).

Results: P1 had compound heterozygous nonsense variants in SKIV2L. P2 had compound heterozygous splicing variants of TTC37, one of which was a deep intronic variant only identified with the aid of RNA sequencing. Both patients had a history of intrauterine growth restriction (IUGR) and presented with watery diarrhea and failure to thrive. Persistent diarrhea and dependence on parenteral nutrition prompted genetic workup for congenital causes of diarrhea. The patients underwent endoscopy at 2 years old with significant histologic overlap. Histologic sections of the stomach biopsies demonstrated chronic, active gastritis with atrophic features, confirmed by gastrin and chromogranin immunohistochemical (IHC) stains, and negative Helicobacter IHC. Duodenal and terminal ileum biopsies showed villous atrophy, plasmacytosis and variable eosinophilic infiltrate of the lamina propria, and variable neutrophilic infiltrate. Colon biopsies demonstrated features of chronic active colitis (cryptitis and crypt abscesses, prominent eosinophilic infiltrate, basal lymphoplasmacytosis, crypt architectural irregularity, and Paneth cell metaplasia). There were also scattered foci of apoptotic bodies in the small intestine and colon biopsies. Neither patient developed hepatic manifestations.

Conclusion: The GI findings described are designated as VEOIBD-like changes in THES given the pathogenic variants in SKIV2L (P1) and TTC37/SKIC3 (P2), and current literature.

However, with the overlapping treatment, and the ongoing investigation into the complex underlying genetic mechanisms in VEOIBD, classification may change in the future. To our knowledge atrophic gastritis-type pattern seen in these cases of THES has only been rarely reported.

Table 1. Clinicopathological Features of THES Patients

	Patient 1	Patient 2
Gender	Male	Female
IUGR	Yes (severe)	Yes
Presenting symptoms	Lethargy, poor oral intake, weight loss. Watery diarrhea (large bouts)	Diarrhea and weight loss
Other clinical manifestations	Bicuspid aortic valve, patent foramen ovale	Ventricular septal defect, recurrent infections, cardiac arrest with subsequent limb ischemia and amputation
Age of onset of diarrhea	2 weeks	7 weeks
Anti-enterocyte AB panel	Negative	Negative
Genomic variants	c.848G>A, p.Trp283*l c.1612del, p.Ala538Profs*91	Variant 1: NM_014639.4(TTC37):c.2921-1G>A (maternally inherited) Variant 2: NM_014639.4(TTC37):c.544-470T>G (paternally inherited)
Transcriptional Consequence	Not performed	Variant 1: Exon 29 skipping Variant 2: Creation of novel exon in intron 8
Age at THES diagnosis	4 months	20 months
Diagnostic Immunology Work-up	Essentially normal lymphocyte phenotyping (T, B and trivial NK cell lymphopenia), a mild type I interferon (IFN) signature on monocytes (CD196/SIGLEC1+) during the initial presentation with acute symptoms. SKIV2L protein expression, assessed by flow cytometry, was normal in all lymphocyte and monocyte subsets. Peripheral B cell subset quantitation and differentiation was normal	CD4+ T cell lymphocytosis and a trivial reduction in cytotoxic NK cells. Normal switched memory (sm) B cells, though very few IgA+ sm B cells observed. There was also a mild decrease in early transitional B cells (CD24++38++). T cell phenotyping indicated normal distribution of naïve and memory CD4+ and CD8+ T cells for age.
Hair clippings	Not tested	Features consistent with trichorrhexis nodosa and trichoptilosis.
Endoscopic Findings	Spontaneous oozing from body of stomach, erythema; otherwise atrophic appearing, gastrostomy in place; duodenum had villous blunting in the blub with few scattered ulcerations is distal part. The rest of the examination was normal.	Diffusely erythematous and granular gastric and colonic mucosa. The rest of the examination was normal.
Biopsy Findings	Villous atrophy in duodenum and TI. Chronic atrophic gastritis of stomach. Chronic active colitis of colon.	Villous atrophy in duodenum and TI. Chronic atrophic gastritis of stomach. Chronic active colitis of colon.
Treatment & Course	Budesonide DR-ER 3 mg capsule once daily. Improving enteral feeding tolerance and signs/symptoms with plan for endoscopic re-assessment in 9 months from last endoscopy (Summer 2024).	Budesonide DR-ER 3 mg capsule once daily. Improving enteral feeding tolerance and signs/symptoms with plan for endoscopic re-assessment 9 months from last endoscopy (Summer 2024).

1722711

Constitutional Mismatch Repair Deficiency Manifesting as Burkitt Lymphoma and High-Grade Glioma

R Wyma [1], X Liang [2], K Teehera [2], A Toland [2], N Willard [2]; [1] University of Colorado Anschutz Medical Campus Department of Pathology, [2] University of Colorado

Background: Constitutional mismatch repair deficiency (CMMRD) is an autosomal recessive (AR) cancer predisposition syndrome resulting from biallelic inactivation of a mismatch repair (MMR) gene. We present a case of Burkitt lymphoma (BL) and high-grade (HG) glioma in a likely CMMRD patient.

Methods: Two resection specimens from one patient were concurrently sent to our institution for consultation with limited clinical historyOur evaluation included histologic examination and standard validated immunohistochemistry (IHC) protocols. Molecular genetic testing via next generation sequencing analysis was performed. Nucleic acid was isolated using standardized methodology and was quantified. Target enrichment of the regions of interest was carried out by a hybridization-based methodology using long biotinylated oligonucleotide probes followed by polymerase chain reaction and sequencing on an Illumina NovaSeq 6000 generating 150bp paired reads. Only exons and canonical splice sites were captured.

Results: A 2-year-old male was found to have a rectal mass. Four years later, he was found to have a brain mass. Histology of the rectal mass showed sheets of monotonous medium-sized cells with round nuclei, clumped chromatin, and squared-off cytoplasmic borders. Many mitotic figures and tingible body macrophages were present (Figure 1A). Immunohistochemical (IHC) stains CD10, CD20, and MIB-1 showed diffuse expression in the neoplastic cells, characteristic of Burkitt lymphoma. EBV RNA in-situ hybridization showed no labeling. Fluorescence in-situ hybridization for MYC was unsuccessful. Histology of the brain mass showed markedly atypical cells with glial cytomorphology, few multinucleated giant cells, atypical mitoses, necrosis, and microvascular proliferation (Figure 1B). Positive GFAP and OLIG2 IHC stains confirmed glial phenotype, and p53 had an overexpressed pattern. MSH2 and MSH6 IHC showed loss of nuclear expression in both neoplastic and non-neoplastic cells (Figure 1C and 1D). Next generation sequencing showed hypermutation with tier 1/2 alterations in TP53, NF1, SETD2, and ATRX. A heterozygous copy number deletion of exons 9 and 10 in MSH2 was also present.

Conclusion: In contrast to Lynch syndrome, CMMRD is an AR tumor predisposition syndrome with increased risk of T-cell leukemia/lymphoma (TLL) and brain tumors by the second decade. In our case, germline testing was not available to confirm the mutation. However, a young patient with two distinct neoplasms, at least one of which is hypermutated, and lack of MSH2/MSH6 expression in non-neoplastic cells strongly suggests a germline biallelic inactivation. A study showed 100% sensitivity and specificity of IHC in diagnosing MMR deficiency. While TLL is more prominent in CMMRD, our and few other BL cases suggest an underrecognized association. Our case likely represents a compound heterozygous

MSH2 mutation. The second hit is likely a deep intronic variant, unable to be detected with a whole exome backbone capture. MMR-deficient gliomas show promising response to immune checkpoint inhibitors compared to conventional chemotherapy. Our case highlights the need for greater access to molecular testing for diagnosis and therapy.

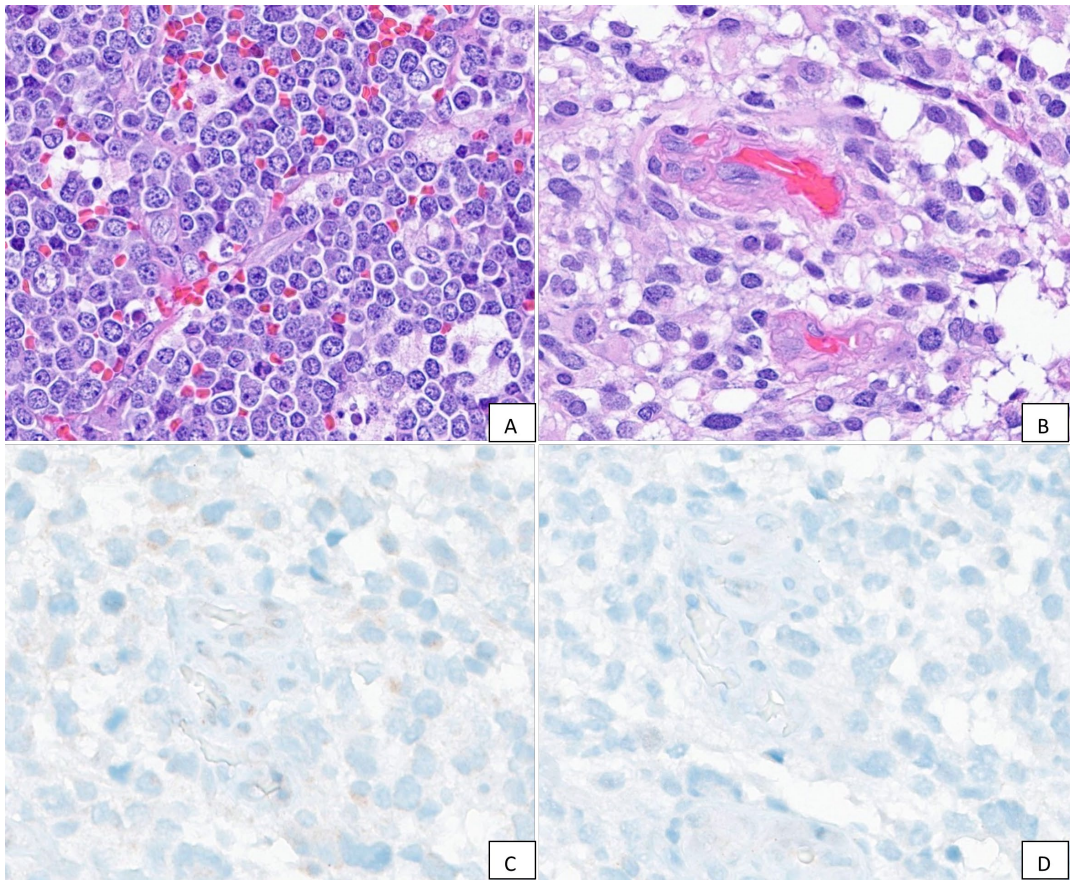

1722839

Is Isolated Collagenous Gastritis and Associated Corpus Atrophy Underdiagnosed in Pediatric Patients? Report of Two Cases and Literature Review

K Tejada K Cote, H Chen, P Church, V Ng, I Siddiqui; The Hospital for Sick Children

Background: Collagenous gastritis (CG) is a rare disease, histologically characterised by thickened subepithelial collagen band and chronic inflammation. In children, CG is usually limited to stomach, without concurrent collagenous colitis. This is in contrast to CG in adults, which tends to involve the colon. Patients with isolated CG typically present with iron deficiency anemia and nodular gastric mucosa. An association with other autoimmune diseases has been reported but pathogenesis is uncertain. Although case reports of CG have limited long term follow-up, none of them reported development of collagenous colitis.

Methods: We present two patients with new diagnosis of CG, who had similar clinical presentations, endoscopic and biopsy findings.

Results: Case 1 is a 17-year-old male who presented with severe iron deficiency anemia and weight loss. Endoscopy showed nodularity in the stomach. Gastric biopsy revealed Helicobacter-negative pan CG with moderate to severe atrophy of the oxyntic mucosa. Patient was treated with iron supplement for three months which resolved the anemia. Case 2 is a 9-year-old male with a 2-year history of recurrent iron deficiency anemia, managed with blood transfusion and iron supplementation. Endoscopy showed atrophic gastric body and cardia with gastritis and antral nodularity. Gastric biopsy revealed Helicobacter-negative pan CG with mild to moderate atrophy of the oxyntic mucosa. For both cases, biopsies from other sites of upper and lower GI tract showed no diagnostic abnormality.

Conclusion: Isolated CG typically occurs in children and presents with iron deficiency anemia and nodular mucosa. The pathophysiology of isolated CG is unclear. The anemia is presumed to be associated with rupture of entrapped capillaries within the subepithelial collagen band. Three histologic patterns have been described, including lymphocytic gastritis-like, eosinophilic rich and atrophic. The evolution of CG in one pediatric patient during a 12-year period has been described. That patient had progressive corpus atrophy with linear hyperplasia of enterochromaffin-like cells, not noted in our patients. Marked inflammation in CG often precludes the assessment of the subepithelial collagen band, thus CG can be erroneously diagnosed as chronic active gastritis. Furthermore, atrophy of the corpus can easily be mistaken as antral mucosa. Therefore, careful assessment of subepithelial collagen in all cases of gastritis presenting with iron deficiency anemia is warranted. It is important to assess for atrophy in all cases of isolated CG, as it precedes metaplasia. There is no standard treatment protocol for CG, and the long-term outcome is unknown. The follow-up biopsies of the reported cases in literature showed either persistence/increase in collagen despite therapy or resolution.

1722963

Clear cell sarcoma of the kidney: Two consecutive cases, with distinct histomorphology and molecular alterations, at a single institution

P Zamiara [1], A Minja [2], V Karne [3], M Warren [3], S Zhou [3], R Schmidt [3], N Shillingford [3], L Wang [3]; [1] Children's Hospital Los Angeles, [2] Harbor-UCLA Medical Center, [3] Children's Hospital Los Angeles

Background: Clear cell sarcoma of the kidney (CCSK) is a rare malignancy of childhood, accounting for 3-5% of malignant renal tumors in the pediatric age group. It is characterized by diverse histologic appearances and three mutually exclusive molecular alterations. We present two consecutive cases of CCSK diagnosed at our institution, highlighting the morphologic spectrum of this entity and the role of molecular testing to confirm the diagnosis.

Methods: Microscopic examination with H&E and immunohistochemical stains was performed. Ancillary techniques included targeted next generation sequencing (NGS) panel, chromosomal microarray, and internal tandem duplication (ITD) assay.

Results: The first patient, an otherwise healthy 18-month-old boy, presented to medical attention with hematuria. Diagnostic workup revealed a 7.8 cm right kidney mass with invasion of infrahepatic inferior vena cava and enlarged retrocaval lymph nodes. Open biopsy was performed. Histology showed sheets of small- to medium-sized polygonal cells with increased nuclear to cytoplasmic ratio and eosinophilic cytoplasm. There were interspersed thin-walled blood vessels but no distinct nested pattern. BCOR, SATB2, and TLE1 immunostains were diffusely positive. NGS panel detected a YWHAE::NUTM2B fusion. The second patient, a 14-month-old otherwise healthy boy, presented to the emergency department with a palpable abdominal mass and hematuria. Diagnostic imaging disclosed a 10 cm left renal mass with possible involvement of the renal vein. Radical nephrectomy was performed. The H&E sections revealed “classic” morphology characterized by nests of monotonous spindled to ovoid cells with clear cytoplasm, with interspersed thin-walled vessels. In addition, areas with abundant myxoid matrix, including cystic degeneration, were also present. The BCOR immunostain was diffusely positive. BCOR-ITD assay was positive, while the NGS panel did not detect clinically established variants.

Conclusion: We present two consecutive cases of CCSK diagnosed at our institution, with differing histologic appearances and two mutually exclusive molecular alterations. Given the spectrum of pediatric kidney tumors, comprehensive diagnostic workup including immunohistochemistry and molecular testing, is essential for establishing this diagnosis.

1722992

Congenital Multifocal Cutaneous and Systemic Histiocytoma with CLTC::SYK Fusion: Expanding the Spectrum of Fusion-Driven Histiocytic Proliferations

J Sookdeo [1], S Koo [2], F Malik [2]; [1] University of Tennessee Health Science Center, [2] St. Jude Children's Research Hospital

Background: Histiocytic neoplasms are characterized by a proliferation of mononuclear phagocytes of myeloid origin. Approximately 80% of these lesions are now known to be driven by gene mutations that increase downstream activation of the mitogen activated protein kinase (MAPK)/ extracellular-regulated kinase (ERK) pathway. A fusion of the gene encoding clathrin heavy chain 1 (CLTC) to the functional domain of spleen tyrosine kinase (SYK) has been recently identified in some cases of solitary, non-Langerhans type histiocytic lesions. Herein, we describe the first case of a congenital CLTC::SYK fusion-driven multifocal cutaneous and systemic histiocytic proliferation.

Methods: A 4-month-old male patient without significant perinatal history presented with a history of skin lesions present since birth with variation in size over time, but without any constitutional symptoms. Physical examination revealed multiple variably sized, mobile, non-tender, yellow papular lesions on the skin of the face, scalp, chest, back, leg, and scrotum. Magnetic resonance imaging revealed multiple pulmonary nodules of variable size. A biopsy of the patient's left buttock lesion was performed.

Results: Microscopic examination revealed skin with a diffuse, cellular infiltrate involving the dermis. The cells showed a uniform spindled appearance, with moderate eosinophilic and vacuolated cytoplasm, with oval, elongated nuclei. No Touton-type giant cells or foamy xanthomatous cells were identified. Immunohistochemical studies showed that these cells were diffusely positive for histiocytic markers (CD68, CD163, Factor XIIIa), whereas CD1a and Langerin were negative. BRAF V600E, S100, SOX10, Melan A, HMB45, CD45, CD43, and SMA were also negative. Next generation sequencing for fusion transcripts revealed an in-frame fusion of exon 31 of CLTC with exon 6 of SYK. Targeted DNA sequencing did not reveal any potential pathogenic gene variants. The patient was managed conservatively and at 6-month follow-up showed spontaneous regression of cutaneous lesions.

Conclusion: Herein, we expand the spectrum of these fusion-driven histiocytic lesions, which was previously considered to be associated only with solitary histiocytomas. The absence of Touton-type giant cells within a uniform-appearing histiocytic proliferation seen in our case is similar to the previously described examples. The fusion transcript of CLTC::SYK may lead to aberrant activation of the MAP/ERK pathway. Although follow-up is limited, short term surveillance showed favorable clinical behavior despite systemic involvement. Identification of this rare histiocytoma subtype may help in avoiding unnecessary treatment or surgical procedures. Further, FDA-approved SYK inhibitors may be a potential therapeutic option in aggressive or unresectable disease.

1723022

BRG1-Deficient Malignant Neoplasm of Bone as the Initial Presentation of a Patient With Rhabdoid Tumor Predisposition Syndrome

J Sookdeo [1], S Koo [2], F Malik [2]; [1] University of Tennessee Health Science Center, [2] St. Jude Children's Research Hospital

Background: The SMARCA4 gene encodes BRG1, a catalytic subunit of the ubiquitous SWI/SNF complex responsible for chromatin remodeling and transcription regulation. SMARCA4 loss is a rare driver in the pathogenesis of various neoplasms. Germline heterozygous loss-of-function mutation of SMARCA4 causes rhabdoid tumor predisposition syndrome type 2 (RTPS2); affected patients are at increased risk for developing malignant rhabdoid tumors and small cell carcinoma of the ovary, hypercalcemic type. However, this molecular alteration has not been described to date in bone tumors. We present a case of a primary osseous high-grade malignant neoplasm with BRG1-loss in a patient with germline SMARCA4 mutation.

Methods: The patient was a previously healthy 13-year-old male who presented with a five-week history of right lower extremity pain that increased in severity. Magnetic resonance imaging (MRI) revealed a 15.4 cm intramedullary mass in the right distal femur metaphysis with heterogeneous enhancement and periosteal reaction. The tumor extended into the adjacent soft tissue. Additional skip lesions were also seen proximally in the right femur. MRI of the thorax showed bilateral small pulmonary nodules representing metastasis. The patient underwent a needle core biopsy of the right femur mass.

Results: Histologically, the tumor showed varying morphology characterized by a high-grade, primitive cellular aggregates with intermixed tumor cells showing rhabdoid features, with frequent mitoses. Small foci of well-formed epithelial component were present, characterized by squamoid nests and irregular glands with mucinous lining. The intermixed mesenchymal component showed cellular fascicles of spindle cells with low-grade histology. There was unequivocal loss of BRG1 immunostaining in all components of the tumor, with retained INI1 expression. Variable positivity for SALL4, CD99, TLE1, WT1, and TTF1 was present. The epithelial components were positive for CK7, CK20, and Cam5.2. Transcriptome sequencing was negative for recurrent fusion transcripts. Whole exome sequencing revealed a heterozygous nonsense mutation in SMARCA4 in the patient’s germline, with apparent copy-neutral loss of heterozygosity leading to loss of the normal copy of SMARCA4 in the patient’s tumor.

Conclusion: We present a case of a primary malignant bone neoplasm with SMARCA4 loss as the initial presentation in a patient with RTPS2. This presentation is previously undescribed, to the best of our knowledge. BRG1-deficient malignant neoplasms should be considered in the histologic differential when polyphenotypic malignant histology is seen, especially in unusual sites. Our case broadens the spectrum of tumors found in patients with RTPS2, which can potentially have implications for surveillance guidelines for this rare syndrome.

1723030

Clinicopathologic Factors Influencing Pediatric Renal Biopsy Adequacy

L Parsons [1], J Jarzembowski [2]; [1] Children's Wisconsin, [2] Children's Wisconsin

Background: Renal biopsies require adequate representation of the cortex to successfully evaluate for a variety of medical kidney disorders. At our children's hospital, renal biopsies are performed under real-time ultrasound guidance by pediatric interventional radiologists or by pediatric nephrologists following ultrasound-guided marking of the site. Historically, a pathologist assistant would perform a gross assessment of the biopsy tissue on-site, but we discontinued this practice in 2014 due to a perceived lack of utility. The tissue is then processed and examined by H&E staining of three levels, immunofluorescence (IF) staining for IgA/IgG/IgM/C3/fibrinogen (native) or C4d (transplant), and electron microscopy (EM; primarily for native biopsies). Recently, we experienced an increase in diagnostically insufficient renal biopsies anecdotally proposed to be related to a switch to new biopsy instruments, and changing the instruments and resuming on-site gross examination were both suggested as potential solutions. We therefore initiated a quality review seeking to determine whether certain clinical parameters are associated with an increased risk of insufficient renal biopsies.

Methods: We used the laboratory information system and the electronic medical record to collect the following data on 367 consecutive patients with renal core biopsies obtained from January 2008 to November 2023: patient age, sex, and body mass index; native or allograft kidney; performing specialty; performance of gross tissue evaluation; number and length of cores obtained; number of glomeruli present on H&E, IF, and EM sections; and ability to interpret for diagnosis (each individual modality and overall). We then performed statistical correlations of these clinical and pathologic variables with each other and with the diagnostic rates using Student t-tests.

Results: Overall, a diagnosis could be rendered on 95.9% of renal biopsies. There was no significant difference in the diagnostic rate, tissue volume, or glomerular content with regard to patient age or sex, kidney type, gross evaluation of the tissue, or performing specialty. Non-diagnostic rates were higher for patients with BMIs above the 75th or 90th percentiles for age (6.1% and 7.5%, respectively; p=0.027 and 0.011); within this latter population, performance by a nephrologist lowered the non-diagnostic rate (11.8% vs. 2.4%; p=0.045).

Conclusion: Ultrasound-guided renal biopsies have high utility for diagnosing medical kidney disease in children, but it may be more difficult to obtain diagnostic tissue in patients with higher BMIs. Gross tissue evaluation appears unnecessary, but having a nephrologist perform the biopsy may improve the diagnostic rate.

1723049

Which Grading Scheme is best? A Comparative Analysis of Current Grading Schemas for Pediatric Pheochromocytomas and Paragangliomas using the PASS, GAPP, and COPPS scores

S Kelley [1], C Timmons [2]; [1] UTSW Medical Center/Children's Medical Center Dallas, [2] UTSW Medical Center/Children's Medical Center Dallas

Background: Pheochromocytomas and paragangliomas are catecholamine secreting tumors arising from chromaffin cells of the sympathoadrenal system and classified as pheochromocytomas (adrenal) or paragangliomas (non adrenal) based on location. Pheochromocytomas are rare, with an incidence of 3 per million, increasing to 1 in 300,000 when combining both entities. 10-20% of these cases are in kids, and these tumors are a rare and potentially life-threatening cause of pediatric hypertension. Although multiple schemes exist for evaluating the aggressiveness, metastatic potential, and progression free survival of these neoplasms, few studies focus on evaluating these strategies in children. The Pheochromocytoma of the Adrenal gland Scaled Score (PASS) relies on histologic criteria and is intended for pheochromocytomas. The more inclusive Grading system for Adrenal Pheochromocytoma and Paraganglioma score (GAPP) and Composite pheochromocytoma/paraganglioma prognostic score (COPPS) both incorporate immunohistochemical findings, while COPPS adds tumor size and mutation status, an important factor in our population, but neither scoring device has been well studied in the pediatric population.

Methods: Between 2017 and 2023, two patients diagnosed with multiple catecholamine secreting tumors underwent resections at our institution. Both patients had at least one tumor that showed a potential for aggressive behavior by at least one grading schema.

Results: An 8 year old girl with refractory hypertension began experiencing headaches and blurry vision and imaging identified bilateral soft tissue retroperitoneal tumors without adrenal lesions. Three separate paragangliomas were seen without significant atypia or mitoses. Although not evaluable by PASS score, irregular cell nests, capsular invasion, and necrosis indicated an intermediate risk GAPP score of 3. No specific germline mutation associated with these lesions was identified. Three years later a pheochromocytoma and bilateral paragangliomas were also identified. Evaluation by PASS criteria showed capsular invasion, increased mitoses, and sheet like growth, yielding an aggressive PASS score of 7. Increased Ki-67 indicated a likelihood of metastasis with a COPPS score >3. Both paragangliomas showed increased Ki-67 and some variable/loss SDHB staining, features of greater COPPS scores. The second patient, an 11 year old with a history of Von Hippel Lindau syndrome, had bilateral adrenal masses with newly elevated normetanephrines and increased positron emission tomography uptake. Right adrenalectomy showed pheochromocytoma with aggressive features, including pleomorphism and comedonecrosis, indicating a PASS score of 3, and focally increased Ki-67 indicating GAPP score of 6 and COPP score of 5. Left adrenalectomy performed one year later again showed aggressive features including tumor necrosis, capsular invasion, and pleomorphism indicating a PASS

score of 6, a GAPP score of 4, and a COPPS score of 6.

Conclusion: Features indicating potentially aggressive behavior were seen in specimens for both patients, and the presence of certain criteria seemed more consistent in predicting further behavior. Evaluation of a larger group will aid in clarifying which features are more concerning in pediatrics.

1723052

A Case of Wiskott Aldrich Syndrome with Lymphadenopathy: Novel Syndrome Associated Morphologic and Immunophenotypic Changes in a Lymph Node Biopsy

B Kaumeyer [1], O Abobarin-Aofolaju [2], L Balikani [2], R Abraham [2]; [1] Nationwide Children's Hospital, [2] Nationwide Children's Hospital

Background: Wiskott Aldrich syndrome (WAS) is a rare X-linked inborn error of immunity (IEI), caused by pathogenic variants in WAS which encodes a protein involved in the function of the actin cytoskeleton and immunological synapse. WAS is characterized by microthrombocytopenia, immunodeficiency and eczema. Due to the key immunoregulatory role of the WAS protein, WAS patients frequently develop lymphadenopathy and have increased risk of autoimmune diseases and hematologic neoplasms. There are limited descriptions of the morphologic findings of lymph nodes in WAS. We describe both previously reported and novel morphologic and immunophenotypic findings in the lymph node of a WAS patient.

Methods: A seven week old male was admitted with failure to thrive and found to have severe thrombocytopenia. WAS protein expression was decreased in all lymphocyte subsets. Genetic testing revealed a hemizygous nonsense variant, WAS, c.121C>T, p.Arg41*. Though originally classified as X-linked thrombocytopenia (XLT), the diagnosis was revised to WAS as his clinical phenotype evolved to include recurrent infections, eczema, and thrombocytopenia poorly responsive to TPO-mimetics. At 12 months, he developed generalized lymphadenopathy and underwent a post-auricular lymph node excision to rule out malignancy.

Results: The lymph node showed scattered germinal centers in the cortex with variable degrees of atrophy. There was paracortical lymphocyte depletion with increased dendritic cells, macrophages, mast cells, and polytypic plasma cells. Immunohistochemistry (IHC) confirmed a decrease in CD3+ T cells in the paracortex. Of note, IHC and flow cytometry showed a markedly abnormal CD4:CD8 ratio (29:1) in the T-cell population without additional antigenic aberrancies. However, the overall lymph node architecture was intact and there was no diagnostic evidence of lymphoma. The paracortex showed areas of nodular expansion which were predominately composed of dendritic cells enriched with CD1a+ and Langarin+ Langerhans cells. These findings, along with scattered pigment laden macrophages and history of rash, were suggestive of dermatopathic-type changes.

Conclusion: Lymphadenopathy can develop in WAS as a result of the underlying immune dysfunction/dysregulation. Two previous descriptions of lymph nodes in WAS patients also noted the paracortical lymphocyte depletion, plasmacytosis and atrophic germinal centers described here. However, this report is the first to describe a WAS lymph node with a skewed T-cell CD4:CD8 ratio and nodular paracortical expansions enriched with Langerhans cell. It is important to understand the full spectrum of possible morphologic changes in WAS lymph nodes to avoid erroneous classification of these syndrome-associated changes as evidence of

malignancy.

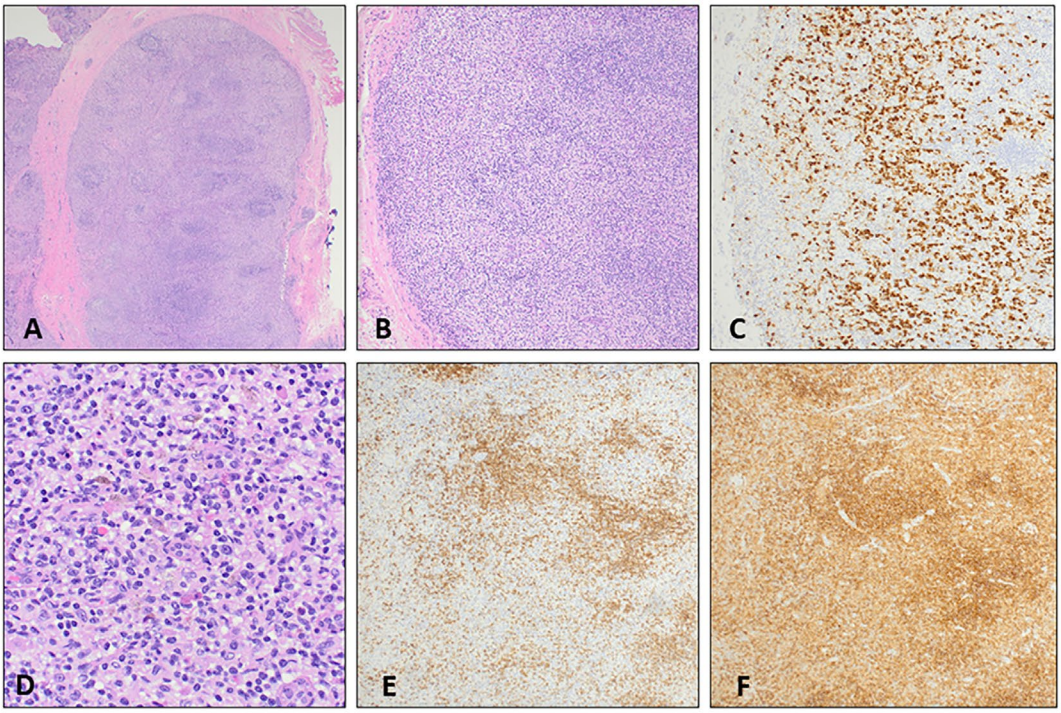

1723054

Spectrum of liver histology findings in patients with transient abnormal myelopoiesis (TAM).

L Dodson [1], K Fisher [2], T Elghetany [2], J Punia [2], K Patel [2]; [1] Baylor College of Medicine, [2] Texas Children's Hospital and Baylor College of Medicine

Background: Transient abnormal myelopoiesis (TAM) is characterized by the presence of increased peripheral blasts with acquired mutations in GATA1 in a neonate with Down syndrome (DS). Most cases resolve spontaneously without sequelae, but there is a risk of progression to myeloid leukemia and increased early mortality due to liver failure. Detailed studies on liver histology are limited and interpretation is often challenged by other co-existing conditions such as prematurity, total parenteral nutrition, congenital heart disease (CHD), biliary atresia (BA), etc. We aim to characterize the liver histopathologic changes in patients with TAM.

Methods: Pathology database was queried to identify patients with TAM with sampled liver tissue; from 2006 to 2022. All available pathology material was studied and electronic medical records were reviewed.

Results: Seven patients with DS and TAM were identified; with 10 liver samples - biopsies (n=5) and autopsies (n=5). Age at sampling ranged from 1.25 to 6 mo, mean 2.9 mo with M:F 4:3. Liver failure was a significant cause of demise in 4 out of 5 patients all of whom had resolution of peripheral blasts. Both surviving patients did not have liver failure. Only 1 had significant CHD with potential effect on liver. Conjugated bilirubin (c-bil) was elevated at the time of all except one sample. Liver biopsy was performed either to rule out BA or for persistent liver panel elevation after the resolution of peripheral blasts. Clinical findings are summarized in table 1. Pericellular fibrosis, pericentral fibrosis, and giant cell change were the most frequent histopathologic abnormalities (80% each) followed by hepatocellular/canalicular cholestasis (70%), central vein obliteration (60%), portal/periportal fibrosis (50%), and ductular reaction/bile plugs (40%). Some of these findings are in keeping with published reports of hepatic changes in TAM. There were no peripheral blasts at the time of any sample (biopsy/autopsy). Only 2 out of 10 samples showed tissue extramedullary hematopoiesis along with atypical megakaryoblasts; of whom one was tested (patient 6) and showed p.Met1 frameshift variant in the GATA1 gene at a variant allele frequency of 23.7% by targeted Next-Gen sequencing of the formalin-fixed paraffin embedded liver biopsy, confirming direct hepatic involvement by TAM in the absence of peripheral blasts. Additional immunohistochemistry and molecular testing are underway.

Conclusion: Our series extends the hepatic histology in TAM to include a mixed pericellular and perivenular pattern of fibrosis with frequent central vein obliteration. It also highlights that about 40-50% of patients can show portal changes mimicking BA, posing a diagnostic challenge. The high mortality in our series is consistent with the known contribution of liver failure.

Clinical characteristics										
Study ID	**1**	**2a**	**2b**	**3**	**4**	**5**	**6**	**7a**	**7b**	**7c**
Type of sample	A	Bx	A	A	A	Bx	Bx	Bx	Bx	A
Indication for biopsy		LF				ELE	ELE	ELE	ELE	
Age, sex	5 wk, M	3 mo, M	3 mo, M	6 wk, F	5 mo, M	5 wk, M	6 wk, F	2 mo, F	5 mo, F	6 mo, F
Gestational age	34-5/7 wk	38 wk		37-5/7 wk	38 wk	36 wk	38 wk	37-1/7 wk		
Cytarabine	x1	No [1]		x1	x1	x1	No [2]	x2		
Liver failure	Y	Y		Y	Y [3]	No	No	Y		
Ascites	Y	No		No	No	No	Y	Y		
Congenital heart defect	No	ASD, PDA		ASD, VSD	No	PDA	VSD	Complete AV canal defect, Rastelli type B.		
Biochemical parameters										
AST (U/L), fold increase	185,3.08	NA	89, 1.48	170, 2.83	62, 1.03	150, 3	115, NA	190, 3.16	360, 6	276. 4.6
ALT (U/L), fold increase	100, 2	NA	98, 2.18	116, 2.58	49, 0.98	150, 3	96	266, 5.32	95, 1.90	189, 3.78
ALK phos (U/L)	72	NA	291	44	136	80	637.1 (H)	134	100	71
GGT (U/L)	290	NA	40	46	116 (H)	70	234 (H)	147	226 (H)	163 (H)
Bili conj (mg/dL)	22.9	NA	10.5	23.1	0.0	7	6.9	23.2	11.7	35.4
Bili unconj (mg/dL)	0.3	NA	11.8	8.1	0.9	5	NA	1.8	1.8	4.7
Histopathologic findings										
EMH (2/10, 20%)	No	No	No	No	No	Y	Y	No	No	No
Megakaryoblasts (H&E) (2/10, 20%)	No	No	No	No	No	Y, rare	Y, rare	No	No	No
Ductular reaction (4/10, 40%)	No	Y	Y	No	No	Y	No	No	No	Y
Bile plugs (4/10, 40%)	No	Y	Y	Y	No	No	No	No	Y, Minimal	No
Hepatocanalicular cholestasis (7/10, 70%)	No	Y	Y	Y	No	No	Y, mild	Y, mild	Y, mild	Y, marked
Giant cell change (8/10, 80%)	Y, rare	Y	Y, rare	No	No	Y	Y	Y	Y	Y, rare
Portal/periportal fibrosis (5/10, 50%)	No	Y	Y	No	No	Nol	No	Y, mild	Y, mild	Y
Pericellular fibrosis (8/10, 80%)	Y	Y	Y	Y	No	Y	No	Y, diffuse	Y, mild	Y, diffuse, marked
Central vein obliteration (6/10, 60%)	Y	Y	Y	Y	No	Y	No	No	No	Y
Pericentral fibrosis (8/10, 80%)	Y	Y	Y	Y	No	Y	No	Y, mild	Y, mild	Y

A: Autopsy; ASD: Atrial septal defect; Bx: Biopsy; F: Female; M: Male; mo: months; PDA: Patent ductus arteriosus; VSD: Ventricular septal defect; wk: weeks; Y: Yes; NA: Not available; LF: Acute on chronic liver failure; ELE: Elevated liver enzymes

No [1] Blasts in peripheral blood resolved without cytarabine

No [2] Blasts were present in the peripheral blood at the time of biopsy

Y[3] Liver failure was followed by recovery

1723094

A Rare Case of Pediatric ALK-Positive Large B-Cell Lymphoma

M Sharobim C Bockoven, E Matkovic, E Ranheim, C Leith; University of Wisconsin Hospitals and Clinics

Background: Anaplastic lymphoma kinase positive diffuse large B-cell lymphoma (ALK+LBCL) is an aggressive neoplasm of ALK+ large, monomorphic B-cells with immunoblast-like morphology. It makes up less than 1% of all large B-cell lymphomas. Most patients present with asymptomatic nodal involvement. Although a wide age range is reported, ALK+ LBCL typically occurs in young immunocompetent patients with a median age of 38 years. Cases are more commonly reported in men than women, with a male:female ratio of 3-4:1. A diagnosis can be quite challenging because of its rare incidence, morphologic overlap with other tumors and unusual immunophenotype. We report clinical and pathologic features of ALK+ LBCL in a pediatric patient.

Methods: We reviewed histopathologic, immunohistochemical, cytogenetic, radiologic, and clinical data with long term follow up for this case. A review of the literature on previously published case reports/series was performed.

Results: A 17-year-old previously healthy male presented with painless left-sided cervical lymphadenopathy. Lymph node enlargement progressed slowly over a period of 2 months without fever, chills, or night sweats. Laboratory studies including CBC, LDH, CMP, and CMV/EBV titers were all within normal limits. Neck CT scan showed bulky left-sided cervical lymphadenopathy compressing the left internal jugular vein. A biopsy of the left neck lymph nodes demonstrated complete effacement of normal lymphoid architecture by nests of large cells with amphophilic cytoplasm, open chromatin, and distinct nucleoli. Immunohistochemical analysis showed neoplastic cells co-expressed ALK with CD138, MUM1, CD45, EMA, and CD4. CD1a, CD3, CD20, CD21, CD30, CD34, CD68, Desmin, MPO, S100, OCT3/4, and EBER were all negative. FISH analysis was positive for rearrangement of the ALK gene at the 2p23. An individualized treatment protocol with 6-cycles of CHOP plus one year of crizotinib (ALK inhibitor) starting at cycle 3 CHOP was started. At three-year follow up, the patient remained in first complete remission.

Conclusion: Recognition of ALK+LBCL as a large B-cell lymphoma with loss of CD20 is important. Tumor cells infrequently express mature B-cell markers, although transcriptional factors such as BOB1 and OCT2 can help confirm the lineage. Chromosomal translocations and rearrangements involving ALK at chromosome 2p23 are the hallmark of tumor pathogenesis. Prognosis is poor and the clinical course is more aggressive than in typical diffuse large B-cell lymphoma, but low-stage disease is associated with a better outcome. An accurate diagnosis is paramount to deliver appropriate treatment as recent studies suggest that ALK inhibitors may be an effective therapeutic option.

1723104

Placental Features Associated with Laminar Decidual Necrosis

M Bezerra Gondim; University of Louisville School of Medicine

Background: Laminar decidual necrosis is a placental feature of unclear causation. The literature is poor and has been associated with preeclampsia, preterm premature rupture of membranes, and preterm abruption. To evaluate possible causation, we retrospectively reviewed the placenta reports from our database and retrieved other placental features present.

Methods: A retrospective search was conducted over approximately two years in our database. Laminar decidual necrosis was described in 61 placentas. A statistical analysis was performed.

Results: The most common features present were distal villous hypoplasia (31%), villous infarcts (28%), and hypertrophic decidual vasculopathy (25%). Other features also present were intervillous hematoma, acute chorioamnionitis, villitis of unknown etiology, and umbilical cord vasculitis. The clinical history of gestational hypertension was present in over 30% of the cases.

Conclusion: Laminar decidual necrosis is a feature associated in the literature with preeclampsia and gestational hypertension. Our study demonstrated that the presence of distal villous hypoplasia, villous infarcts, and hypertrophic decidual vasculopathy further supports those studies.